SKB P-18-23

ISSN 1651-4416

ID 1700631

November 2022

Field test of seismic equipment in borehole HFM42 in Forsmark

Site management in Forsmark

Björn Lund, Christopher Juhlin, Michael Roth, Michael Schieschke
Uppsala University

Carl Nygren
HydroResearch

Andy Clarke, Simon Dathan, Ariana David, Anna Stork
Silixa

Keywords: AP SFK-18-010, Geophones, Fibre optics, Seismic survey

Summary

In preparation for a high sensitivity local seismic network at the Swedish nuclear waste repository site at Forsmark, the Swedish Nuclear Fuel and Waste Management Co. (SKB) proceeded with instrument tests at the Forsmark site in August 2018. Initially a test of downhole noise levels with high sensitivity geophones and digitisers, the test suite was expanded with fibre-optic cables and interrogators and an active seismic investigation. The study is a collaboration between Uppsala University, Silixa, HydroResearch AB and SKB. A number of different objectives were defined for the study:

1. Investigate the suitability of a variety of digitisers.
2. Investigate how the background seismic noise levels vary with depth and time, and if the noise “hump” at approximately 200 Hz found by Lund et al. (2017) was due to natural causes.
3. Test a variety of fibre-optic technologies in a 200 m deep borehole.
4. Compare fibre-optic measurements to geophone measurements.
5. Provide input data to the selection of instruments for the future local seismic network.
6. Investigate attenuation and near-surface structures in the area.

A 195 m deep borehole (HFM42) was drilled under SKB supervision in early April 2018 and installation of equipment took place in August 2018. Two three-component high sensitivity geophones from the Institute of Mine Seismology (IMS; similar instruments to those used in Lund et al. (2017)) were installed at 188 m and 74 m depth respectively, and a vertical component IMS geophone was installed at 6.5 m depth. Three fibre-optic cables were installed in the borehole, two helical cables and one linear cable. The borehole was grouted from bottom to top for optimal coupling of the instruments and cables to the formation rock. In addition, a vertical component geophone was installed in a 60 cm deep borehole in the vicinity of the deep borehole, and a surface seismometer was located close to the shallow borehole.

Uppsala University performed laboratory test of digitisers from Guralp, Nanometrics and the IMS. Suitability for the field test purposes was evaluated and noise measurements carried out. The Guralp Affinity digitiser was found to be best suited for the field experiment and was used during most of the field work but the IMS digitiser, with its lower noise level, was also used for a shorter time period.

Silixa performed continuous passive data acquisition from the interrogators on the fibre-optic cables in HFM42 between 14 and 17 August 2018. Data from the HFM42 borehole geophones have been collected by Uppsala University since 15 August 2018. On 16 August 2018, active source seismic data were acquired from a 1.35 km long line with a weight drop seismic source, activated every 10 m and 10 times per source point.

Using geophone night-time data for the ambient seismic noise investigation we found, similar to Lund et al. (2017), that there is significant broad-band noise in the Forsmark area between approximately 3 – 100 Hz. Superposed on the broad-band noise are high amplitude spectral peaks at 25 Hz, 50 Hz, 100 Hz, 150 Hz and further overtones. Above 150 – 300 Hz the ground motion noise reaches the digitizer noise levels, depending on digitizer. For the geophones cemented into the HFM42 borehole, there were no signs of the spectral “humps” observed in Lund et al. (2017). Such a hump was, however, observed on the free-standing geophone in the shallow nearby borehole, further supporting the conclusion that the humps are due to resonances due to inadequate coupling between sensor and borehole. There was a very clear decrease in the noise amplitudes between the geophone at 74 m depth and the one at 188 m depth. The deeper sensor is quieter over most of the spectrum by 10 – 20 dB, whereas the upper and middle sensors have very similar noise amplitudes, the uppermost being a little noisier. Interestingly, the deeper geophone records more high frequency ground motion than the middle and upper sensors, indicating that although it is less noisy at depth, the more competent rock transmits high-frequency signals better.

The ambient noise levels were found to be surprisingly stable over time, from August 2018 to March 2019. There is a small amplitude increase later in the time period, perhaps due to winter conditions and increased production in the nuclear power plants, but the overall difference is small. However, at specific frequency bands, such as 50 Hz and 100 Hz, there are significant temporal variations in the energy at the three different depth levels in HFM42. The broad-band noise is strongest at 6.5 m depth and decrease lower in the borehole. At 100 Hz, the contrary is true and the 188 m geophones sees higher noise amplitudes than the upper geophones, again potentially pointing to less high-frequency attenuation at depth.

For the fibre-optic test measurements the linear fibre and one helically wound fibre were connected to an iDASv2 interrogator and the second helical fibre, a Constellation fibre, was connected to a Carina interrogator. The systems ran in parallel for most of the recording period. Fibre data were collected with a gauge length (GL) of 10 m (measurements are made between two points on the fibre 10 m apart) for most of the acquisition period but on 16 August some 30 m data were also acquired using the Carina interrogator.

One aim was to test the differences between data collected on linear and helically wound fibre. One characteristic of DAS data is that it is one-component and it is insensitive to P-waves arriving broadside (perpendicular) to the fibre. A more even P-wave sensitivity can theoretically be achieved using helically wound cables (HWC). This is demonstrated in practice here where the linear fibre data has generally lower SNR for near-broadside arrivals.

A second aim was to demonstrate the improved SNR of data collected using a Carina system, with engineered Constellation fibre, over data collected using an iDAS v2 on standard single mode fibre. Indeed, the Carina data generally has higher SNR by a few dB. However, the system did not perform as well as expected, up to 20dB better. The reasons for this are not clear but the interrogator was an early prototype unit.

It was not possible to fully explore the effect of GL in this survey because the borehole length (195 m) was too short to evaluate the 30 m GL data in comparison to the 10 m GL data.

The fibres make it possible to have a large number of "receivers" in a borehole while the geophones give a clear indication of true ground motion in three dimensions. A direct comparison between the two systems is difficult as there are inherent differences in the measurements and also differences in the coupling with the formation of the geophones and the fibres. We made the following observations:

- All systems are able to record data with good signal-to-noise (SNR) out to 500 m for stacked weight drop data. Comparing single weight drops (a single, non-repeating source) we found that the geophones have significantly better signal-to-noise (SNR) characteristics than any of the fibre systems. If the three-component geophones are rotated to the ray direction, SNR increases further and is good out to 1.1 km. However, further investigations into the application of array techniques and data stacking of DAS data over longer length fibres should improve the SNR due to the dense spatial sampling.
- The fibre systems show high spatial resolution arrivals throughout the borehole, with the Carina system having the highest SNR.
- The fibre systems and the geophones tend to be in phase in the early part of the signal waveform but then grow increasingly out of phase.
- iDAS measures strain-rate on a fibre and therefore a direct comparison with geophone data requires conversion. As true ground motion is difficult to measure with the fibres due to varying frequency and incidence angle response we do not find good agreement between fibre and geophone amplitudes, neither in time series data nor in the spectra. This area of DAS processing is still under continuous development.
- Comparing SNR for weight drops along the active seismic profile, instead of true amplitudes, we find that even for stacked shot data the geophones have generally higher SNR than the fibre systems, when measured versus distance or incidence angle. The Carina system is better than the iDAS helical system, and the linear system shows the poorest response, which is to a large degree due to the fact that the seismic signals are incoming almost perpendicular to the fibre.
- We find that the geophones have good SNR to above 500 Hz and the Carina system to 250 – 300 Hz, depending on the distance to the source.

During acquisition of data with sample rates from the geophones at 1 kHz or 2 kHz, a few earthquakes and a number of nearby blasts have been recorded. A magnitude 0.4 earthquake 14 km away from HFM42 was recorded with high SNR at the lowermost geophone and on the horizontal components at the middle geophone but less well on the vertical components of the middle and upper geophones. At frequencies from 50 – 250 Hz the SNR is good on all geophones. A regional M2.9 earthquake at 65 km distance is well recorded on all geophones in HFM42. During blasting in the nearby Söderviken area we recorded data with 2,000 samples per second, which showed that the blasts produced ground motion above the instrument noise levels on the lower and middle geophones all the way up to about 800 Hz.

The active source weight drop data was used to manually inspect how well the signals were recorded at different distances. However, due to the different coupling of the source to the ground at different locations, depending on the amount of soil, sand or gravel between the drop point and the underlying bedrock, we could not produce good attenuation data. As another SKB project at Forsmark was investigating attenuation down to 500 m depth we did not purse attenuation studies further.

The active source data was also used to investigate potential reflectors in the underlying rock, and seismic velocities. The Carina fibre data is somewhat noisy but shows that velocity between 10 and 195 m depth is almost constant at 5.75 km/s, with the uppermost layer being slower. There is also an indication of a reflected S-wave incoming at 30 degrees angle to the borehole. The surface seismic recordings were CDP processed and found a similar velocity of 5.6 km/s below the uppermost layer. A number of sub-horizontal reflections at 150 – 300 m depth were identified in the section. These reflections appear to be localized to certain areas and do not have lateral extents of more than a few 100s of meters. It is not currently clear whether these reflections originate from fracture zones or lithological boundaries. In receiver gathers from the three geophones we found that the lower geophone, at 188 m depth, estimates a velocity of 5.8 km/s for the P-wave and 3.25 km/s for the S-wave. The middle geophone observes slightly lower velocities, 5.5 km/s for P and 3.0 km/s for S whereas the upper geophone observes similar velocities of 5.5 km/s and 2.9 km/s albeit with larger uncertainties.

Comparing geophones and fibre-optics for a seismic network, three-component geophones provide data on true ground motions for magnitudes, focal mechanisms and moment tensors which the fibre data cannot easily do without significant calibration (usually with geophone data). Geophones of the type tested here are also more sensitive than the fibre systems. Fibre-optics, on the other hand, provides high density measurements, can be used for simultaneous multi-parameter measurements (strain, temperature and seismic) and can remain in the ground for decades without requiring maintenance. The DAS interrogators are currently relatively expensive but can be used with tens of kilometres of fibre cable.

For a future seismic network in Forsmark we primarily recommend a network of high-sensitivity borehole geophones at various depths in order to detect events and obtain magnitudes, focal mechanisms and potentially moment tensors. To increase detection and location capabilities, now or in the future, we suggest that fibre-optic cables be installed in the boreholes in preparation for later connection to interrogators, either as part of the monitoring system or during campaign measurements. The design of the fibre-optic cable network needs careful analysis as individual cables in boreholes would require multiple interrogators, while continuous buried cables from borehole to borehole would reduce the number of interrogators and provide additional surface ground motion data.

Sammanfattning

I förberedelsearbetet inför installationen av ett lokalt seismiskt nätverk i slutförvarsområdet i Forsmark genomförde SKB instrumenttester i augusti 2018. Projektet startade som en undersökning av brusnivåerna på olika djup i ett borrhål, med högkänsliga geofoner och tester av olika digitaliseringsinstrument, men utökades kraftigt med tester av fiberoptisk seismisk registrering med olika typer av optiska fibrer och mätinstrument, samt en aktiv seismisk undersökning med ytgeofoner och en 400 kg viktsläppsmaskin. Studien är ett samarbete mellan Uppsala universitet, Silixa, Hydroresearch AB och SKB. Ett flertal mål definierades för studien:

1. Undersöka olika digitaliseringsenheters lämplighet för dessa mätningar.
2. Undersöka hur det seismiska bakgrundsbruset variera med djup och i tid, samt undersöka om den brustopp vid cirka 200 Hz som identifierades av Lund et al. (2017) har naturliga orsaker.
3. Testa flera olika fiberoptiska tekniker i ett 200 m djupt borrhål.
4. Jämföra de fiberoptiska mätningarna med geofonresultaten.
5. Producera data med olika instrument som kan användas när instrumentering till det lokala seismiska nätet ska bestämmas.
6. Undersöka berggrundens dämpningsegenskaper och struktur nära ytan i området.

Ett 195 m djupt borrhål (HFM42) borrades av SKB i april 2018 och instrumenten installerades i augusti 2018. Två tre-komponentgeofoner från Institute of Mine Seismology (IMS; instrument liknande de som användes av Lund et al. (2017)) installerades på 188 m och 74 m djup. En en-komponentgeofon av samma typ från IMS installerades på 6,5 m djup. Tre fiberoptiska kablar installerades i borrhålet, två heliska kablar och en linjär kabel. Borrhålet betongfylldes från botten till topp för att ge optimal koppling mellan berget och instrumenten. Dessutom installerades ytterligare en en-komponentgeofon i ett 60 cm djupt borrhål nära det djupa hålet, samt en ytseismometer nära det grunda borrhålet.

Uppsala universitet genomförde labbtester på digitaliseringsenheter från Guralp, Nanometrics och IMS. Lämpligheten för fältmätningarna utvärderades och brustester genomfördes. Guralps Affinity-digitaliseringsenhet bedöms vara bäst lämpad för fälttesterna och användes under större delen av mätperioden. Digitaliseraren från IMS har ett lägre internt brus och användes under en kortare tidsperiod.

Silixa samlade in kontinuerligt data från fiberinstrumenten i HFM42 mellan den 14 och 17 augusti 2018. Data från geofonerna i HFM42 har samlats in av Uppsala universitet sedan 15 augusti 2018. Den 16 augusti 2018 genomfördes en 1,35 km lång aktiv seismiska undersökning med ett 400 kg tungt viktsläpp som källa. Källan aktiverades var tionde meter med 10 gånger per källpunkt.

Mätningar av det seismiska bakgrundsbruset under nätterna visade på liknande resultat som de i Lund et al. (2017). En bred brustopp mellan cirka 3 Hz och 100 Hz med kraftiga smala brustoppar vid 25, 50, 100, 150 Hz och fler övertoner. Över cirka 150 – 300 Hz minskar bakgrundsbruset ner under egenbruset i digitaliseringsenheten, beroende på vilken enhet som användes. I data från de geofoner som gjutits in i HFM42 finns inte den breda topp runt 200 Hz som observerades av Lund et al. (2017). Däremot observerades den igen i data från den fristående geofonen i det grunda borrhålet, vilket stärker hypotesen att den brustoppen beror på resonanser mellan sensor och borrhål när sensorn inte är ingjuten. Brusnivåerna minskade tydligt mellan sensorn på 74 m djup och den på 188 m djup. Den djupare sensorn ser mindre brus över stora delar av spektret, med 10 – 20 dB, medan de mellersta och översta sensorerna har likartade brusnivåer, med den översta något mer brusig. Intressant nog registrerar den djupa sensorn mer högfrekvent markrörelse än den mellersta eller översta sensorn, vilket indikerar att den mer kompakta berggrunden på djupet fortplantar högfrekventa signaler bättre än berget högre upp.

Brusnivåerna visade sig vara förvånansvärt stabila över tid, mellan augusti 2018 och mars 2019. De ökade något senare i tidsintervallet, kanske beroende på vintern och ökad produktion i kärnkraftverket, men skillnaderna var små. Vid specifika frekvenser, som vid 50 Hz och 100 Hz, registrerade vi signifikanta tidsvariationer vid alla tre geofonerna i HFM42. Det bredbandiga bruset är störst på 6,5 m nivån och minskar med djup i borrhålet. För 100 Hz bruset är förhållandena de omvända och sensorn på 188 m djup ser högre nivåer än sensorerna högre upp, vilket igen tyder på mindre högfrekvent dämpning på djupet.

Under de fiberoptiska testerna kopplades den linjära fibern och en av de heliska fibrerna till ett iDASv2 instrument och den andra heliska fibern, en Constellation-fiber, kopplades till ett Carinainstrument. Systemen kördes parallellt under större delen av mätperioden i Forsmark. Fiberdata samlades in med ett mätintervall på 10 m (mätningar på fibern med 10 m avstånd) under större delen av perioden men även data med 30 m mätintervall samlades in med Carinainstrumentet den 16 augusti.

Ett av målen med mätningarna var att undersöka skillnaderna mellan en linjär fiberkabel och en där fibern lindats i en helix. DAS data är mätningar i en riktning och en linjär fiber är därmed okänslig för P-vågor som kommer in vinkelrätt mot fibern. En bättre P-vågskänslighet kan teoretiskt uppnås genom att linda fibern som en helix (Helically Wound Cable, HWC). Vi visar här att det stämmer i praktiken, då det linjära fiberdatat har generellt lägre signal-till-brus (SNR) nivåer än den heliska kabeln för P-vågor som kommer in vinkelrätt mot kabeln.

Ett annat mål var att visa hur Carina systemet med Constellationfibern har bättre SNR än systemet med en iDASv2 och en standard optisk fiber. Carina systemet visade mycket riktigt en förbättrad SNR, men endast med några få dB vilket var mindre än de förväntade 20 dB. Orsakerna till detta är inte klarlagda men Carinainstrumentet vara en tidig prototyp.

Det var inte möjligt att undersöka effekterna av olika mätintervall i detalj eftersom borrhålet var för kort för att få in tillräckligt med data för att kunna jämföra 30 m intervallet med 10 m intervallet.

Fibern gör det möjligt att ha ett stort antal ”sensorer” i ett borrhål medan geofonerna ger en tydlig bild av markrörelsen i tre dimensioner. En direkt jämförelse av de två systemen är svår eftersom det finns fysikaliska skillnader i vad som mäts och eftersom kopplingen mellan berget och fibern eller geofonen kan skilja. Vi gjorde dock följande observationer:

- Alla system ger data med god SNR ut till cirka 500 m avstånd för stackat data från viktsläppet. Om man jämför enstaka viktsläpp (en enda källa som inte upprepas) har geofonerna signifikant bättre SNR än alla fibersystem. Om geofonernas tre-komponentdata roteras till strålgångens koordinatsystem ökar SNR ytterligare och det är god SNR ut till 1,1 km avstånd. Om arraytekniker och stackning över längre fiberintervall tillämpas bör dock SNR från kabeln också öka.
- Fibersystemen visar hög rumslig upplösning på ankomsterna i hela borrhålet, där Carinasystemet har högst SNR.
- Fibersystemen och geofonerna tenderar att vara i fas i den tidiga delen av signalen men den kopplingen avtar med tid i signalen.
- iDAS mäter töjningshastigheten i fibern och därför kräver en direkt jämförelse med geofonernas amplitud en omvandling av fiberdatat. Fibrernas registrering av markrörelse beror både på frekvensinnehåll och infallsvinkel vilket gör mätningen svår och våra testmätningar visar på dålig överensstämmelse mellan fiber och geofondata, varken i tidsserier eller i spektra. Detta område inom DAS-processering är under intensiv utveckling.
- När vi jämför SNR för viktsläppsdata längs den seismiska profilen fann vi att geofonerna har systematiskt högre SNR än fiberdatat både relativt avstånd och infallsvinkel, även när viktsläppen stackas. Carinasystemet är bättre en det heliska iDAS-systemet, som i sin tur är bättre än det linjära systemet, vilket till stor del beror på att de seismiska signalerna till stor del inkommer närmast vinkelrätt mot fibrerna.
- Vi ser att geofonerna har god SNR till över 500 Hz, och att Carinasystemet har god SNR till 250 – 300 Hz, beroende på avståndet till källan

Under tiden geofondatat digitaliserades med 1 eller 2 kHz hastighet registrerades ett par jordskalv och några sprängningar i närheten. Ett jordskalv med magnitud 0.4 inträffade 14 km från HFM42 och registrerades med god SNR på den nedersta geofonen och på horisontalkomponenterna på den mellersta sensorn, men mindre väl på de vertikala komponenterna på den mellersta och övre sensorn. På frekvenser mellan 50 – 250 Hz är SNR bra på alla geofonerna. Ett regional skalv 65 km bort med magnitud 2,9 registrerades väl på alla geofonerna i HFM42. Registreringar av sprängningar i Söderviken, i närheten av HFM42, visade att dessa producerar markrörelser som är större än instrumentens egenbrus ända upp till cirka 800 Hz.

Det seismiska viktsläppsdatat användes till att manuellt inspektera hur väl signalerna registrerades för olika avstånd. Däremot visade det sig att kopplingen mellan viktsläppet och berggrunden varierade så pass mycket längs profilen, till stor del beroende på varierande tjocklek av sand och grus över berget, att vi inte kunde genomföra en bra studie av signalernas dämpning i berget. Eftersom en annan studie undersökte dämpningsförhållandena i Forsmark i ett 500 m djup borrhål beslöt vi att inte vidare försöka analysera vårt data med avseende på dämpning.

Det aktiva datat användes också för att undersöka eventuella reflektorer i berget under profilen och för att uppskatta seismiska hastigheter. Carinadatat är delvis brusigt men visar att P-vågshastigheten mellan 10 och 195 m djup är i det närmaste konstant med 5,75 km/s, och lägre i det översta lagret. Det visar också en indikation på en S-vågsreflektion som kommer in med 30 graders vinkel mot borrhålet. Datat från de seismiska ytstationerna CDP-processerades och en liknande P-vågshastighet om 5,6 km/s identifierades under det översta lagret. Ett flertal subhorisontella reflektioner på 150 – 300 m djup identifierades i sektionen. Dessa reflektorer verkar lokaliserade till specifika platser och är inte längre än några få hundra meter. Det är ännu inte klart om dessa reflektioner kommer från sprickzoner eller litologiska gränser. Det aktiva datat registrerat på geofonerna i HFM42 visade att geofonen på 188 m djup uppskattar en P-vågshastighet på 5,8 km/s och en S-våghastighet på 3,25 km/s. Den mellersta geofonen gav 5,5 km/s för P och 3,0 km/s för S medan den översta geofonen gav 5,5 km/s för P och 2,9 km/s för S, dock med större osäkerheter.

När resultaten för geofoner och fiber jämförs med tanke på instrumentering för ett seismiskt nätverk ser vi att trekomponentgeofoner är värdefulla för uppskattningar av korrekta markrörelser, och därmed för magnituder, fokalmekanismer och momenttensorer, något fibern inte gör utan avancerad kalibrering (ofta med en geofon). Geofoner av den typen som testats här är också mer känsliga än fibersystemen. Fiberoptiken däremot ger mätningar med hög täthet längs fibern, kan användas för samtidiga mätningar av töjning, temperatur och markrörelse och kan lämnas i marken i decennier utan underhåll. DAS-instrumenten är ännu relativt dyra men kan användas med tiotals kilometer kabel.

För det framtida seismiska nätet i Forsmark rekommenderar vi primärt ett nätverk med högkänsliga borrhålsgeofoner i olika djup för att detektera seismiska händelser och beräkna magnituder, fokalmekanismer och momenttensorer. För att öka detektabilitet och lokaliseringskapabilitet, nu eller i framtiden, föreslår vi att fiberoptiska kablar installeras i borrhålen för att senare kunna kopplas till DAS-instrument, antingen som en del av övervakningssystemet eller för tillfälliga mätningar. Hur ett fiberoptiskt nätverk ska utformas behöver planläggas med eftertanke eftersom individuella kablar i borrhål kräver individuella DAS-instrument medan långa kablar, från borrhål till borrhål, reducerar antalet DAS-instrument och dessutom ger ytterligare data från markytan.

Content

1 Introduction

For safety and environmental hazard assessment a nuclear waste repository should be monitored with a local seismic network. The main reasons to carry out seismic monitoring are to provide information on the natural baseline seismicity before the start of civil works at the site; to understand the responses of the rock to stress redistribution (expressed as induced seismicity) due to e.g., excavation or blasting; and to use the seismic waves generated by such events to gain knowledge about the rock mass. Key parameters include seismic event source parameters, recurrence intervals and the spatial distribution of events. The location of induced seismicity can also be used to constrain the geometry of geological structures and to assess the potential for fluid flow in such structures. Improved operational safety can be achieved through seismic monitoring by providing indications of volumes with near critical rock conditions.

The field test reported here was conducted to understand the seismic monitoring needs at Forsmark, the proposed site for long-term nuclear waste storage in Sweden, and to compare the capabilities of different technologies to fulfil this role. The monitoring at the site will be performed both before and during construction and operation. For the selection of instrumentation and design of a seismic network in Forsmark, it is important to understand the seismic background noise conditions and seismic wave attenuation properties of the rock at the site (e.g., Lund et al., 2017). These properties determine both the necessary sensitivity of the instruments and the density of recordings to detect and analyse seismic events down to a certain magnitude. The current study focuses of noise conditions, comparisons of the capabilities of different digitisers and recordings of several geophone systems and a fibre-optic Distributed Acoustic Sensing (DAS) systems. It also determines the near surface velocity in the vicinity of borehole HFM42

The bedrock in the area for the repository consists of an upper unit (FFM02) with elevated fracture density and a significant anisotropy, and a lower unit (FFM01) with lower fracture density. In some areas the boundary between the upper and lower units coincides with a deformation zone, ZFMA02.

Both geophones and fibres of the DAS system were deployed in a 200 m borehole and an active seismic survey was conducted to provide data for studies of instrument sensitivity with distance, seismic imaging and near-surface seismic velocity. This report describes the installation of three geophones and two fibre optic cables in the percussion drilled hole HFM42 (Figure 1-1), and the field tests and related analysis performed after the installation. Short holes (PFM007946 and PFM007947) have been drilled nearby, where the noise at the surface was measured to enable a comparison between previous tests (Lund et al., 2012; Lund et al., 2017) and results from borehole HFM42. Controlling documents for performing this activity are listed in Table 1-1.

Table 1-1 Controlling documents for performance of the activities.

Document	Number	Version
Activity plan		
Field test of seismic equipment in HFM42	AP SFK-18-010	1.0

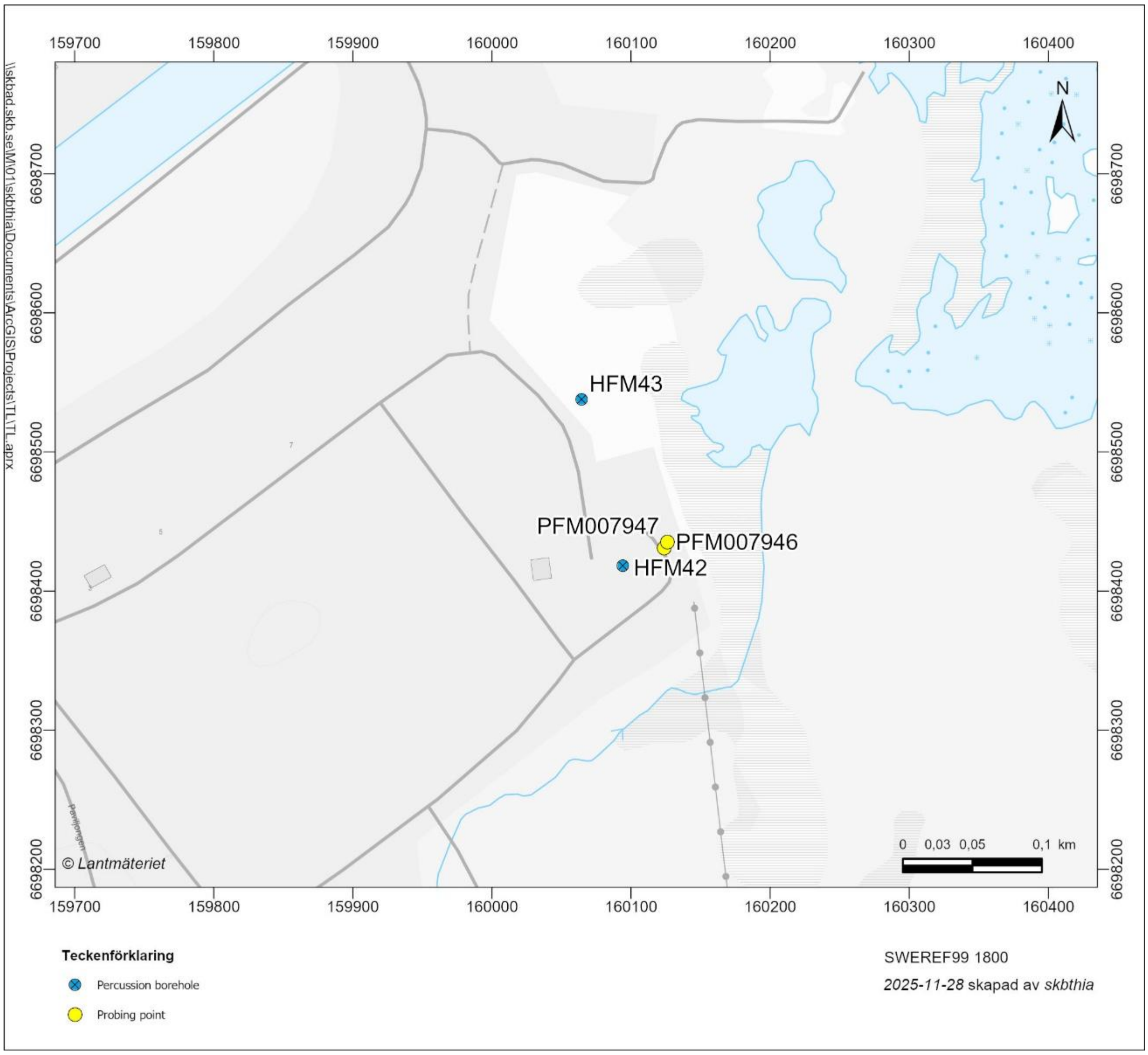

Figure 1-1. *Map showing location of percussion hole HFM42 and short holes PFM007946 and PFM007947.*

2 Instrumentation

2.1 Seismic sensors

In this project we utilized a similar type of custom-made borehole geophone from the Institute of Mine Seismology (IMS 2020) as was used in the previous noise tests (Lund et al., 2017). Two three-component geophones were purchased by SKB for installation at approximately 100 m and 200 m depth in the HFM42 borehole (see Figure 1-1). At shallow depth, just below the upper casing, a vertical component geophone from the Lund et al. (2017) survey was installed, Figure 3-1. In addition, during the active source survey we installed another vertical component geophone in a nearby shallow borehole, PFM007946 (Figure 1-1), and a three-component Guralp ESPC sensor at the surface by the shallow borehole, see Table 3-1 for serial numbers and installation locations.

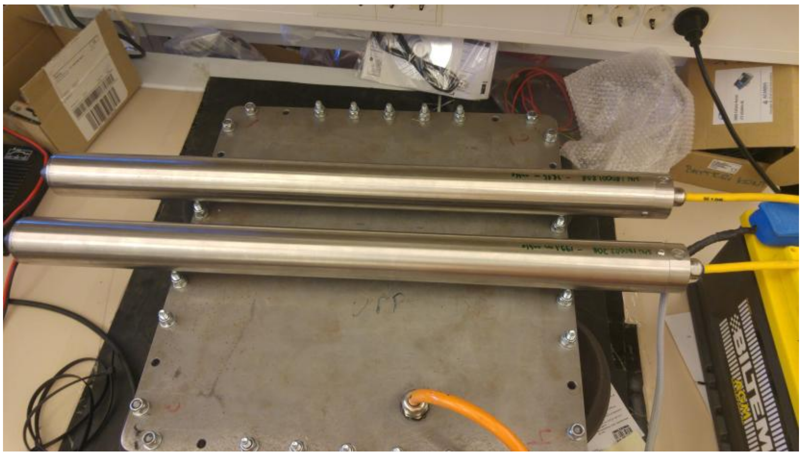

Figure 2-1. *IMS three-component geophones during testing on a shake table.*

The three-component IMS geophones consist of five stacked SM6 14 Hz OB (Brass-type) omnidirectional elements for each component, for a total of 15 elements per geophone, in a 51 mm wide (55 mm at protruding screws) and 70 cm long cylindrical steel casing, see Figure 2-1. The geophones measure motion along the instrument and in two perpendicular directions across the instrument. These geophones are not equipped with an internal accelerometer, as are the older vertical component geophones. Some further characteristics are listed in Table 2-1 (see Appendix 4 for a full set) and Figure 2-2. The three-component geophones were delivered connected to cables of 100 m and 200 m length. The original delivered geophones had serial numbers 180001.208 (100 m cable) and 180002.208 (200 m cable). The 100 m cable was damaged prior to delivery so that geophone was exchanged for geophone number 180003.208 (100 m cable), see Appendix 4 for the Production Test Records.

Table 2-1. IMS geophone specifications

	Geophone element
Natural frequency	14 Hz ± 7%
Configuration	Uniaxial, vertical
Open circuit sensitivity	80 V/m/s +5 /-10%
Coil resistance	3500 Ω
Open circuit damping	0.185
	Geophone assembly
Coil resistance	17500 Ω
Open circuit sensitivity Nominal damping resistor	400 V/m/s 41 kΩ
Combined resistance Damping ratio with the above	12.2 kΩ 0.49
Resulting sensitivity	250 V/m/s

2.1.1 Polarity test

The three-component geophones were engineered according to the IMS polarity convention (email from Dolf Bredenkamp 2018-05-11):

"The phase goes to -180 degrees to indicate that the movement of the mass to case is in opposite direction to ground motion. That said, the polarity for each sensor, when connected through the IMS system, are verified during production by tap tests, so the following default convention hold:

- The N-S aligned element swings positive for waves travelling in a southern direction
- The E-W aligned element swings positive for waves travelling in a western direction
- The U-D aligned element swings positive for waves travelling in a downwards direction."

This convention is opposite that normally used in seismology, where e.g., waves travelling upward has a positive polarity on the vertical component. The polarities were tested in the laboratory by holding the sensors vertically with the attached cable upward and tapping the sensors from three directions to simulate a P-wave. We found that the geophones did not follow any of the conventions, the test results are detailed in Table 2-2.

Table 2-2 IMS geophone polarity test

P-wave direction	Observed polarity	Expected in IMS convention	Expected in "usual" convention
down → up	negative	negative	positive
south → north	positive	negative	positive
west → east	positive	negative	positive

The wiring for the vertical component thus needed to be swapped prior to the digitiser. This later turned out not to have been done properly, resulting in the wrong polarity for both IMS three-component geophone Z-components until the wires were corrected on 2018-10-18. Unfortunately, the wiring of the one-component, vertical geophone installed at 6.5 m depth in the borehole was not in accordance with the three-component geophones, resulting in the one-component geophone having the correct polarity until 2018-10-18 but after that having the wrong polarity. At the time of writing (2021-08-31) the polarity is still wrong on the one-component geophone. We present data showing these problems in Section 4.3.1.

2.1.2 Shake table test

We compared pairs of sensors against each other using a vibrator source (controlled frequency and amplitude) to check for pair-wise phase and amplitude consistency. The test will also reveal potential resonances in the sensors. The sensors were tested using an oscilloscope.

- Tested triaxial sensors S/N 180003.208 (100m) against S/N 180002.208 (200m)
- Tested uniaxial sensors S/N 130003.184 (20m) against S/N 130002.184 (20m)

The results showed that the amplitude and phase consistency is generally good, except near regions of resonance as the resonance frequencies are slightly different. The triaxial sensors have a case resonance at approximately 380 Hz on the horizontal components. We interpret this to be due to the long sensor body and expect that this resonance will disappear when the sensors are grouted into the borehole. The field measurements in Section 6.1, however, indicate that there may be a weak resonance signal remaining.

2.1.3 Guralp ESPC

The Guralp ESPC (T36021) is a 60 second to 100 Hz broadband seismometer with sensitivity 2x5,000 V/m/s, see Figure 2-2. The sensor is part of the mobile instrument pool at Uppsala University and used in temporary network deployments. We use it here for comparison with the vertical component shallow geophone.

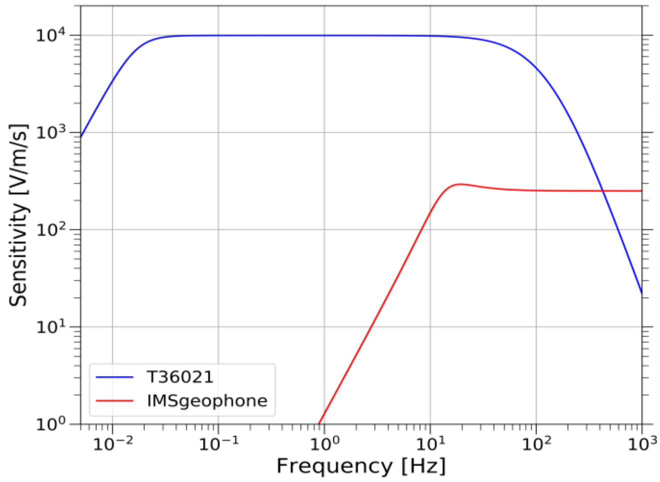

Figure 2-2. *Sensitivity curves for the IMS three-component geophone and the T36021 Guralp ESPC.*

2.2 Digitisers

The project tested five digitisers with respect to the need for high sample rates (4 kHz or more), time keeping and noise characteristics. Specifically, the tests included:

- Digitiser sampling phase lock and synchronicity. Input Pulse-Per-Second (PPS) and record >= 10 minutes. The raising/falling edges should be <1µs offset.
- Digitiser sampling clock accuracy. Input Pulse-Per-Minute (PPM) and record >= 1 hour. Check for offsets >1 second which the previous test would not discover.
- Digitiser self-noise test. Simulate the effective sensor impedance by shortening the digitiser input with a 12.2 or 17.5 kΩ resistor, use continuous recording >= 10 minutes at highest and lowest gain at 6 kHz sampling or maximum sampling rate if lower.

Below are brief descriptions of the digitisers' key features and the test results.

2.2.1 Guralp Affinity

- Picture in Figure 2-3.
- Eight 31-bit analogue-to-digital conversion (ADC) channels (six primary, 2 auxiliary).
- 138 dB of dynamic range at 100 samples per second.
- Output rates between 1 to 4,000 samples per second available, up to four concurrent rates per channel.
- Selectable gain: 1x, 2x, 4x, 8x, 16x, 32x, 64x.
- Sensitivity: 1µV/count at 1x gain.
- Timing precision < 0.1 µs with GNSS (GPS, GLONASS, Galileo, BeiDou) connected.
- Power consumption 1.2 to 1.55 W at 12 V DC, input voltage 9 – 36 V DC.
- Linux operating system, configuration via web-browser or Scream!, with RS232, Ethernet and USB communication.
- GCF and miniSEED data formats with Scream!, SEED-link and other seismic data protocols.

The Affinity passed the tests for sampling phase lock, synchronicity and clock accuracy. The noise tests are presented below.

Figure 2-3. *Guralp digitisers. Left: Affinity. Centre: Minimus (above) and Minimus+ (below). Right: DM24.*

2.2.2 Guralp Minimus+

- Picture in Figure 2-3.
- Eight 24-bit analogue-to-digital conversion (ADC) channels.
- 142 dB of dynamic range at 100 samples per second.
- Output rates between 1 sample per hour to 5,000 samples per second available.
- Selectable gain: 1x, 2x, 4x, 8x, 12x.
- Sensitivity: 2.441 uV/count at 1x gain.
- Timing precision ±50 ns with GNSS (GPS, GLONASS, BeiDou) connected.
- Power consumption 1.65 – 1.75 W at 12 V DC, input voltage 10 – 36 V DC.
- Operating system compatible with Linux, Windows and MacOS, configuration via web-browser, Guralp Discovery or mobile phone app, with Ethernet or Bluetooth communication.
- miniSEED data format with Scream! and SEEDlink seismic data protocols.

The Minimus+ was tested in 2017 and showed time offset of 758 µs, which was acknowledged by Guralp. It passed the test of accuracy for offsets above 1s. The Minimus+ does not have an analogue low-pass filter which implies that there is a risk of aliasing, especially at higher sampling frequencies. Because of these limitations we did not include the Minimus+ in further tests.

2.2.3 Guralp DM24S x EAMU

- Picture in Figure 2-3.
- Four (or seven) 24-bit analogue-to-digital conversion (ADC) channels (three/six primary plus one auxiliary).
- 137 dB of dynamic range at 40 samples per second.
- Output rates between 1 to 1,000 samples per second available.
- Unity gain.
- Sensitivity 3.2 µV/count.
- Timing precision 0.8 µs with GPS connected.
- Power consumption 1.96 – 2.85 W at 12 V DC, input voltage 12 – 28 V DC.
- Linux operating system, configuration using web-browser, terminal-based menus or Linux control line, with RS232, Ethernet and USB communication.
- GCF, GDI & miniSEED data format with Scream!, SEED-link and other seismic data protocols.

The DM24 digitisers from Uppsala University used in the project are older versions of the one detailed above and do not have the EAM communication module. The results here may therefore differ slightly from those that would have been obtained with the latest model. Newer versions of the DM24 can also be obtained with varying gain levels, from unity to x64. The DM24 used here passed the tests for sampling phase lock, synchronicity and clock accuracy, and as they will be used only for comparison to earlier surface instruments tests the low sampling rate is sufficient. The noise tests are presented below.

2.2.4 Nanometric Centaur, high gain model

- Picture in Figure 2-4.
- Six 24-bit analogue-to-digital conversion (ADC) channels.
- 142 dB of dynamic range at 100 samples per second.
- Output rates between 1 to 5,000 samples per second available, up to two concurrent rates per channel. Only 3 channels support 5,000 sps sampling, maximum sampling rate with 6 channels is 2,000 sps.
- Selectable gain: 4x, 8x, 16x, 40x, 80x, 160x (high gain model). In addition, digital gain control.
- Sensitivity: 0.625 uV/count at 4x gain (lowest).
- Timing precision < 5 µs with GNSS (GPS + one of GLONASS, Galileo, BeiDou, QZSS) connected.
- Power consumption 0.85 to 2.0 W, input voltage 9 – 36 V DC.
- Web-based graphical configuration, with Ethernet, WiFi and USB communication.
- miniSEED data format with Nanometrics NP and SEED-link seismic data protocols.

Lab tests showed that the Centaur digitizer could not record continuous data with a sufficient sample rate (5 kHz) for more than 3 channels. The maximum stable sample rate for recording continuously on 6 channels was 2000 samples per second which was insufficient for the planned field measurements. The timing and noise tests were not completed.

Figure 2-4. *Digitisers. Left: Nanometrics Centaur. Right: IMS netADC.*

2.2.5 Institute of Mine Seismology, NetADC + NetSP

- Picture in Figure 2-4.
- Eight 24-bit analogue-to-digital conversion (ADC) channels.
- 147 dB of dynamic range at 50 samples per second.
- Output rates between 1 to 192,000 samples per second available.
- Unity gain.
- Sensitivity 0.021 µV/count
- Timing: generally needs external timing, input over Ethernet or RS232. We used a special solution with an attached GPS.
- Power consumption 0.38 to 3.0 W, input voltage 9 – 18 V DC.
- Configuration with IMS software, with Ethernet or RS232 communication.
- IMS data format and seismic data protocol.

The IMS netADC/netSP standalone unit was tested in the SKB project in 2013 and the unit we received for this test was of a similar type. As discussed in the report Lund et al. (2017), the unit did not pass the tests for sampling phase lock, synchronicity and clock accuracy. According to IMS this is, however, not a problem when the digitiser is integrated in a network with central timing.

2.2.6 Summary

Some of the digitiser specifications are presented in Table 2-3 below. For the field tests we will use the Guralp Affinity and IMS NetADC+NetSP digitisers for the geophones in the deep borehole. We will also use two Guralp DM24 digitisers, one each for the vertical geophone in the shallow PFM007946 borehole and for the broadband Guralp instrument. The lack of an analogue anti-alias filter in the Guralp Minimus and the insufficient sampling rate of the Nanometrics Centaur for the intended downhole geophone measurements precluded use in the field.

Table 2-3. Digitiser comparisons. *The Nanometric Centaur only provides up to 2,000 samples per second for more than 3 channels and is a high-gain model with lowest gain x4.

Digitiser	Sample rates	Gain levels	Sensitivity at gain 1 [µV/cnt]	Timing test	Power consumption [W]	Seed-link
Guralp Affinity	1 – 4,000	1x, 2x, 4x, 8x, 16x, 32x, 64x	1.0	Pass	1.2 – 1.55	Yes
Guralp Minimus+	1 – 5,000	1x, 2x, 4x, 8x, 12x	2.441	Not tested	1.65 – 1.75	Yes
Guralp DM24	1 – 1,000	1	3.2	Pass	1.96 – 2.85	Yes
Nanometrics Centaur*	1 – 5,000	4x, 8x, 16x, 40x, 80x, 160x	0.625*	Not tested	0.85 – 2.0	Yes
IMS NetADC+NetSP	1 – 192,000	1	0.021	Pass	0.38 – 3.0	No

2.3 Digitiser noise

We carried out noise tests in the lab on the Guralp Affinity, Guralp DM24 and IMS digitisers. To simulate the IMS geophones we would use in the field experiment we terminated the digitiser input channels with resistors matching the geophone nominal impedance. Depending on the digitiser used, the resistors were either 12.2 kΩ or 17.5 kΩ. The signals recorded will then be due only to internal noise in the digitiser. We show results below as power spectral densities (PSDs) in dB relative to 1 V2/Hz. Calculations are performed on 5 minutes of data using Welch's method in Obspy (Obspy, 2020) with 50% overlapping segments. The segments are tapered with a Hanning window. To assess the noise levels relative to ground motion (System Noise) we also present results where the digitiser output is convolved with the IMS geophone response, red line in Figure 2-2.

The noise level PSD in V2/Hz are compared to the theoretical levels of quantization (spectral) noise in an ideal analogue to digital converter in order to determine the number of effective noise free bits (e.g., Sleeman et al., 2006):

$$Spectralnoise = \frac{(2\,A/2^B)^2}{12 * f_N}$$

where: Spectral Noise has units of V^2/Hz, A is the digitiser peak full scale (half peak-to-peak) in Volt, B is the number of ideal bits of resolution and fN is the sampling Nyquist frequency in Hertz.

The dynamic range (SNR) in a specific frequency band is calculated as the ratio of the RMS of a full-scale sine wave (A as above) and the noise RMS:

$$SNR = 20log\left(\frac{A/\sqrt{2}}{RMSnoise}\right)$$

where the RMS is calculated as

$$RMS = \sqrt{\frac{1}{T_s N}\sum_{k=n}^{m}|P_{xx}[k]|}$$

and T_s is the sampling period in seconds, N the number of samples in the window and P_{xx} the PSDs.

2.3.1 Guralp Affinity

The Affinity was tested using 4,000 samples per second sampling rate at three different gain levels with three channels terminated by 17.5 kΩ resistors. The tested gain levels are x1, corresponding to 40 V peak-to-peak input voltage, x8 (5 V peak-to-peak) and x64 (0.625 V peak-to-peak). The sensitivity of the Affinity is 1 µV/cnt at gain x1. PSDs are calculated on segments of data with 16384 samples, corresponding to 4.096 seconds of data. As we are interested in the high frequency performance we show data from 1 Hz upward.

Figure 2-5 shows how the noise levels for each gain level are constant in the frequency interval 1 to 2,000 Hz. The noise levels decrease with increasing gain, there is an approximate 11 dB decrease from x1 to x8 and then approximately 1 dB decrease from x8 to x64, indicating that there is a diminishing return for increasing the gain. Similarly, the number of effective bits decrease with increasing gain and is 19.1 bits at x1 gain, 17.8 at x8 and 14.9 bits at x64 for the 4 kHz sampling frequency. Figure 2-5 also shows that the three tested channels have virtually identical noise levels, for gain x8, as expected, but that the East channel picked up more of the 50 Hz noise from the power grid. This could be due to how the channel terminators were located.

Convolving the digitiser noise PSDs with the response function of the IMS geophone shows how the digitiser noise would affect measurements of ground motion by the IMS geophone, see Figure 2-6. We use the velocity proportional response function shown in Figure 2-2 above. These so-called system noise measurements will be used below to compare to the noise data recorded in the field.

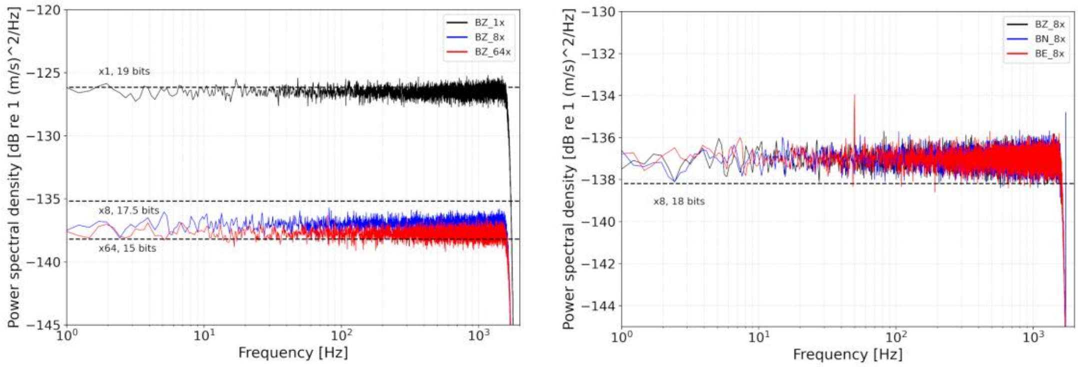

Figure 2-5. *Power spectral densities (PSD) for the Affinity digitiser sampling at 4 kHz in dB relative to 1 V^2/Hz. The input channels are terminated by 17.5 kΩ resistors. Horizontal dashed lines show levels of theoretical quantization noise for different gain levels and bits of resolution. Left) PSDs for gain levels x1 (black), x8 (blue) and x64 (red). Right) PSDs for three different channels at x8 gain.*

Table 2-4 contains the calculated RMS and dynamic range values for the different components and gain levels in the passband 15 – 1,000 Hz, suitable for the IMS geophone. We include both the RMS in volts and the corresponding system noise in nm/s for gain level x8. We note that as the gain is increased, the RMS goes down but as the full-scale input is reduced, the dynamic range decreases with increasing gain.

Table 2-4. Affinity digitiser noise RMS and dynamic range (SNR), estimated between 15 - 1,000 Hz for gains of x1, x8 and x64. Sample rate 4,000 samples per second.

Channel	RMS x1 [µV]	RMS x8 [µV]	RMS x64 [µV]	SNR x1 [dB]	SNR x8 [dB]	SNR x64 [dB]	System RMS x8 [nm/s]
E	15.0	4.43	4.06	119	112	95	17.5
N	14.8	4.44	4.08	120	112	95	17.6
Z	14.9	4.43	4.06	120	112	95	17.5

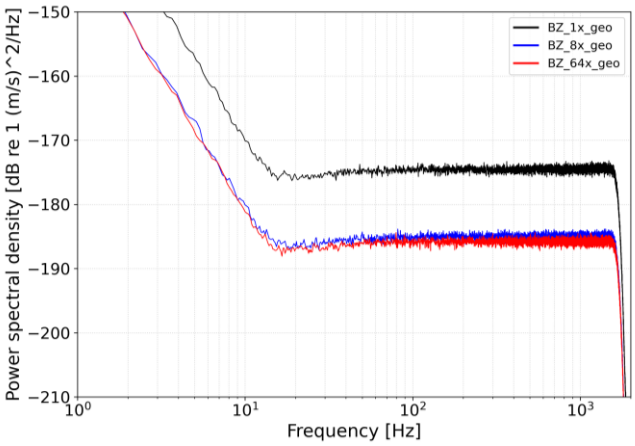

Figure 2-6. *System noise as power spectral densities (PSD) for the Affinity digitiser at gains x1 (black), x8 (blue) and x64 (red) at sampling rate 4 kHz. The digitiser noise has been convolved with the response of the IMS geophone to show noise relative to ground motion in terms of velocity.*

2.3.2 IMS digitisers

Test result for the IMS digitiser were reported in Lund et al. (2017). We revisited the test data to produce results comparable to those presented for the Affinity above. The IMS digitiser was tested with two different terminating resistors to investigate how different geophones would affect the noise recorded from the digitiser. We present results here both for a 12.2 kΩ resistor, simulating the IMS geophone, and a 50 Ω resistor simulating an active geophone. Sample rates at 6,000 and 24,000 samples per second were tested. The IMS digitiser has unity gain, corresponding to an input voltage span of 0 to 5.65 V. The sensitivity of the IMS digitiser is 0.021 µV/cnt. For the calculations, the 6 kHz data use segments of 16384 samples, corresponding to 2.73 seconds of data, and the 24 kHz data use segments of 131072 samples, corresponding to 5.46 seconds of data.

Figure 2-7 shows how the noise levels are almost independent of sample rate, differences are probably due to different environmental conditions as the recordings with 6 kHz and 24 kHz were done during two consecutive days. We also see how the noise decreases when the resistance on the input is decreased, by approximately 2 dB, as does the tendency to pick up noise from the surrounding electromagnetic fields. Since the time when the digitiser was tested in Uppsala, IMS has worked on improved shielding which is likely to have decreased the tendency to pick up environmental signals. The number of effective bits decrease with increasing sample rate, they are 21.3 bits at 6 kHz sample rate and 20.6 bits at 24 kHz sample rate. Figure 2-7 also shows the characteristic 1/frequency increase in noise at lower frequencies which is characteristic of active electronic components.

Convolving the digitiser noise PSDs with the response function of the IMS geophone shows how the digitiser noise would affect measurements of ground motion, to the right in Figure 2-7. We use the velocity proportional geophone response function shown in Figure 2-2 above. These measurements will be used below to compare to the noise data recorded in the field.

Table 2-5 contains the calculated RMS and dynamic range values for the two resistors and sample rates in the passband 15 – 1,000 Hz, suitable for the IMS geophone. We include both the RMS in volts and the corresponding ground motion in nm/s for the 12.2 kΩ resistor. We note that as the sample rate is increased, the RMS goes up (in agreement with e.g., Merchant & Slad (2018), but perhaps also in response to different strengths of the external fields at specific frequencies) and thus the dynamic range goes down. Similarly, as the RMS is decreased when the resistance is increased, the dynamic range increases. The RMS estimated here agrees well with measurements performed at the IMS lab in response to our inquiries, where they estimated an electronic noise RMS of 1.144 µV, corresponding to 4.1 nm/s (D. Bredenkamp, IMS, personal communication 2013-11-22). It is not clear to us over which exact frequency range IMS estimated the RMS.

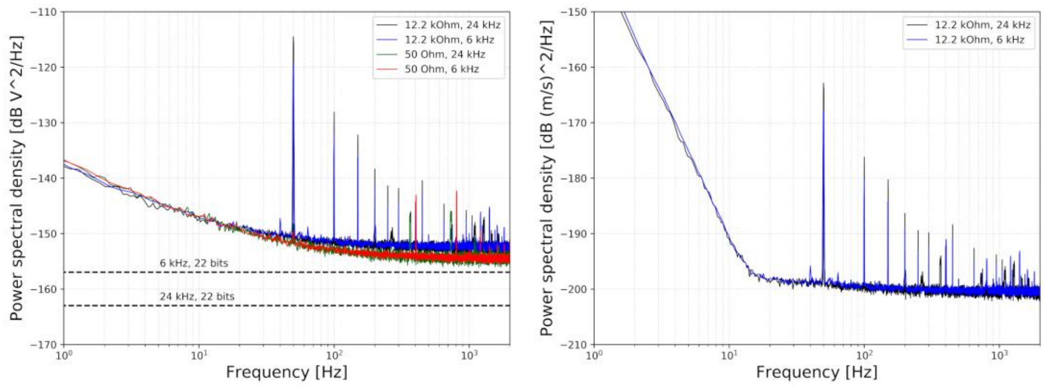

Figure 2-7. *Left) Power spectral densities (PSD) for the IMS digitiser sampling at 6 kHz (blue, red) and 24 kHz (black, green) in dB relative to 1 V2/Hz. The input channels are terminated by 12.2 kΩ (black, blue) and 50 Ω (green, red) resistors. Horizontal dashed lines show levels of theoretical quantization noise for different sampling rates and 22 bits of resolution. Right) System noise as PSDs for the IMS digitiser with a 12.2 kΩ resistor at 6 kHz (blue) and 24 kHz (black). The digitiser noise has been convolved with the response of the IMS geophone to show noise relative to ground motion in terms of velocity.*

Table 2-5. IMS digitiser noise RMS and dynamic range (SNR) for two termination resistors of 12.2 kΩ and 50Ω, estimated between 15 - 1,000 Hz. Unity gain, sampling 6,000 and 24,000 samples per second, respectively.

Resistor	RMS 6 kHz [µV]	RMS 24 kHz [µV]	SNR 6 kHz [dB]	SNR 24 kHz [dB]	System RMS 6 kHz [nm/s]	System RMS 24 kHz [nm/s]
12.2 kΩ	1.26	1.39	124	123	4.87	5.40
50 Ω	0.67	0.67	129	129	-	-

2.3.3 Guralp DM24

One of SNSNs Guralp DM24 digitisers (serial number A1667) was tested using 1,000 samples per second sampling rate on one channel terminated by a 12.2 kΩ resistor. The DM24 only has one gain level, corresponding to 40 V peak-to-peak input voltage, and sensitivity 3.2 µV/cnt. PSDs are calculated on segments of data with 16384 samples, corresponding to 16.384 seconds of data. As we are interested in the high frequency performance, we show data from 1 Hz upward.

Figure 2-8 shows that the DM24 noise level at 1 kHz sampling rate is constant over the frequency interval 1 to 500 Hz and that it is very similar to the Affinity noise levels at x1 gain and 4 kHz sampling rate. The DM24 picked up more of the 50 Hz electric field disturbance than the Affinity, but at similar levels as the IMS digitiser, although at fewer frequencies.

Convolving the digitiser noise PSDs with the response function of the IMS geophone shows how the digitiser noise would affect measurements of ground motion, see Figure 2-8. We use the velocity proportional response function shown in Figure 2-2 above. As the digitiser noise level is similar to that of the Affinity at x1 gain, so is this system noise curve. These measurements will be used below to compare to the noise data recorded in the field.

Table 2-6 contains the calculated RMS and dynamic range values for the different components and gain levels in the passband 15 – 400 Hz, suitable for the IMS geophone. We include both the RMS in volts and the corresponding ground motion in nm/s. As the passband is smaller for the DM24 than that used for the Affinity RMS above, the RMS is also smaller and the dynamic range larger.

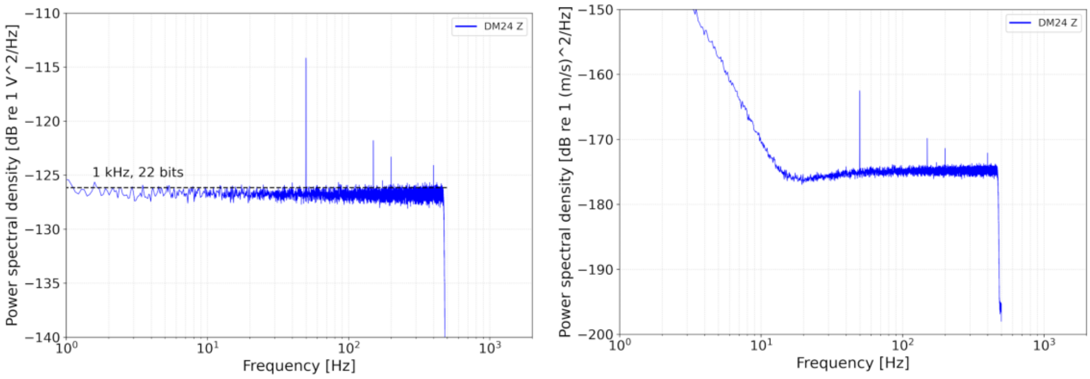

Figure 2-8. *Left) Power spectral densities (PSD) for the DM24 digitiser (A1667) sampling at 1 kHz (blue) in dB relative to 1 V^2/Hz. The input channels are terminated by 12.2 kΩ resistors. Horizontal dashed line shows level of theoretical quantization noise for 1 kHz sampling rate and 22 bits of resolution. Right) System noise as a PSD for the DM24 digitiser with a 12.2 kΩ resistor at 1 kHz (blue) sampling rate. The digitiser noise has been convolved with the response of the IMS geophone to show noise relative to ground motion in terms of velocity.*

Table 2-6. Guralp DM24 digitiser noise RMS and dynamic range (SNR) for a termination resistor of 12.2 kΩ, estimated between 15 - 400 Hz. Unity gain, sampling 1,000 samples per second.

Resistor	RMS [µV]	SNR [dB]	System RMS [nm/s]
12.2 kΩ	9.04	124	37.8

2.3.4 Nanometrics Centaur

As the Centaur did not meet the sampling rate requirements for the downhole geophone test we did not test it further. However, Sandia National Laboratories have thoroughly tested the Centaur digitiser (Merchant & Slad, 2018) and we copy relevant results from that report here.

The Sandia test were performed at significantly lower sampling rates than the ones tested for Forsmark. The highest sample rate used at Sandia was 100 Hz, and the Centaur was tested at gain levels from x1 to x40 and with shortening resistors of 50Ω, 500Ω, 4kΩ and 9.4 kΩ. The noise levels were calculated in various frequency bands, none of which compare well to our measurements above. In Table 2-7 below we show results for the 0 – 50 Hz, as that contains the widest high frequency band.

The Centaur noise measurements were convolved with various seismometer responses to produce system noise curves. However, as the Sandia test was focused on broadband seismology, most of the instrument were high sensitivity broad-band instruments. The only short period instrument used was the Geotech GS13 but Merchant & Slad (2018) note that the tested digitiser was of a low impedance model and not suitable for a high impedance instrument. They do not present integrated RMS values but show system noise curves which indicate that the Centaur with a GS13 instrument reaches noise levels of -200 to -215 dB (m/s)2/Hz between 1 – 15 Hz.

Table 2-7. Nanometrics Centaur digitiser noise RMS and dynamic range (SNR) for various termination resistors and gain levels, estimated between 0 and 50 Hz. Sample rate 1,000 samples per second.

Resistor	Gain	RMS [µV]	SNR [dB]
50 Ω	x1	1780	138
500 Ω	x1	1770	138
4 kΩ	x1	1840	138
500 Ω	x10	185	138
4 kΩ	x10	204	137
9.4 kΩ	x10	204	134

2.3.5 Summary

The Guralp Affinity, DM24 and IMS digitisers are designed for slightly different applications, with the Guralps focusing on traditional seismology and more recently induced seismicity applications and thus lower frequencies, whereas the IMS digitiser is designed for high frequency near-field recordings in mines. This is evident both in the frequency response between 1 and 10 Hz (Figure 2-9), where the IMS loses sensitivity but the Affinity does not, and in the available sampling rates where the IMS is capable of 192 kHz and the Affinity 4 kHz. We see that the IMS has approximately 11 dB lower noise than the Affinity (x8 gain) at frequencies above the IMS geophone corner frequency when compared as ground motion (system RMS). The IMS digitiser is, however, more sensitive to noise at high frequencies and we are uncertain if this is internally generated noise or signals picked up through the resistors.

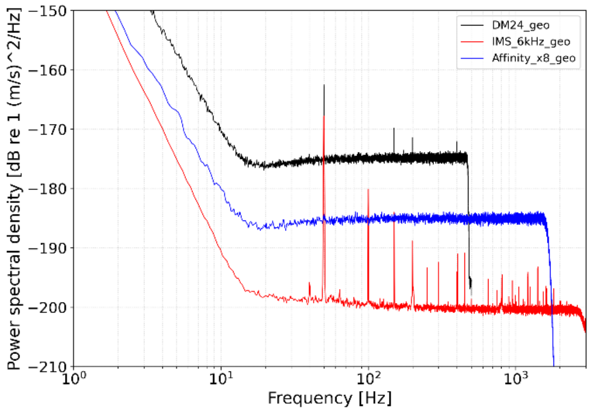

Figure 2-9. *Comparison of the system noise power spectral densities, simulated for the IMS geophone, from the three digitisers tested above. Black: DM24 at 1 kHz sampling. Blue: Affinity at 4 kHz sampling and gain x8. Red: IMS at 6 kHz sampling rate.*

2.4 Distributed measurements

2.4.1 Introduction

Distributed acoustic measurements are made on both fibre-optic cables deployed downhole. Data is recorded simultaneously from the two cables using intelligent Distributed Acoustic Sensor (iDAS™) interrogators. Below is a description of the cables and interrogators used in the test.

2.4.2 Cables

Two fibre optic cables were used for the survey:

Cable #1 (Figure 2-10 bottom)

- Referred to as the helical cable (HWC) in the following text.
- An optical cable with 12 optical fibres split into 3 helically wound loose tubes. The helical path required an extra 13.5% of fibre length compared to the linear fibre. The fibres are divided as follows into the tubes:
  - Tube #1: 2 single mode standard fibres and 3 Constellation fibres (two of these fibres are optimised for 10 m spatial resolution, and one for 30m spatial resolution).
  - Tube #2: 2 single mode standard fibres and 1 Constellation fibre. The Constellation fibre is optimized for 10m spatial resolution.
  - Tube #3: 4x multi-mode fibres (for temperature measurements).
- Further information is provided in Table 2-8.
- Cable has an outer diameter of 25mm and length 203m. Specifications for the cable can be found in Appendix 1. However, note that the number of fibres and configuration within each tube is different and the description given within this section should be used.

Cable #2 (Figure 2-10 top)

- Referred to as the linear cable in the following text.
- An optical cable with a hybrid structure including 2 single mode fibres (for acoustic); 2 multi-mode fibres (for temperature); and 2 18AWG copper conductors (for cable heating).
- Cable has an outer diameter of 6.35mm and length 220m. Specifications can be found in Appendix 2.

Note, Constellation fibres are engineered for enhanced acoustic response and can only be used with Silixa's Carina® interrogator (Figure 2-13).

Using the two cables allows comparisons between standard single mode fibre and Constellation fibre and between linear and helical fibres.

Downhole terminations were used for both the linear cable and the helical cable to protect the fibres from mechanical damage and water ingress while providing a return upgoing fibre path (Figure 2-11). At the bottom end of both cables, the fibres are spliced in a u-bend configuration (duplexed) within Silixa's engineered downhole termination. This duplexed fibre configuration allows a double-ended measurement, i.e., the possibility of measurement on both the upgoing and downgoing portions of the fibre. It also provides a great deal of flexibility, allowing multiple boreholes to be connected and monitored simultaneously using a single DAS or distributed temperature sensing (DTS) unit. It also enables robust length and temperature calibration methods. The fibre-optic cable deployments have no electronic components and therefore are unaffected by electrical noise.

Table 2-8 Helical cable fibre configuration. SM – single mode; MM – multi-mode; CF – constellation fibre; SE – single-ended; DE – double-ended (up- and down-going measurements).

Tube	Fibre Type	Label	Gauge Length	Configuration
Blue	SM	SM1		DE
Blue	SM	SM2		DE
Blue	Constellation	CF1	10m	DE
Blue	Constellation	CF2	10m	DE
Blue	Constellation	CF3	30m	SE
Orange	SM	SM3		DE
Orange	SM	SM4		DE
Orange	Constellation	CF4	10m	SE
Green	MM	MM1		DE
Green	MM	MM2		DE
Green	MM	MM3		DE
Green	MM	MM4		DE

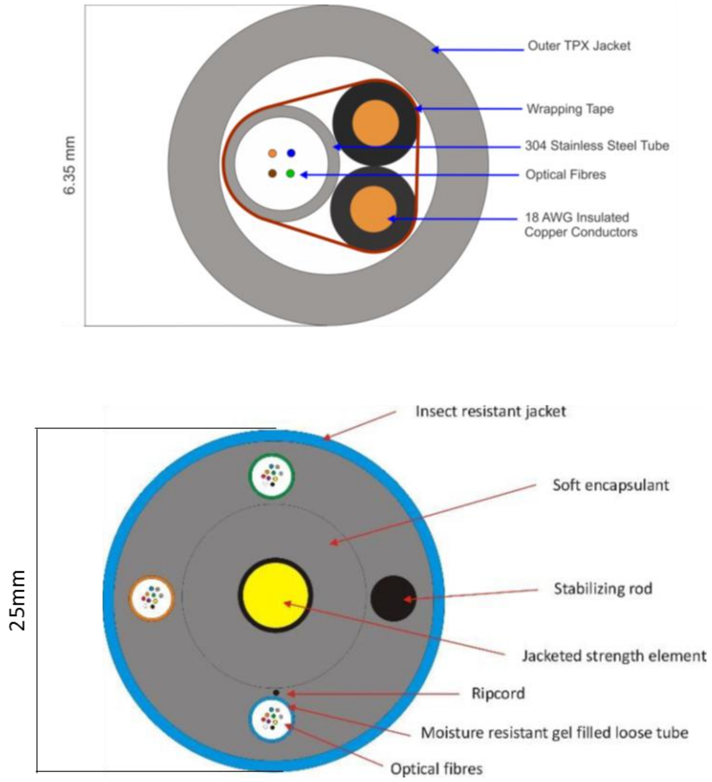

Figure 2-10 *Heatable linear cable (top) and helical cable (bottom).*

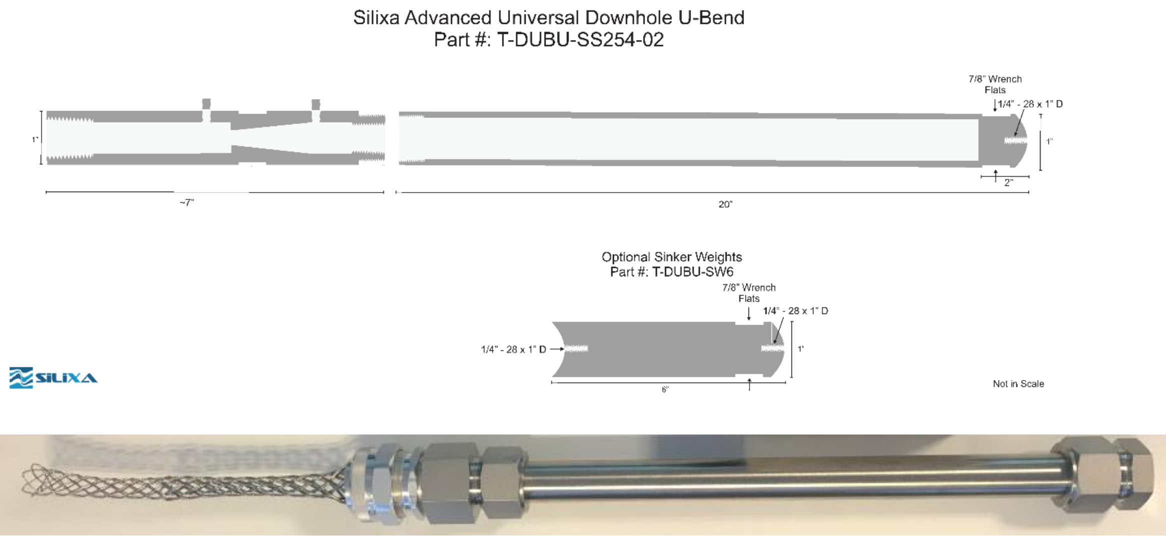

Figure 2-11 *Downhole termination used for heatable linear cable (top) and helical cable (bottom).*

2.4.3 Instruments

iDAS interrogator

Silixa's iDAS (Figure 2-12) is an optoelectronic system which records the complete acoustic signal (phase and amplitude) continuously along the path of sensing fibre up to tens of kilometres long.

When a pulse of light travels down an optical fibre, a small amount of the light is naturally backscattered (through Rayleigh, Brillouin and Raman scattering) and returns to the sensor unit (Muanenda et al., 2019). The nature of this scattered light is affected by tiny strain events within the optical fibre structure which themselves are determined by the localised acoustic or seismic environment. The iDAS interrogator records the returning signal against time, a measurement of the acoustic field all along the fibre can be determined. Silixa's iDAS has broadband sensitivity and is sensitive to frequencies ranging from millihertz to hundreds of kilohertz. The iDAS also offers the flexibility to operate on single mode or multi-mode fibre without the introduction of any external or additional apparatus, with no loss of signal quality and while preserving the true acoustic nature of the measurement. This unique feature makes it possible to access legacy DTS installations for new acoustic surveys, for example, borehole seismic surveys or flow measurements.

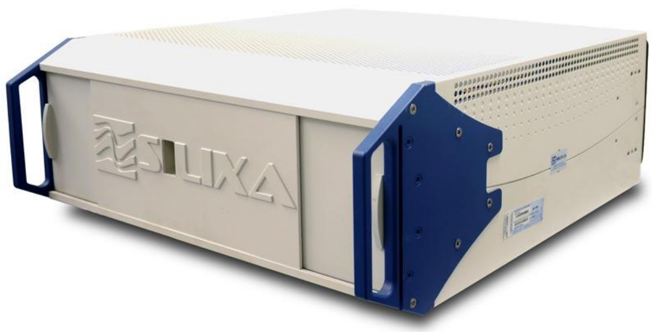

Figure 2-12 *The Silixa iDAS interrogator.*

Carina Sensing System

Carina is a versatile fibre optic sensing system and comprises an advanced optoelectronics interrogator (Figure 2-13) and sensing cables, which are equipped with the new family of engineered Constellation fibres. This system enables a gain of two orders of magnitude (100 times) better signal to noise ratio (SNR) over that achieved with standard fibres. This is equivalent to a 20dB improvement.

The transformative performance improvement has been achieved by advancing the state of the iDAS optoelectronics interrogator architecture, together with the introduction of new and proprietary Constellation fibre. This fibre is engineered to increase the scattered light from points along the length of the fibre and reflect more light back to the interrogator. This is achieved without introducing significant loss to the forward propagating laser pulses. With Carina Sensing System it is possible to achieve the wide coverage of distributed sensors without having to compromise on signal quality because the SNR achieved with this system is similar to traditional geophone instrumentation.

This step change in performance is most acute in applications with low acoustic signal levels such as is common with leak detection, production monitoring and borehole active seismic and microseismic applications. In these situations, the acoustic signal can be present at, or below, the inherent system noise floor of previous technology and can therefore be difficult to detect.

In addition to standard single mode and multi-mode optical fibres, a family of Constellation fibres can be incorporated into different cable types for downhole and surface deployment.

Figure 2-13 *Silixa's Carina interrogator.*

3 Installation of equipment in borehole HFM42

The main borehole for the instrument tests is HFM42, located as in Figure 1-1, at coordinates 6700137.380N, 1631076.445E in RT90 2.5 gon west (Gunnar Rauseus, email 2019-01-23). This corresponds to latitude, longitude (60.39789,18.18310) and SWEREF99 TM (6699961.956, 675363.6150). The borehole is 195.3 m long, from the head, approximately vertical at the top (89°) with an inclination of 86.5° at the bottom. The bottom of the borehole is offset by 7.5 m from the top. The technical design and data are given in Figure 3-1. The borehole is cased to a depth of 6.3 m from TOC. More information on the drilling can be found in (Nilsson, et al. 2018). In addition, a 60 cm shallow borehole, PFM007946, was drilled approximately 30 m east of the main borehole, see Figure 1-1, in order to repeat noise test conditions similar to those described in Lund et al. (2017). The closest measurement site in Lund et al. (2017) is site 2, 275 m north of HFM42.

The installation of equipment was initially scheduled for June 2018 but was postponed due to late delivery of the geophones where one of the geophones did not work. The installation took place 7 - 10 August 2018. Personnel from SKB, GNC, HydroResearch, Protek, Silixa, TSB and Uppsala University were present during the installation.

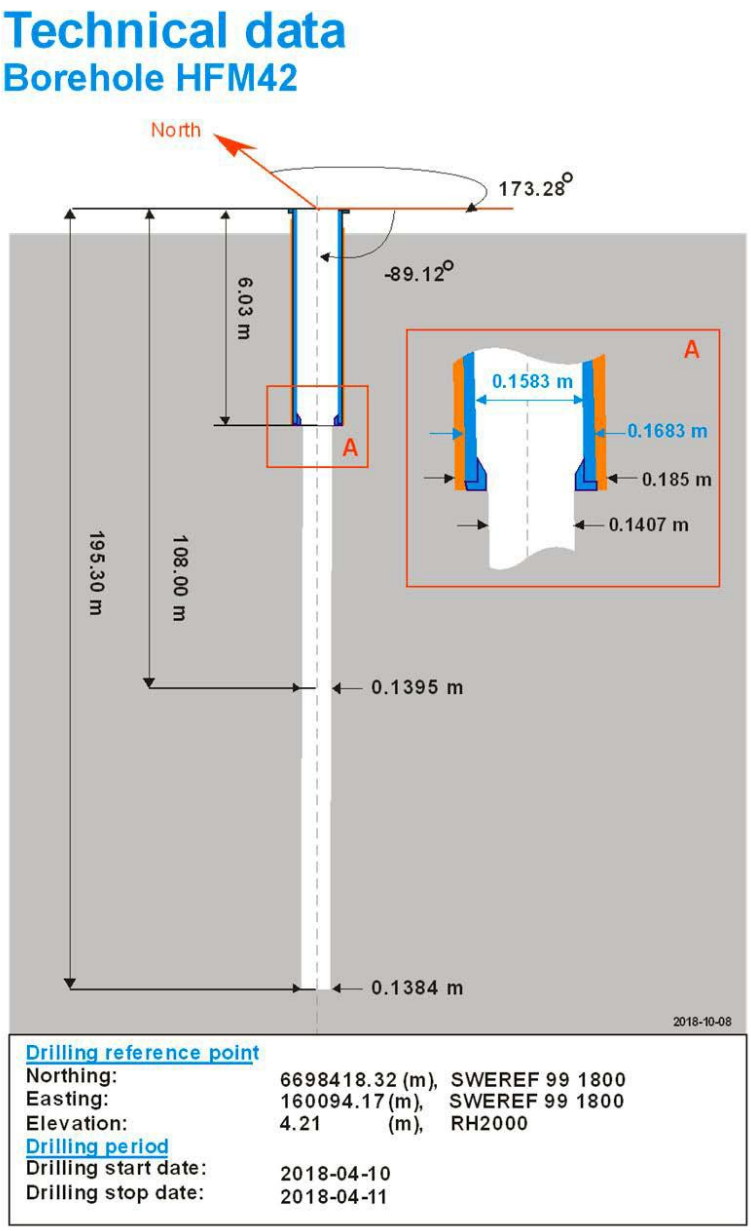

Figure 3-1 *Technical data for borehole HFM42.*

3.1 Installation procedure

A two-stage working podium was placed above the borehole. Six-meter-long grouting pipes were handled from the upper stage, and the cables and geophones were handled from the lower stage (Figure 3-2 left). Cable drums for the fibre optic cables and geophone cables were placed on cable drum jacks (Figure 3-2 right). The geophone cables and the heatable linear cable were passed through a pulley hung over the drill hole. The helical cable has a high stiffness compared to the other cables and therefore was deployed by hand.

The deployment started at 12:00 CET on 8 August 2018 (the following timestamps in this section are all CET). On the first grouting pipe, a bullnose was welded to protect the downhole terminations of the fibre optic cables during the descent (Figure 3-3). To this pipe, an 8 mm steel wire with an electric winch was also attached to control the descent.

The downhole terminations for the two fibre optic cables were placed inside the bullnose, with the downhole termination for the helical cable at the bottom (Figure 3-4 left). Geophones were attached using both heavy-duty cable ties and tape (Figure 3-4 right).

During the descent, all cables were attached to the grouting pipe using heavy-duty cable ties. At each grouting pipe two centralizers were installed to keep the pipe centred in the borehole to keep the cables and geophones off the borehole wall (Figure 3-5 left).

The deployment process was finished at 18:00 The final positions of the geophones were at 187.5 m, 74.5 m and 6.5 m from TOC (top of casing). The bottom of the grouting pipe was at 193.3 m from TOC.

Figure 3-2 *Left: Installation in HFM42 using a two-stage podium (photo: HydroResearch). Right: Drums with fibre optic cables (blue, helical and grey, linear) and cables for geophones placed on cable drum jacks (photo: Sanna Andrén, SKB).*

Figure 3-3 *Bullnose welded at the first grouting pipe for protection of the downhole terminations of the fibre optic cables. Dimensions in mm.*

***Figure 3-4** Left: Deployment of the downhole termination of the helical cable inside the bullnose (photo: HydroResearch). Right: Fastening of the lowest geophone using heavy-duty cable ties and tape (photo: Sanna Andrén, SKB).*

The borehole was grouted to improve coupling of the sensors, both geophones and fibres, and hence provide better quality data. The grouting of the borehole took place on 9 August. The cement mixture had a water cement ratio of 0.8 (40 litres water and 50 kg cement). The mixture was pumped through the grouting pipe to the bottom of the borehole meaning that the water filled borehole was filled with the mixture from the bottom to the top. Separate mixers were used to keep a constant pumping flow of the grout into the borehole.

One stop of the pumping took place at 11:50 to 12:30 while waiting for more cement. The pumping resumed at 12:30. At 12:47 the water level had raised to TOC. At that time, 2736 litres of grout had been pumped into the borehole. The cement reached TOC at 13:38 and the cement pumping ended at 13:43 (Figure 3-5 right). At that time, 3,933 litres of grout had been used. The total volume of the borehole minus the installed equipment is approximately 2,800 litres meaning that approximately 1,100 litres of grout was injected into fractures along the borehole.

An OTDR (Optical Time-Domain Reflectometer, an instrument for signal control of optical fibres) was used to check the integrity of the fibre optic cables. OTDR measurements were performed before, during (at 50 m and 120 m descent) and after the deployment and after the grouting. No signal changes could be seen. The geophones were also checked by looking at the signals coming out from the digitiser before, at 50 m and 120 m descent and after grouting. No issues were identified.

In borehole settings, DTS measurements are often made to monitor cement curing processes and warm-back phenomena. In this survey, Silixa Ultima DTS measurements were made during the grouting to follow the progress of the grouting and the curing process as both affect the temperature along the borehole. Additionally, active distributed temperature measurements are possible with the heatable linear cable deployed here but do not form part of this report.

Figure 3-5 *Left: Centralizer attached to the grouting pipe (photo: Sanna Andrén). Right: Cement mix has reached TOC, meaning that the entire borehole was filled (photo: Sanna Andrén).*

On 10 August a cabin was placed on top of the borehole. The fibre optic cables were fastened in a loop on the left wall and protected with a wooden construction (Figure 3-6 left). A cabinet with inlets in the bottom was placed on the left wall above the cable loops, and the cables were pulled inside the cabinet. All the fibres in both cables were spliced with 10 m patch cords. Single mode patch cords for the helical cable were placed to the left of the cabinet. Multi-mode patch cords for the helical cable were placed to the right of the cabinet together with both single mode and multi-mode patch cords for the linear cable (Figure 3-6 right). A schematic picture over the installed equipment is illustrated in Figure 3-7.

Figure 3-6 *Left: View of wooden cabin placed on top of the borehole for protection of the fibre optic cables entering the borehole. Right: Cabinet with fibre splices, patch cords beside the cabinet, and fibre loops below the cabinet (photo: HydroResearch).*

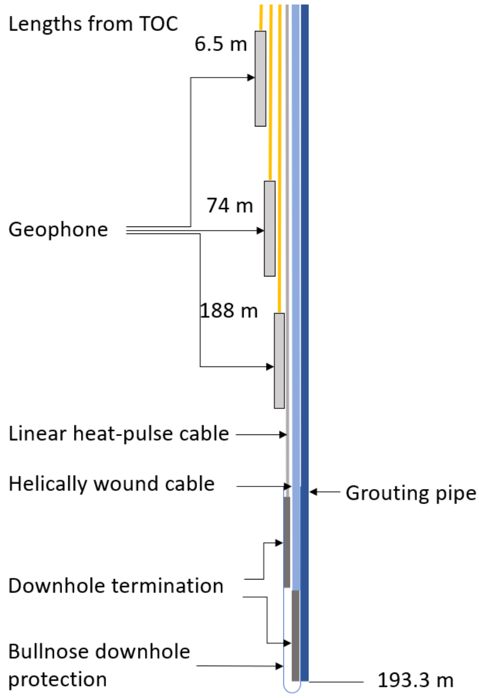

Figure 3-7 *Schematic over installed equipment in HFM42 (not to scale).*

3.2 Instrument setup in HFM42

Geophones were located in the boreholes as described in Figure 3-7 and Table 3-1, the Guralp seismometer is a 60 s to 100 Hz broadband surface instrument located on bedrock next to the PFM007946 borehole for comparison with the IMS sensor, as in Lund et al. (2017). The geophones in the deep borehole are referred to in this report by letters A (deepest sensor, at 188 m), B (middle sensor, at 74 m depth) and C (shallow sensor, at 6.5 m depth), often followed by a component indicator, such as AZ for the deepest z-component or BN, for the middle north component. The depths were measured from the top of the sensor housing at an accuracy of approximately 1 m, for more information about the sensor installation see Nilsson (2018). These sensors were tested with both the Guralp Affinity digitiser and the IMS digitiser. The instruments at PFM007946 used Guralp DM24 digitisers, with serial numbers as indicated by the labels in Table 3-1. Note that, as in Lund et al. (2017), the IMS geophone was not cemented into PFM007946 but just loaded by a lead weight.

The setup of the equipment enabled simultaneous measurements on the different systems. This is possible because the instruments do not interfere with each other, and optical fibre sensing is unaffected by electrical noise or electromagnetic signals. The interrogators for the fibre cables were placed inside a container near the borehole (Figure 3-8). They were controlled from the trailer between the container and the borehole cabin. Equipment for the geophones were placed inside the borehole cabin.

To make simultaneous measurements on the helical and linear cables, they were connected in series at the surface in the cabin. Since the linear cable did not contain Constellation fibres, this was done only for iDAS measurements with single mode fibre. The optical fibre loops are illustrated in Figure 3-9 and the cable mapping determined using tap tests to obtain receiver channel locations is given in Table 3-2.

The acquisition parameters are provided in Table 3-3 for both DAS systems. Data were recorded continuously using a GPS timing reference and extracted in SGY file format.

Table 3-1. Instrumentation in the test boreholes. Depth is measured from the top of the borehole casing. Orientation is the direction of the instrument's north component with respect to geographical North. Instrument north thus has to be rotated westward (counter clock-wise) the number of degrees in the last column to get to correct geographical North.

Borehole	Label	Type	S/N	Measured depth [m]	Orientation [deg]
HFM42	**A**	3-component IMS geophone	180002.208	188	302
HFM42	**B**	3-component IMS geophone	180003.208	74	332
HFM42	**C**	vertical-component IMS geophone	130002.184	6.5	N/A
PFM007946	2598	vertical-component IMS geophone	130003.184	0.6	N/A
PFM007946	2599	3-component Guralp ESPC 60 second seismometer	T36021	0	0

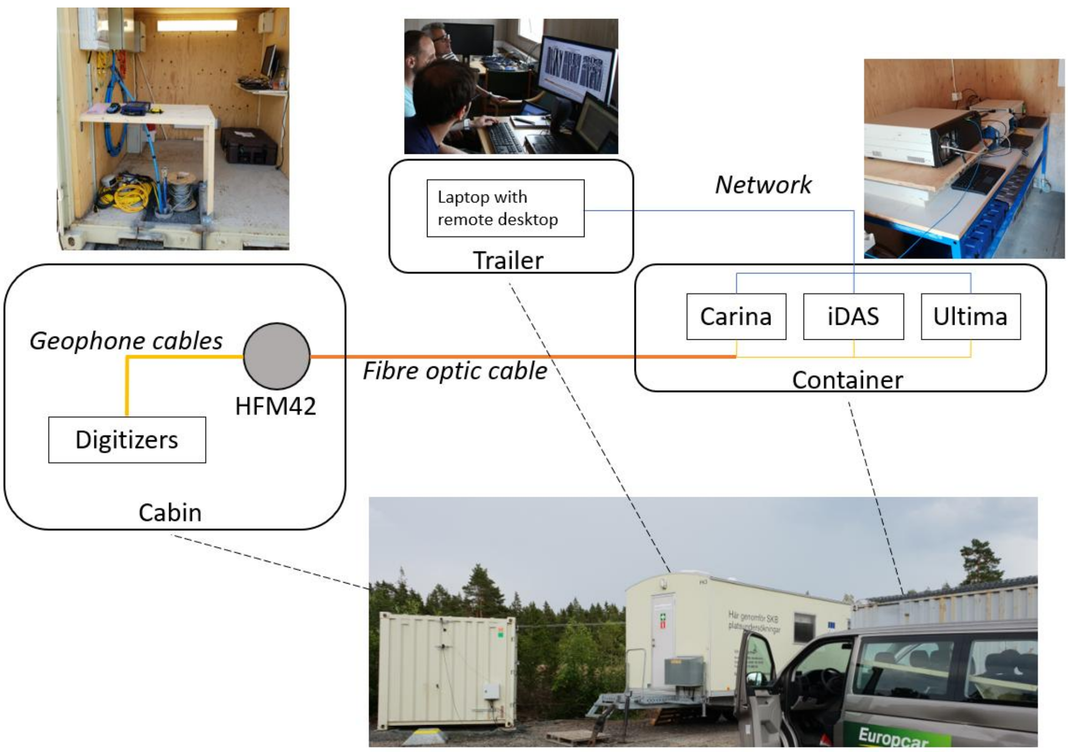

Figure 3-8 *Equipment setup during the measurements.*

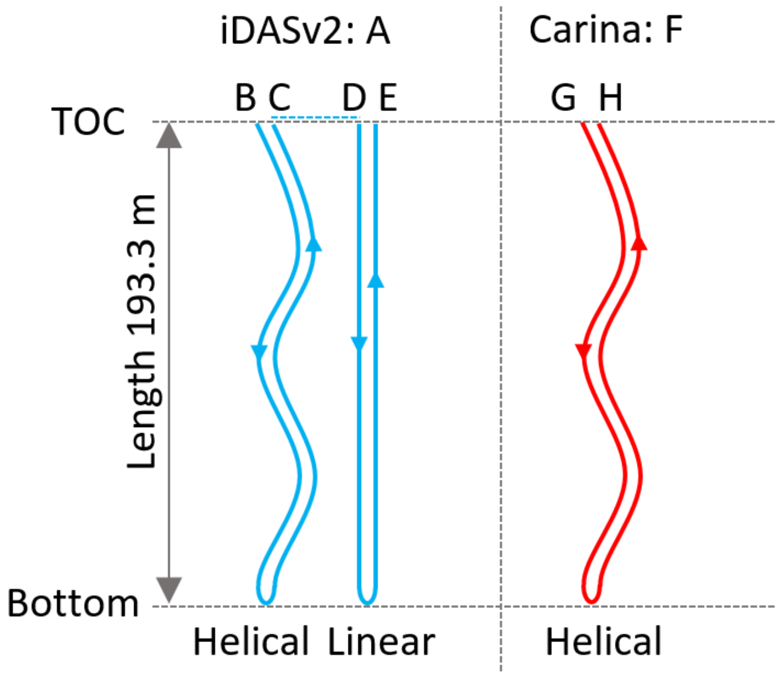

***Figure 3-9** Fibre connectivity diagram.*

Table 3-2 Fibre distance mapping. The fibres are standard (STD) or constellation (CONST10). The labels refer to the letters in Figure 3-9.

Label	Position	Cable	Instrument	Fibre	Fibre Distance (m)	Trace Number
A	Instrument OUT	Surface Cable	iDASv2	STD	0	123
B	TOC IN	Helical	iDASv2	STD	80	202
C	TOC OUT	Helical	iDASv2	STD	521	631
D	TOC IN	Linear	iDASv2	STD	565.1	677
E	TOC OUT	Linear	iDASv2	STD	957.2	1061
F	Instrument OUT	Surface Cable	CARINA	STD	0	200
G	TOC IN	Helical	CARINA	CONST10	50	249
H	TOC OUT	Helical	CARINA	CONST10	490	680

Table 3-3 Data acquisition parameters.

	iDAS	Carina
Serial Number	iDAS16042	Carina-P3
Sample Rate	1kHz	1kHz
Spatial Sampling Resolution	1m	1m
Time Decimation	20	20
Measure Length	1175m	778m
Recording Mode	Continuous	Continuous
File Duration	30s	30s
Timing Source	GPS	GPS

4 Field measurements

4.1 Active source data acquisition

Active source seismic data were generated using a weight drop source mounted on a small excavator (Figure 4-2). The source was activated at a nominal spacing of 10 m along an approximately 1.35 km long stretch of gravel road extending to the south-southeast from the borehole (Figure 4-1). Geophones planted very close to the source and connected to a GPS-synchronized digitiser were used for source timing. Due to infrastructure near the borehole the source could only be activated at a few source points (SP) in this area, i.e., only SPs 1, 2, 9, 10, 11, 15, 16, 17 and 23 were activated, beyond these the source was activated nearly every 10 m. Geophones (10 Hz) were planted every 10 m along the source line. The southern part of the source/receiver profile is coincident with previous profile 4 (Juhlin et al., 2002), but the northern part deviates to the west by 100-150 m from it.

All source points were recorded by the surface receiver line, the borehole geophones, the iDASv2 with both the linear and the helical cable, and Carina with the helical cable. At each source point the weight was dropped at least 10 times to allow stacking of the signals to increase the signal-to-noise ratios.

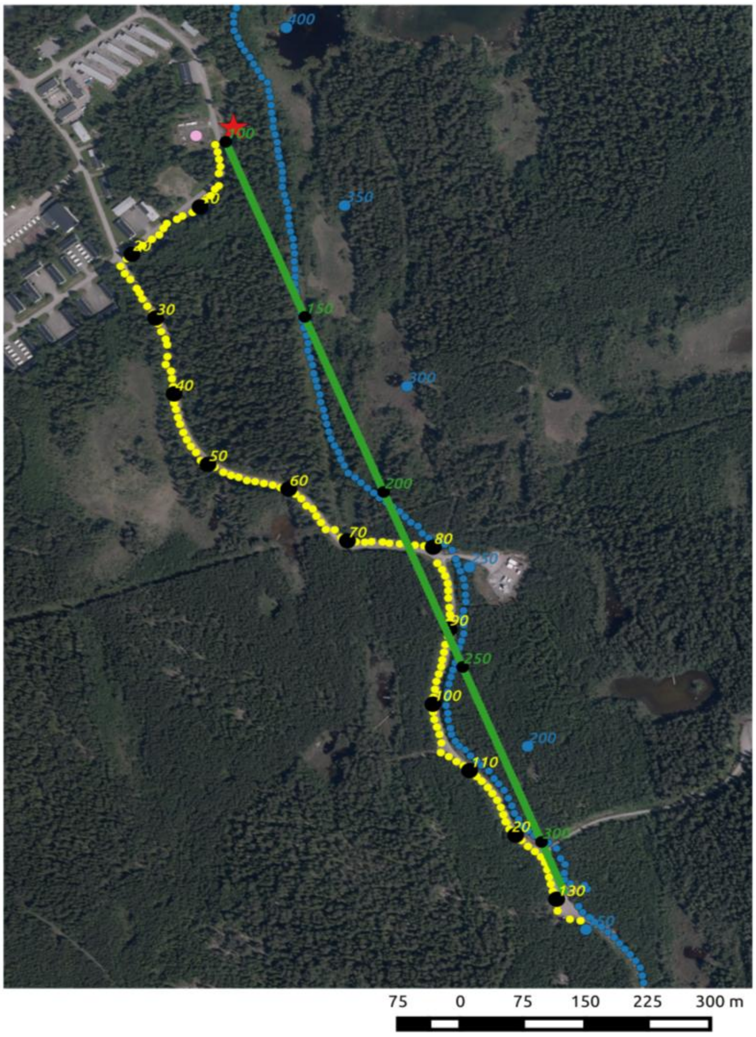

Figure 4-1. *Acquisition geometry. Yellow: surface source/receiver points, green: CDP line that the surface seismic data were stacked along, blue dots: receiver locations for previously acquired profile 4 (Juhlin et al., 2002), blue dots with numbers: CDP point locations for profile 4 for reference, and red star: location of borehole that geophones and fibre-optic cable were installed in.*

Figure 4-2. *Seismic source used for the data acquisition.*

4.2 Fibre length calibration and data quality control

DAS receiver channels, equivalent to a single sensing point on the fibre, are equally spaced in linear distance along the fibre. The position of these channels is very accurately known in the in-line fibre coordinate system by measuring the time of flight of the laser light with a high accuracy, high speed clock. The location of a single channel in physical space is unknown however, until its position is calibrated. To do this calibration an acoustic or optical signature that has a known location in both distance along the fibre and physical space (i.e., measured length in the well) is required, these points are known as length calibration reference points.

A common way to create a length calibration reference point is to tap on the fibre optic cable at the wellhead. The location of the tap is known to have a certain length relative to the well depth reference, in this case the top of the casing. The acoustic tapping signal can also be seen and accurately located along the fibre path. This position can normally be found to an accuracy of approximately +/- 0.25 x gauge length (the spatial resolution of the system). Turnaround points, i.e., the receiver channel at the bottom of a well, can also be used as calibration reference points because the apparent velocity of a signal changes sign at this point. Receiver channel positions are attributed based on a linear interpolation between calibration points. There is no information between these points and therefore any non-linear effects cannot be taken into account but with short distances, as is the case here, this linear assumption is usually accurate.

Example tap test data and turnaround point determination are given in Figure 4-3 and Figure 4-4 respectively. Figure 4-3 shows a tap test signal at Point B (see Figure 3-9) on the helical cable recorded with iDAS16042. The figure shows the tap signal in the centre of the image where the x-axis is distance along the fibre from the front of the interrogator unit and the y-axis is time. The tap signature (the highest amplitude data) is spread over the gauge length of 10 m due to the averaging effect of the gauge length (approx. 75 m – 85 m). However, since multiple measurements are made within a gauge length (the spatial sampling is 1 m) and, for each channel, the measurement is a moving average over a gauge length along the fibre, the true location can be found to a higher precision. In this case, the error in the measured tap location of 80 m is approx. +/- 2 m. As the fibres are looped at the bottom of the well, the tap test can be repeated at Points C, D and E on this cable and for other fibres in the cable.

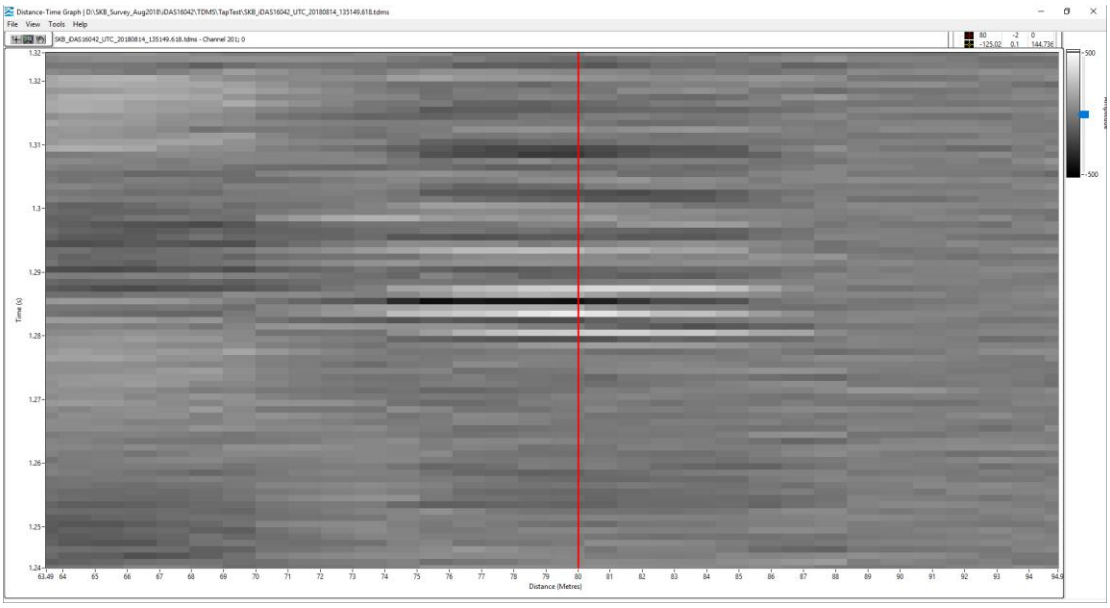

Figure 4-3 *Tap test signal on the helical cable at Point B recorded with iDAS16042. Distance is shown on the x-axis and time on the y-axis. The tapped point on the fibre (the point where the signal has the maximum amplitude) is shown by the red line (at 80m).*

It is not possible to access the fibre at the bottom of the well. Best practice is to locate the turnaround point using a seismic signal and Figure 4-4 shows the turnaround point in two of the fibres in the helical cable on iDAS16042 at 300.5 m. An alternative, but less accurate method, is to use the midway distance between tap tests at the looped fibres as an approximation of the bottom of the well, although this assumes that the two looped fibres are identical in length. The mid-point between the two tap-tests Points B and C was found to be (80 + 521)/2 = 300.5 m, in agreement with the value found from a seismic signal.

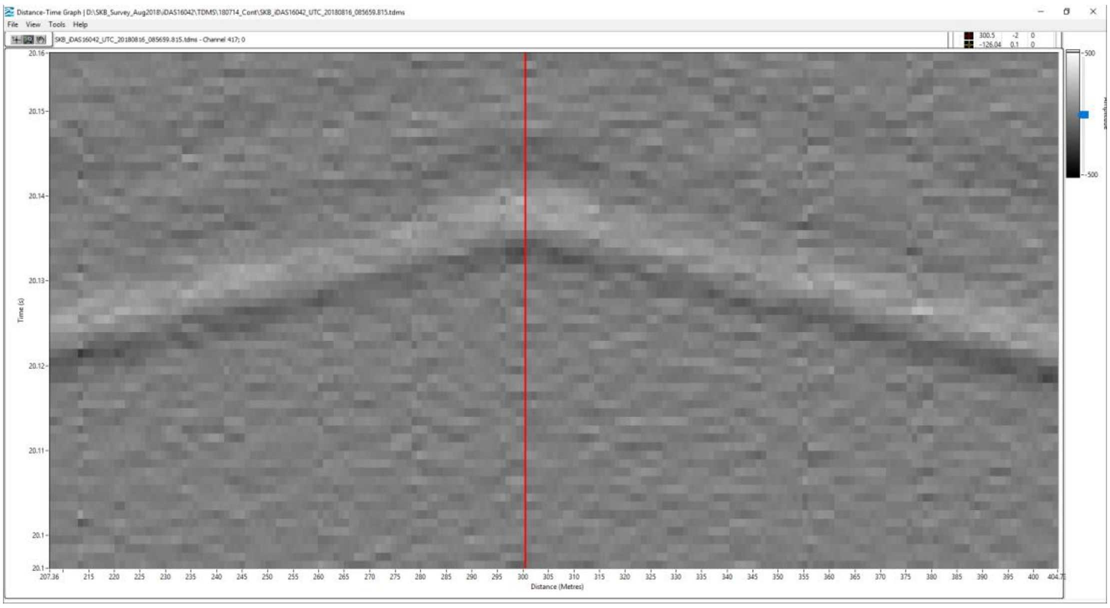

Figure 4-4 *Acoustic signal from an active source recorded with iDAS16042. The apex of the signal (red line) indicates the turnaround point in the helically wounded cable (300.5m)*

After finding the locations of these features in distance along the fibre, they must then be given a location in measured length within the well relative to the TOC. The tap test was performed on the TOC, so each tapping point seen in the fibre is assigned a length of 0m. The turnaround point of the fibres is taken from the completion information. During installation of the fibre, the length from TOC to the bottom of the cable inside the borehole was measured to be 193.3 m. Each turnaround point is therefore given the length of 193.3 m. Receiver channels between these points are assigned a length by linear interpolation.

Table 4-1 and Table 4-2 give the full results of the length calibration for the DAS units.

Table 4-1 iDAS16042: Helical SM1 (single mode fibre 1) – Helical SM2 – Linear SM1 – Linear SM2

Fibre Location	Closest SEGY Trace Number	Fibre Distance (m)	Length from TOC (m)
Top of Helical SM1	202	80	0
Turnaround Helical SM1 – Helical SM2	418	300.5	193.3
Top of Helical SM2	634	521	0
Top of Linear SM1	677	565.1	0
Turnaround Linear SM1 – Linear SM2	869	761.5	193.3
Top of Linear SM2	1061	957.2	0

Table 4-2 Carina-P3: Helical CF1 (Constellation fibre 1) – Helical CF2

Fibre Location	Closest SEGY Trace Number	Fibre Distance (m)	Length from TOC (m)
Top of Helical CF1	249	50	0
Turnaround Helical CF1 – Helical CF2	464	270	193.3
Top of Helical CF2	680	490	0

Quality control of data was done in the field in various ways. During set up the optical signal levels were optimised and then operation tests were carried out to ensure data was being saved correctly. This involved checking that the GPS synchronisation was working and that data saving to disk was stable. The units were found to be operating well after these initial checks were completed.

Seismic quality control was also carried out in the field where possible. Data were acquired in continuous mode, i.e., DAS data were recorded throughout the experiment, which meant individual weight drop recordings could not easily be viewed and quality controlled in real-time. However, data were qualitatively checked with frequent visualisation of the data to ensure data collection proceeded as expected. Once DAS measurements commence the only potential issues are timing and data saving which can be easily checked. There is no need to change acquisition settings during a survey unless new information becomes available or survey parameters change.

Accurate source timestamps were acquired using a trigger geophone located at the source position. Any timing issues would affect the DAS and the geophone data in the same manner, however no problems with timing were reported. Locations and timestamps for weight drops were provided to Silixa and data records were extracted and saved. These records were then plotted and stacked for further quality control, checking both repeatability and signal quality. At near offsets the signal levels were strong enough to be able to see good seismic arrivals but as the offset increased the low SNR meant that it was difficult to see arrivals. However, since the interrogators were still operating well and there was a gradual decrease in SNR, there was a high level of confidence that the data being acquired was of optimum quality. This was found to be true after the job when all active source records were extracted.

Unfortunately, the Constellation fibre installed in the well had a manufacturing defect between 40 m and 60 m measured length from TOC. This means that data in this region was not usable. The cause of this defect has been resolved for future fibre manufacturing.

4.3 Geophone field tests

A number of tests were carried out in the field to establish the correct polarity and orientation of the geophones.

4.3.1 Functionality testing by hammer blows

As a first functionality test of the deep borehole instruments we used a number of sledgehammer blows at distances of 10 m, 30 m and 300 m. The 30 m blows were located close to the shallow borehole PFM007946 (Figure 1-1) and the 300 m distance blows were located at point 2002 (Figure 4-8). The geophones were connected to the Affinity digitiser sampling with 4,000 samples per second during the measurements and we tested both x8 gain and x64 gain.

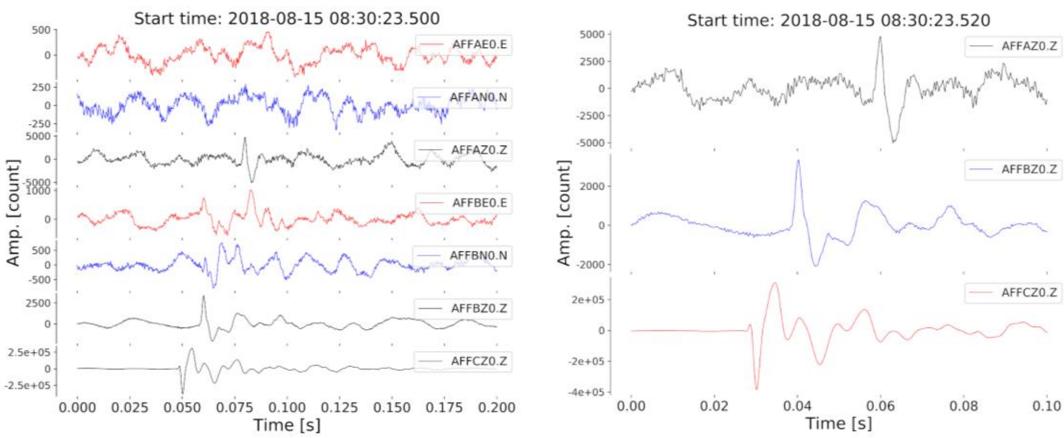

Figure 4-5. *Sledgehammer blow 10 m from the top of the borehole at 2018-08-15 08:30:23. Affinity digitiser and deep borehole geophones. Gain x64 on Affinity channels AZ and CZ, all other channels have gain x8. Left) All channels. Right) Only vertical channels.*

Figure 4-5 shows a hammer blow from 10 m horizontal distance and the signal is nicely visible on all vertical components and on the horizontal components at 75 m depth. At 188 m depth the signal comes in almost vertically and is very difficult to identify on the horizontal components. On the shallow 6.5 m geophone the signal comes in at approximately 57 degrees from vertical (geometrical estimate) and the vertical component first motion is therefore relatively smaller. The two deeper vertical components show clear positive first motions, which is opposite to the usual behaviour where upward travelling signals are considered positive. This is due to the erroneous wiring discussed above, a wiring problem that persisted until 2018-10-18. The uppermost geophone, C, is correctly wired at this time but still show a small positive first motion. It is unclear what the origin of that is. There is however a much larger negative phase corresponding to a downward propagating P-wave.

Moving the sledgehammer to 30 m from the top of the borehole, Figure 4-6 shows that the signal is still well recorded at all three levels. Maximum amplitudes are similar to those at 10 m distance for the two lower geophones, which is expected as the distance from source to receiver is very similar (7% increase for sensor B, 1% increase for A). The increased incidence angles allow for more S-wave energy on the vertical component, which is clearly visible comparing Figures 4-5 and 4-6. At the shallow geophone, C, the signal amplitude is decreased by a factor 3 and the signal waveform extended, due both to the significant increase in distance and the more horizontal incidence of the signal. Reducing the gain from x64 to x8 on channels A and C, Figure 4-6, the recorded amplitude decrease by a similar factor but as the signals are very strong the reduced gain does not affect the signal to noise ratio, as both signal and the natural background noise is significantly above the digitiser noise levels at the frequencies of interest.

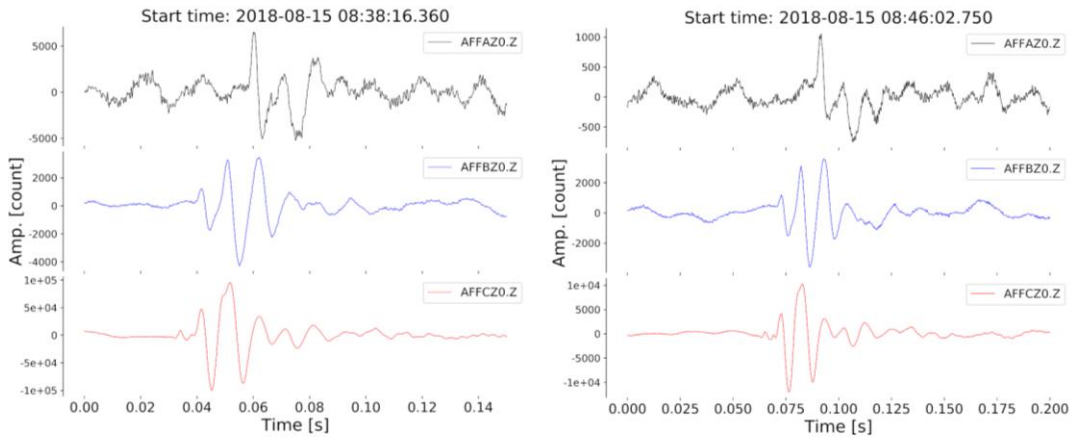

Figure 4-6. Sledgehammer blows 30 m from the top of the borehole on 2018-08-15. Affinity digitiser and deep borehole geophones. Left) 08:38:16, gain x64 on channels AZ and CZ, gain x8 on channel BZ. Right) 08:46:02, gain x8 on all channels.

Hammer blows 300 m from the borehole were not visible in the data, neither at gain x8 nor x64. The sledgehammer tests showed that the polarity of the vertical component of the three-component geophones needed to be reversed, and that a gain of x8 is sufficient in the Forsmark area using this instrument setup. The test also confirmed that all channels were live after installation.

The geophones were connected to the IMS digitiser and the sledgehammer blows repeated. Unfortunately, it was not possible to retrieve the data from the digitiser as the recording spanned less than 10 minutes and the IMS Trace software required full 10-minute blocks for data retrieval. A fact which we had not observed prior to the test.

Sledgehammer blows were also recorded on the two instruments in the shallow borehole PFM007946, see Figure 4-7. We clearly see the long period background signals recorded on the Guralp seismometer (2599) and the offset from zero due to the DM24 digitiser. Zooming in on one of the hammer blows, and using a high-pass filter, to the right in Figure 4-7, it is clear from the ringing signal of 2598 that the IMS geophone is not properly seated in the shallow borehole. The ringing is triggered by the high amplitude impulsive signal and is difficult to discern in the noise data in Section 6.1.1. Both instruments show clear signals and are operational.

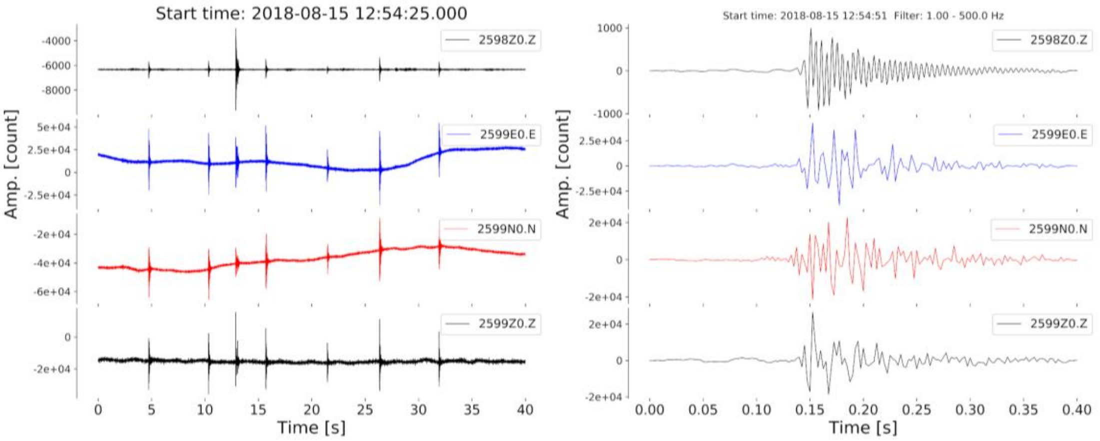

Figure 4-7. Sledgehammer blows near the shallow borehole PFM007946 at 2018-08-15 12:54. Guralp DM24 digitisers, IMS vertical geophone (2598) and Guralp Compact seismometer (2599). Left) All sledgehammer blows, unfiltered. Right) Sledgehammer blow at 2018-08-15 12:54:51, signals high-pass filtered at 1 Hz.

4.3.2 Orientation of the borehole three-component geophones

The initial orientation of the horizontal components of the borehole geophones is arbitrary and needs to be determined after installation. One method is to place an oriented instrument in the immediate vicinity of the borehole and perform a relative orientation of the borehole sensors. This is a very simple and elegant method, but it is based on the analysis of coherent ambient noise recorded simultaneously with the surface sensor and the borehole sensors. Unfortunately, the procedure cannot be applied here, because of the high corner frequency of the sensors (14 Hz) and the relatively large distance between them. The second method, applied for this installation, is to generate seismic signals at well-defined positions at the surface and to perform a polarization analysis of the P-wave signal. The P-wave signal is linearly polarized and the first motion points into the opposite direction of the source (for explosive or single-force impact sources).

Figure 4-8: *Location of the borehole and the 3 source sites (2001, 2002, 2003) where weight drops were performed in order to determine the orientation of the borehole geophones.*

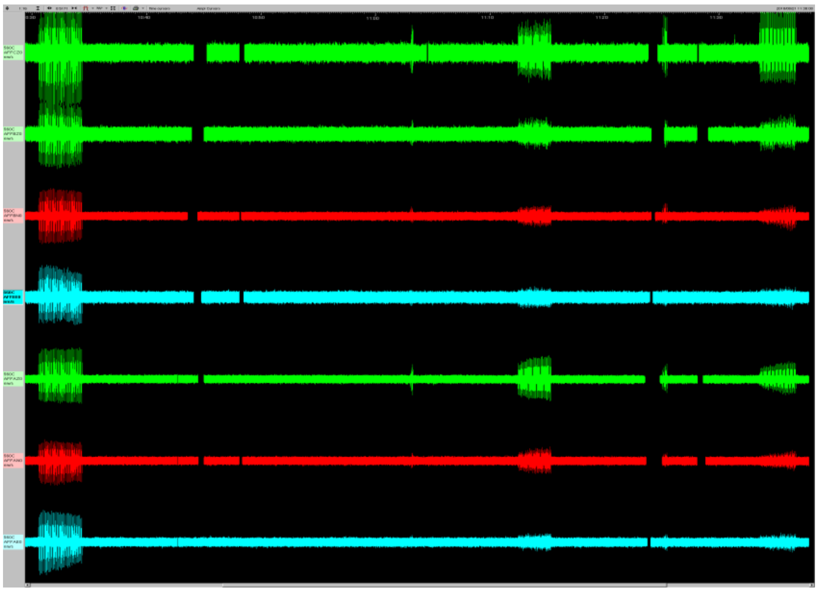

Figure 4-9: *Raw data of the weight drop signals recorded with the borehole geophone C, at the surface (top trace), the borehole geophone B (trace 2-4) and the borehole geophone A (trace 5-7). Weight drops at approximately 10:30 (ID 2001), 11:12 (ID 2002) and 11:33 (ID 2003).*

Table 4-3. Locations of the weight drops relative to the borehole, with geometrical back azimuth (gbaz) and distance.

Source	Rel E [m]	Rel N [m]	gbaz [deg]	Distance [m]
2001	-165	134	309.1	212
2002	-24	263	354.8	264
2003	199	216	42.7	293

We used weight-drops at three different positions north of the borehole, see Figure 4-8 and Table 4-3, where the weight was dropped about 40 times at each site (Figure 4-9).

The following plots show close-ups of the three-components for a signal with good signal/noise ratio, Figure 4-10 upper, and for a signal with typical signal quality, Figure 4-10 lower. Since the source signals are highly similar, it is possible to stack the signals in order to improve the signal to noise ratio. We selected a signal template for each channel and drop sequence and cross-correlated the records in order to obtain accurate repetition times which in turn were used to stack the signals properly. The steps in the polarization analysis are shown in Figure 4-11 to Figure 4-13.

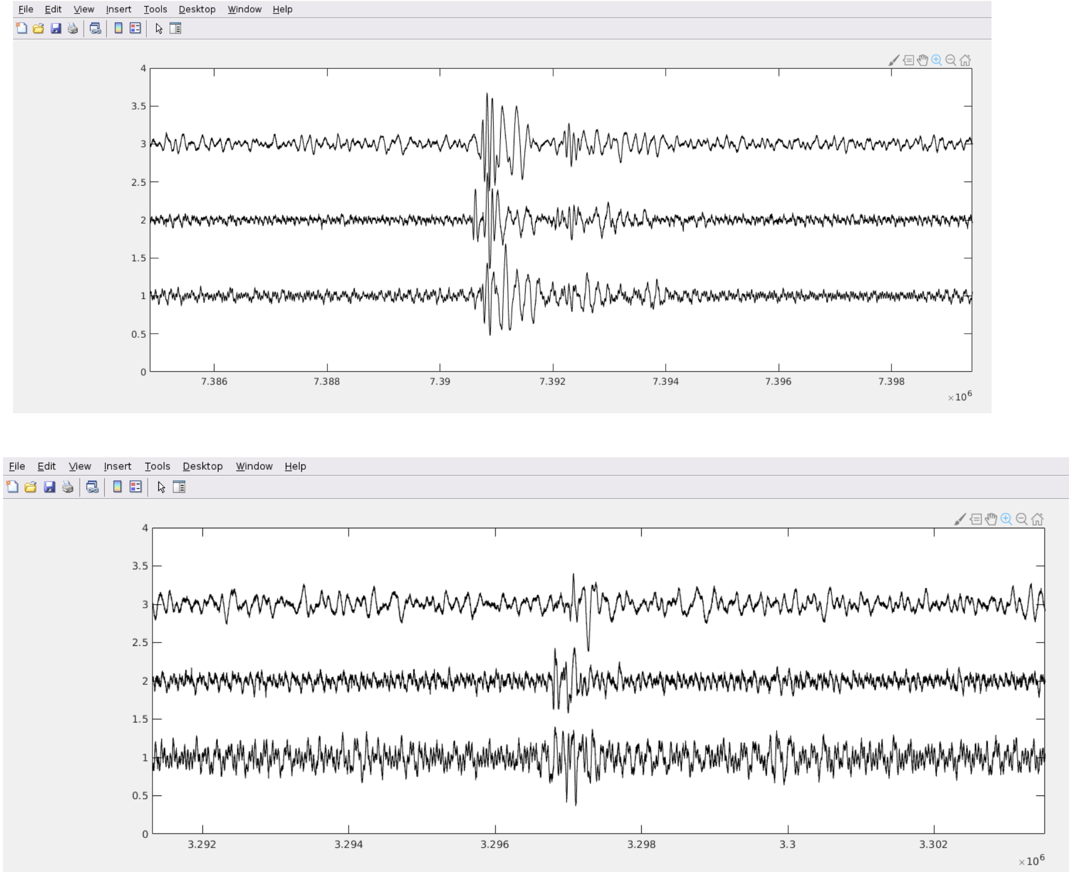

Figure 4-10. *Upper) Drop signal generated at site 2001 and recorded with geophone A. The seismograms are trace-normalized. The channels from top to bottom are the Z and the horizontal components N and E, which are not yet oriented. Lower) Drop signal generated at site 2003 and recorded with geophone B. The seismograms are trace-normalized. The channels from top to bottom are the Z and the horizontal components N and E, which are not yet oriented.*

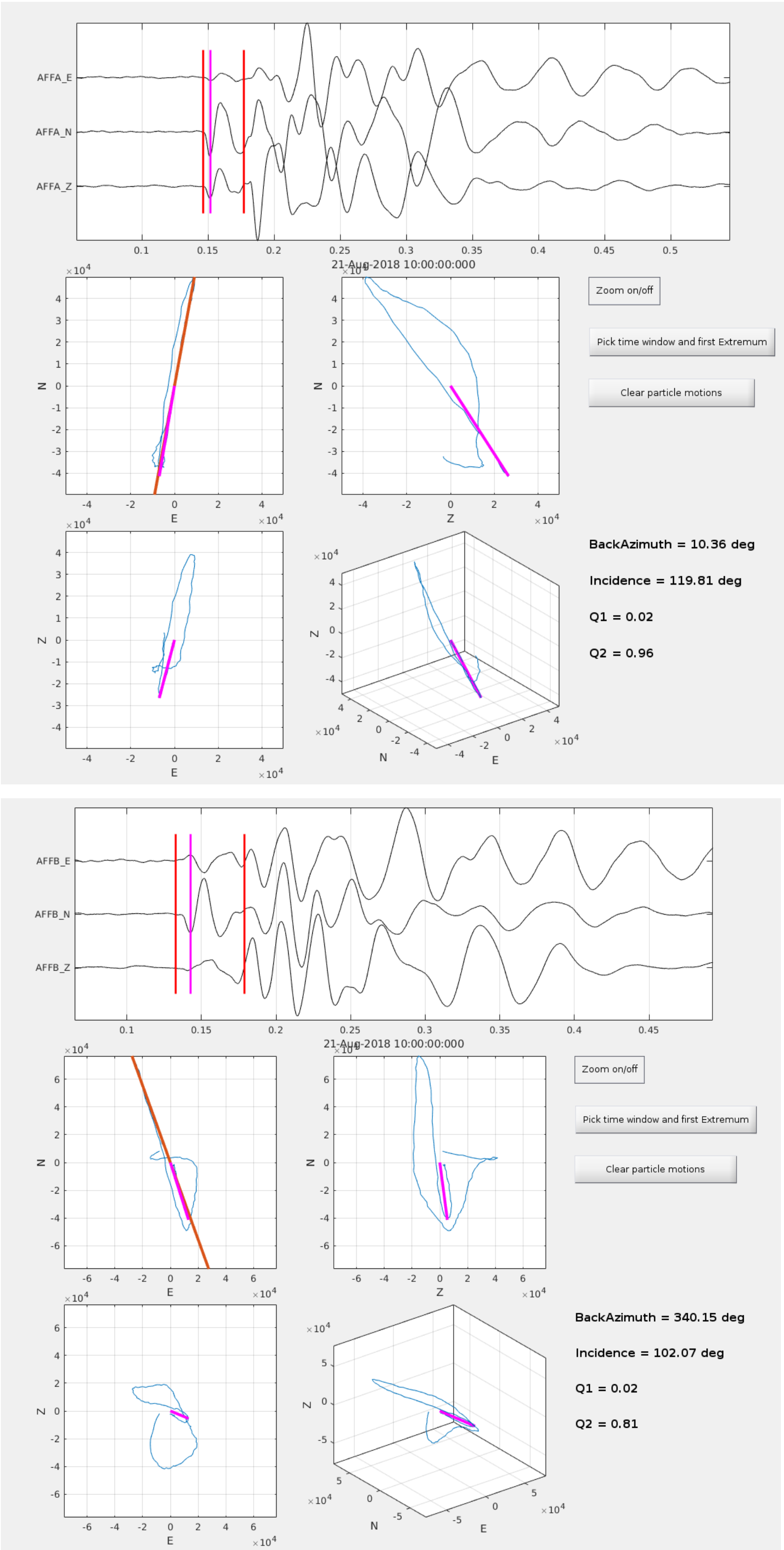

Figure 4-11. *Polarization analyses for drop site 2001 and geophones A (upper panel) and B (lower panel). Each plot shows the stacked traces of the 3C geophones, the selected time window for the P-wave polarization analysis and the particle motion in map view, E and N-cross sections and 3D view.*

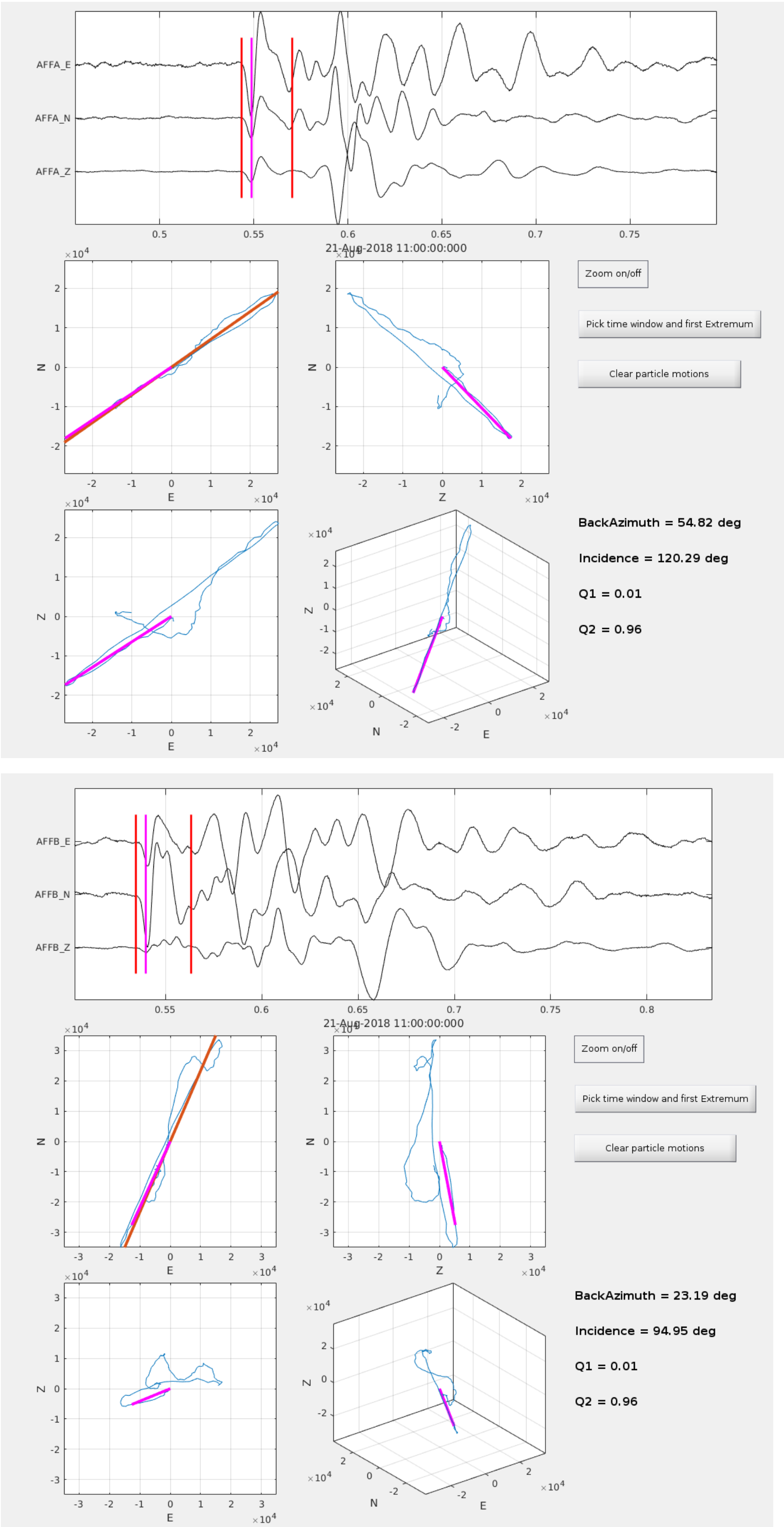

Figure 4-12. *Polarization analyses for drop site 2002 and geophones A (upper panel) and B (lower panel). Each plot shows the stacked traces of the 3C geophones, the selected time window for the P-wave polarization analysis and the particle motion in map view, E and N-cross sections and 3D view.*

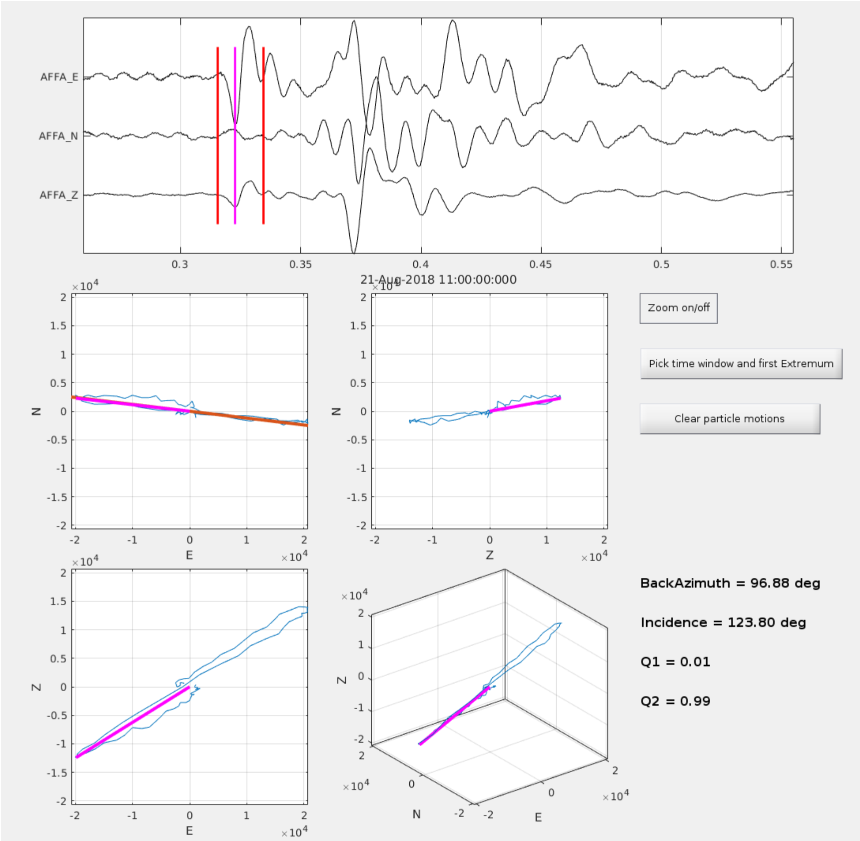

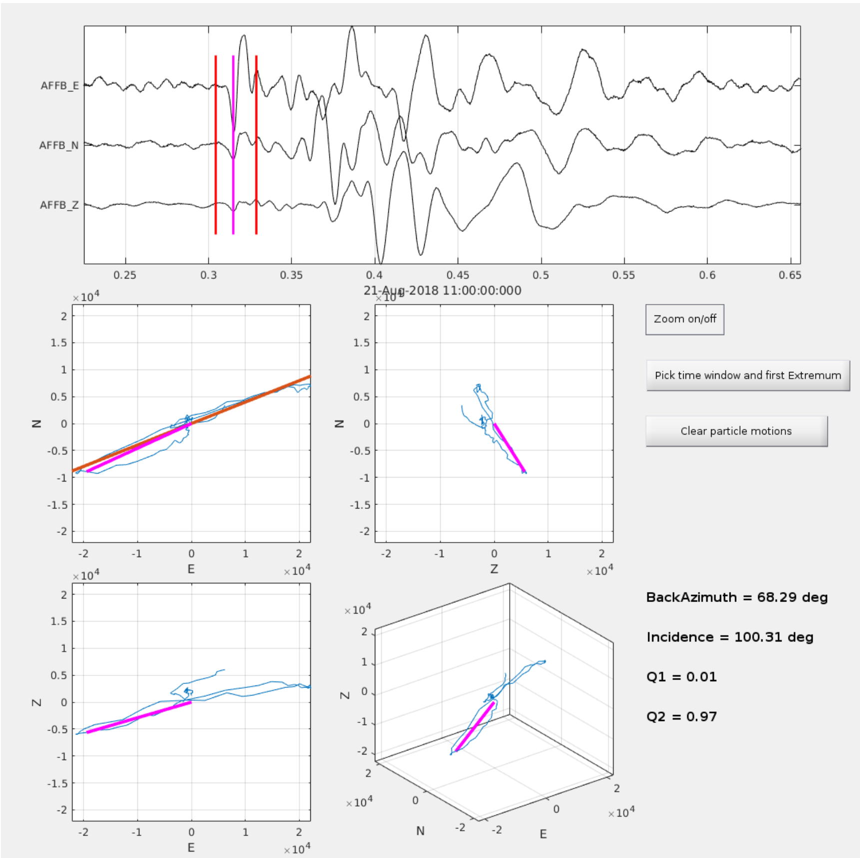

Figure 4-13. *Polarization analyses for drop site 2003 and geophones A (upper panel) and B (lower panel). Each plot shows the stacked traces of the 3C geophones, the selected time window for the P-wave polarization analysis and the particle motion in map view, E and N-cross sections and 3D view.*

Table 4-4. baz_A, baz_B: Back-azimuths for geophone A and B, respectively determined by polarization analysis. gbaz: Geometrical back-azimuth, baz_A-gbaz, baz_B-gbaz: misorientation.

Source	baz_A [deg]	baz_B [deg]	gbaz [deg]	Difference baz_A – gbaz [deg]	Difference baz_B – gbaz [deg]
2001	10.4	340.2	309.1	61.3	31.1
2002	54.8	23.2	354.8	60	28.4
2003	96.9	68.3	42.7	54.2	25.6

Averaging the azimuth differences for the 3 source locations, Table 4-4, results in orientation correction angles of about 58 and 28 degrees for geophone A and B, respectively. Positive correction angles mean the sensor data needs to be rotated counter-clockwise.

4.3.3 Active sources to confirm geophone polarity and orientation

We use recordings from two of the weight drops in the active source profile to confirm that we have the polarity and orientation of the sensors set up correctly. As noted in Section 2.1.1 above, the vertical components of the three-component geophones in the borehole are misconfigured and need to be polarity swapped. This is clearly seen in Figure 4-14 where the Z-components of the recording from source point 1 (SP1), at 14 m distance from the borehole, should be negative due to the down going P-wave, but shows up as positive. To the right in Figure 4-14 are the polarity corrected traces with the horizontals rotated to a radial component (R) and a tangential component (T) using the angles in Table 4-4. We see that this removes most of the P-wave energy on the T-component, which it should. We also see that the radial component has positive first motion, indicating motion away from the source. This is consistent with the North components showing positive motion, as they should since the source point is located south of the borehole.

As SP1 is only 14 m from the borehole, the down going ray comes in almost vertically on the lowermost geophone, at 188 m depth. This is confirmed by the data, with the vertical component amplitude being much larger than the horizontal component amplitudes. It is also seen as a lack of S-wave energy on the vertical component. The effect is smaller at 75 m depth, where the ray comes in with more of a horizontal component. At 6 m depth there is a gain a small positive first motion followed by a later negative P-phase.

In Figure 4-15 we show data from SP61, 483 m approximately to the south of the borehole. Here the ray comes in more horizontally to the borehole, a purely geometrical angle would be 68 degrees from vertical for the lowermost sensor A, and 81 degrees from vertical for the middle sensor B. This is clearly seen on the left in Figure 4-15, where the first motion (the P-wave) is hardly seen on the vertical component but clearly on the radial components of sensors A and B. On the vertical component sensor C, where the ray comes in horizontally, the P-wave cannot be seen. To the right in Figure 4-15, the data has been rotated into the LQT coordinate system of the ray, where the L-component shows motion along the direction of the ray, away from the source (pure longitudinal motion), the Q-component is perpendicular to the ray in the SV-wave plane (vertical and radial plane) and the T-component is the transverse component out of the SV plane. Figure 4-15 shows how there is a large positive L-component, indicating the P-wave away from the source, and a lack of P-energy on the Q and, especially, T-components. These instead clearly show the S-wave.

Taken together the data, and the rotations performed on the data, indicate that we have correctly identified the orientation and polarity of the geophones.

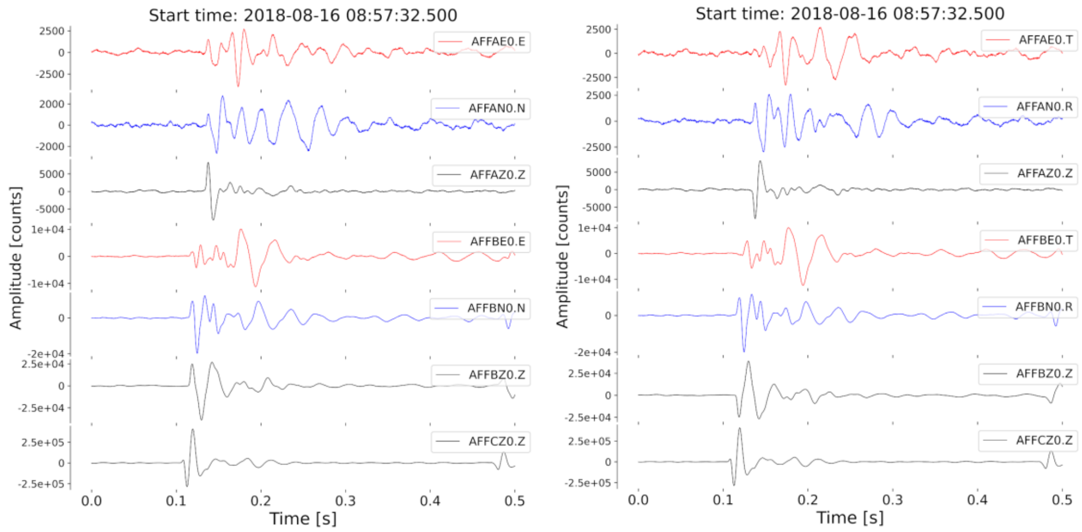

Figure 4-14. *Data from a single weight drop at source point 1 of the active source profile, recorded on the borehole geophones. Left) Original data, recorded on the non-oriented components and with the wrong z-component polarity. Right) Data oriented and rotated horizontally to radial (R) and tangential(T) horizontal components. Vertical components polarity swapped.*

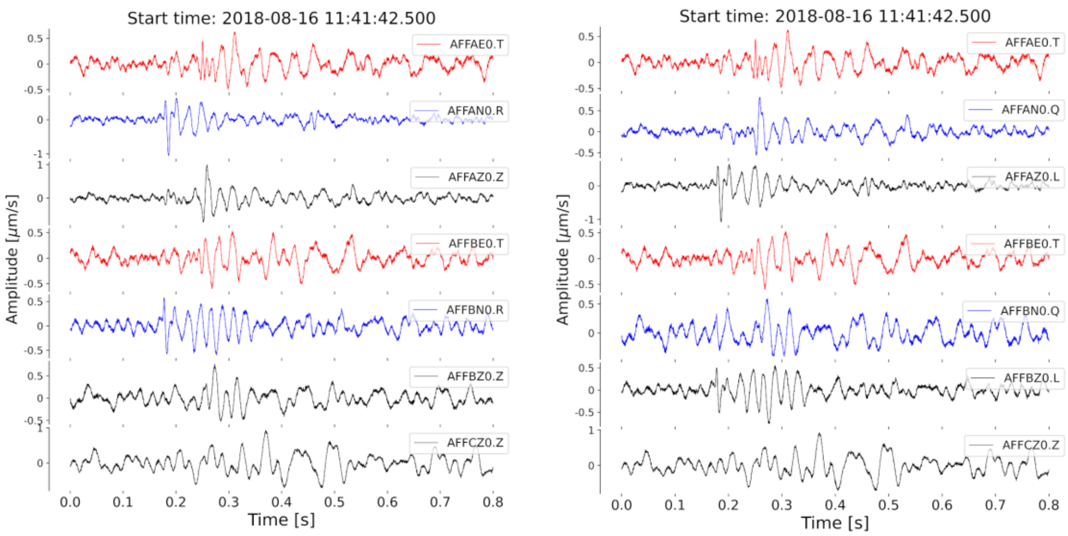

Figure 4-15. *Borehole geophone data from SP61 of the active source profile, 483 m to the south of the borehole. The instrument response has been removed. Left) The horizontal components have been rotated to radial (R) and tangential (T) directions. Right) The lower two geophones (A and B) have been rotated into the ray coordinate system LQT.*

4.3.4 Noise data for amplitude and polarity consistency

Ambient noise data is increasingly used for quality control of seismic sensors, for both amplitude and phase data. Here we use data from recordings on 2019-04-03 17:04, with the Affinity digitiser set to 1,000 samples per second and gain x8 and all three borehole geophones. We also have data from a Guralp Compact seismometer recording on an outcrop by the shallow borehole PFM007946 approximately 30 m to the east of HFM42. As the bottom borehole geophone, A, is 182 m below geophone C, and approximately 190 m from the Guralp, we need to use seismic waves with long enough wavelength to be similar over those distances. Assuming that much of the noise consists of surface waves, with velocities around 3 km/s, we need to look at frequencies below approximately 15 Hz. We chose the 5 – 10 Hz band, even though the geophones have a natural frequency of 14 Hz the noise signal is strong there.

Figure 4-16 upper shows the raw signal in counts, and the instrument deconvolved signal in ground velocity. In the raw data we see that the amplitude of the Guralp is much larger than that of the geophone data, due to different sensor sensitivities and digitizer gain, but also that there is a phase shift between the Guralp and the geophones. Deconvolving the instrument response we find that the signals agree very well. They are all in phase, so both phase and polarity agree, and the amplitudes show the expected behaviour, with the Guralp and the upper C geophone having similar amplitudes, the middle borehole geophone B has slightly lower amplitudes while the bottom geophone A have significantly lower amplitude.

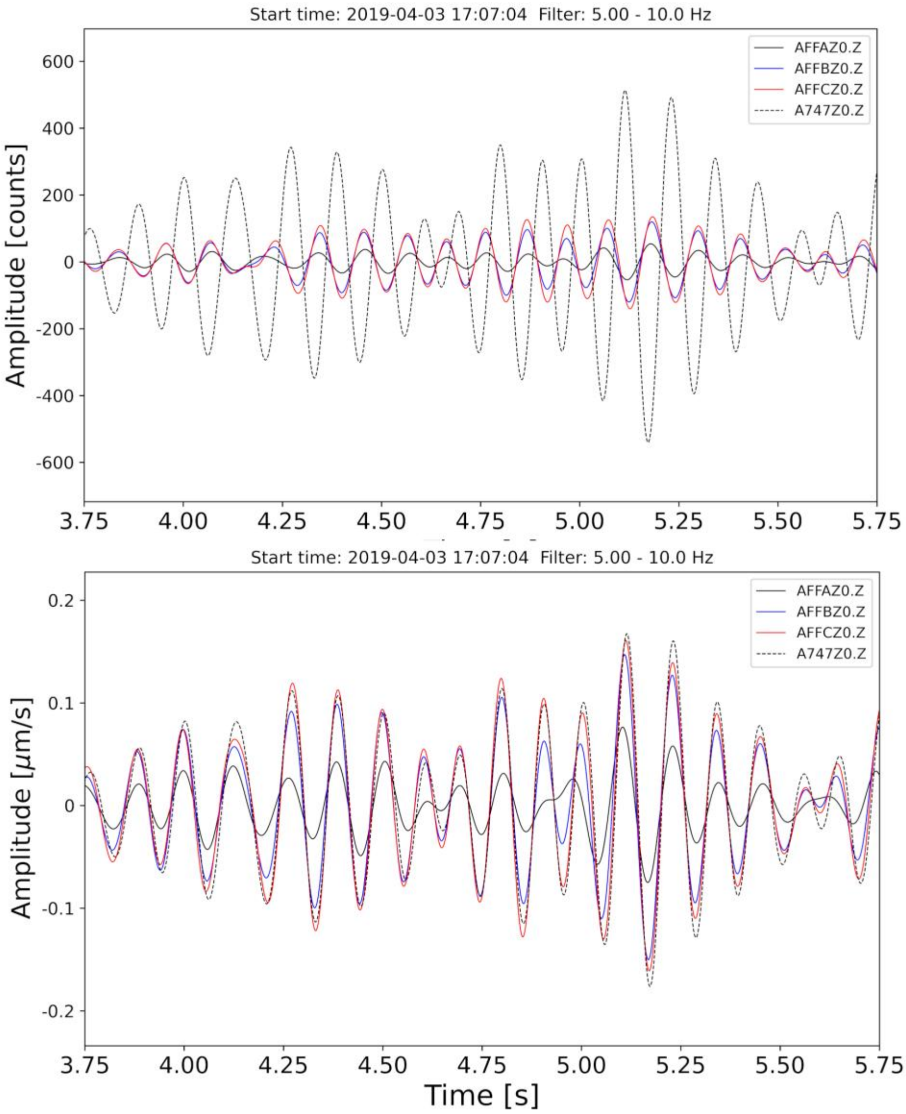

Figure 4-16. *Ambient noise data in the frequency band 5 – 10 Hz recorded on the vertical components of the geophones in borehole HFM42 (AFFA, black; AFFB, blue; AFFC, red; solid lines) and a Guralp Compact seismometer (A747, black dashed). Upper) Raw data in counts. Lower) Instrument deconvolved data in ground velocity.*

5 Results - Distributed measurements

5.1 Data Processing Methods

Following data extraction and length calibration, recordings of all 10 weight drops are stacked for each source location. Data is provided in units of strain rate, nm/m/s. The downgoing and upgoing sections of each fibre, as outlined in Figure 3-9 and Table 3-2, are extracted to enable a comparison between instrument and cable types. An estimate of signal and noise levels are calculated at three borehole depths. These are selected to align with the geophone locations at depths 6.5m, 74m and 188m from TOC. To estimate signal and noise levels, data from each channel is first normalised by its root mean square (RMS) value. A rectangular window of 20m long in depth and 20ms long in time is then selected around each comparison length. The RMS of a time window immediately prior to first arrival is used for the noise estimate and following the first (P-) arrival for the signal estimate. The same processing routine is applied to the geophone data (Z-component). An example of recorded data and these signal and noise windows are shown in Figure 5-1.

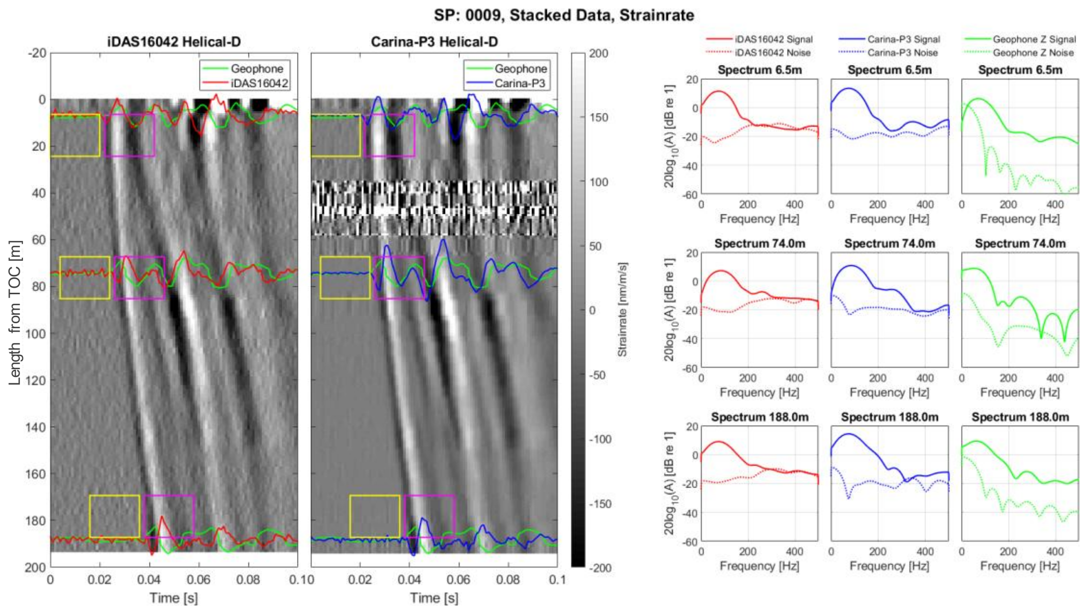

Figure 5-1 Left: Example stacked data recorded for the sources at SP9 on the helical cables using the DAS interrogators. The windows to estimate the noise (yellow) and signal (purple) amplitudes are indicated. The geophone recordings on the Z-component are shown (green), compared to the fibre signal from the channel closest to the geophone. Right: The signal and noise frequency spectra observed on the fibres and the Z-component of the geophone. Note, the geophone data at 75 m and 188 m deep are plotted with the opposite polarity.

5.2 Comparison between iDAS and Carina Sensing System

This comparison is performed using data recorded on the down-going section of the helical cable for both DAS systems.

The first comparison to make is between the noise floor of the DAS systems. The data was first time-integrated to flatten the frequency spectrum and then the last 2 seconds of data within each 4 second record was selected, to minimise contamination by the seismic source signal. However, for long offsets there is some coda signal contamination (i.e., contamination by the latter part of the signal). Finally, the frequency spectrum was calculated for a variety of source points and for each depth corresponding to a geophone location.

At the shallowest depth noise levels are higher because the distributed sensor is affected by noise between 1.5 m and 11.5 m depth and very near-surface noise levels are higher than at depth (for examples see Figure 5-2 and Figure 5-3 for data acquired at SP28 and SP31). At such shallow depths the noise spectra of the iDAS and Carina systems are similar, showing that the background noise levels are above the instrument noise floors. The Forsmark site is close to an operating nuclear power station which could generate significant low frequency noise. At depth, the benefit of the Carina system can be seen because the noise levels are lower than in the iDAS data (Figure 5-2 and Figure 5-3). This is clearest at frequencies >100Hz (which are most likely outside of the frequency range of most sources of the acoustic background noise at these depths) where there is a >10dB improvement in SNR between iDAS and Carina. At lower frequencies, closer to the seismic signal frequency, the Carina system does not show such a significant improvement. Again, this is believed to be due to background noise levels being above the instrument noise floor.

The expected overall improvement afforded by the Carina system is not observed in the data and it is believed that the prototype unit used in this test did not perform to the standard of newer models which have been updated with several improvements following field tests.

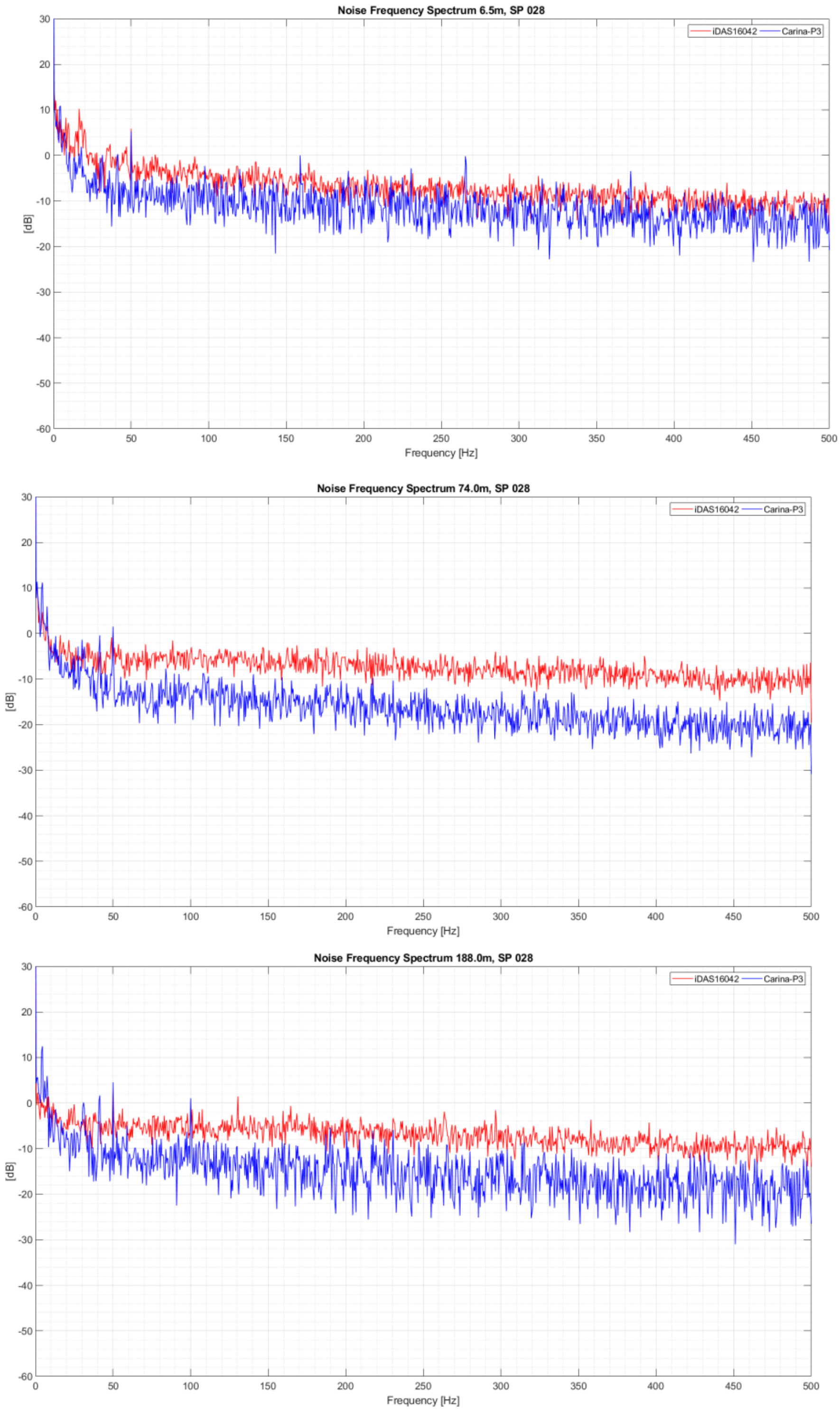

Figure 5-2 *iDAS (red) and Carina (blue) noise floor spectrum comparisons for SP28 for channels at depths of 6.5 m (top), 74 m (middle) and 188 m (bottom) from TOC.*

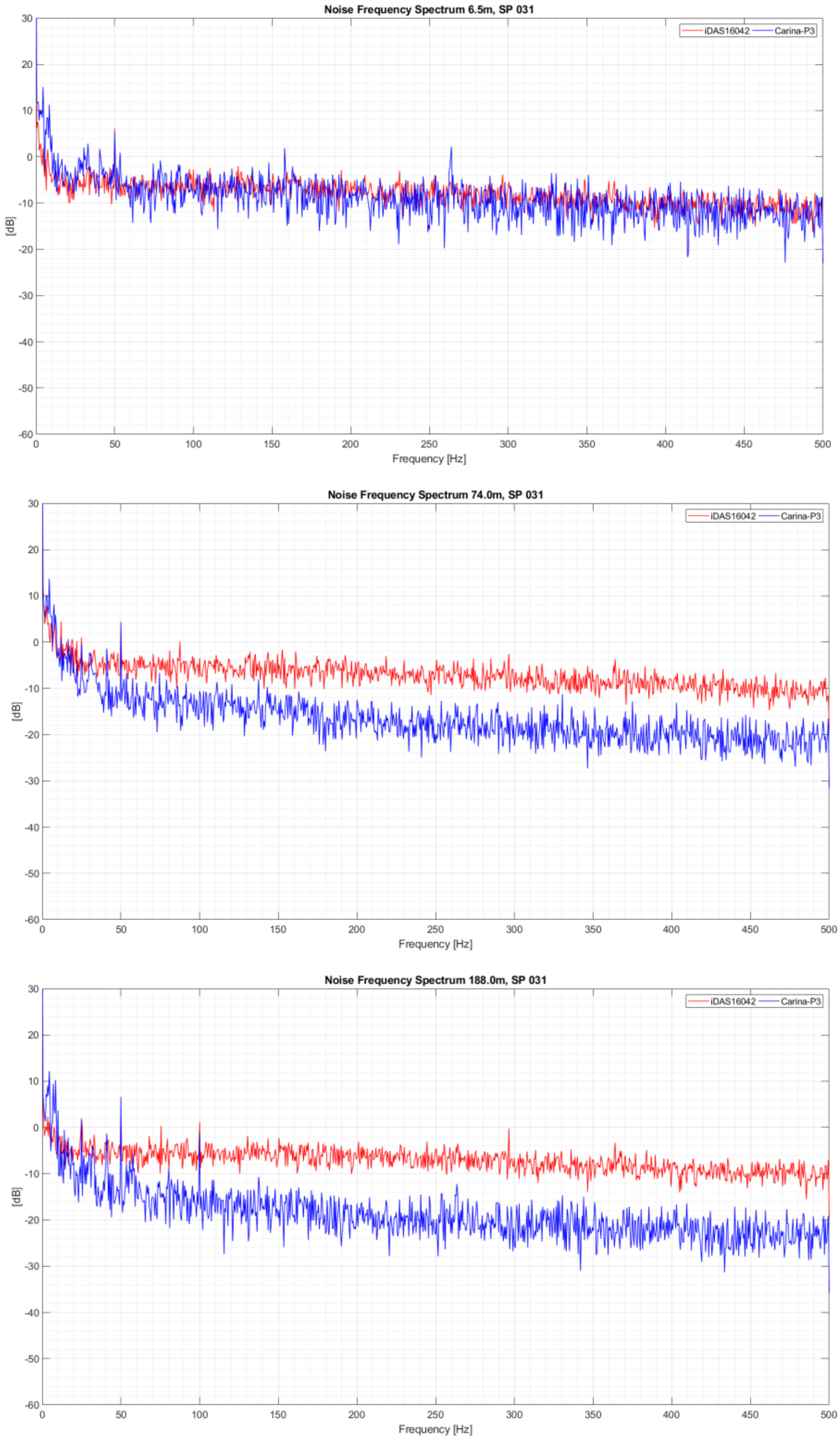

***Figure 5-3** iDAS (red) and Carina (blue) noise floor spectrum comparisons for SP31 for channels at depths of 6.5 m (top), 74 m (middle) and 188 m (bottom) from TOC.*

Figure 5-4 shows the difference in SNR of signals recorded on the helical cables of the Carina and iDAS systems (SNRCarina – SNRiDAS) as a function both of horizontal distance to the source point (offset) and the estimated incidence angle. The approximate incidence angle is calculated based on a straight line between the receiver and source location and is measured from vertical. This calculation will result in an underestimation of the angle of incidence as it does not take into account the true ray-path and refraction effects. The SNR on the Carina system is mostly higher than on iDAS, except at the shallowest receiver depth (6.5m), where the measurement is contaminated with acoustic background noise. The improvement afforded by the Carina system is up to 15dB.

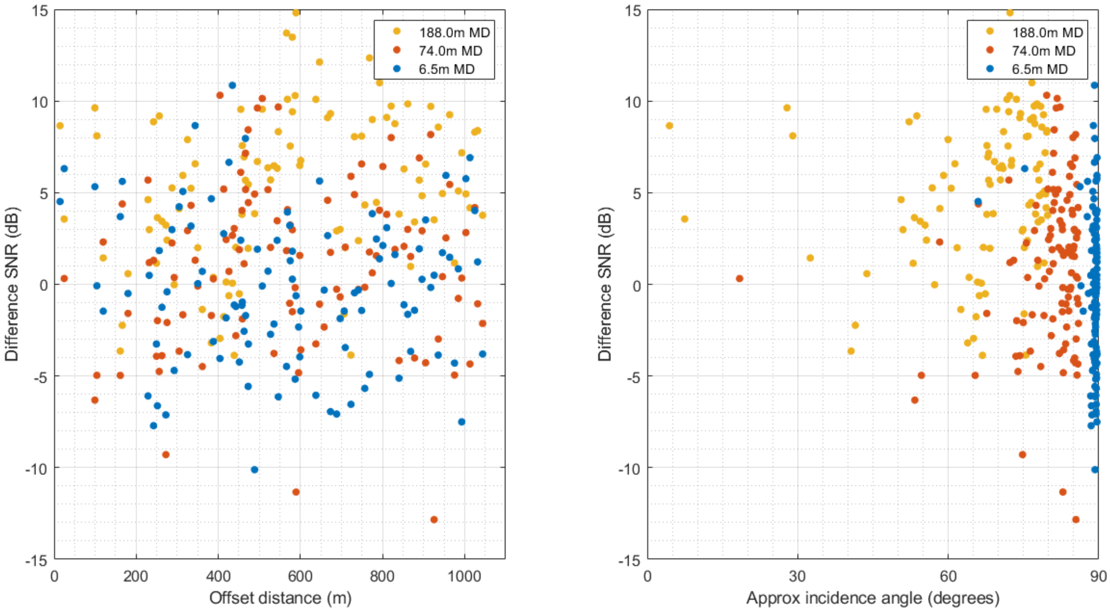

Figure 5-4 *The difference in SNR between Carina and iDAS (helical cable) as a function of offset distance from the borehole (left) and P-wave incidence angle from vertical (right). Data for all three geophone depths are shown.*

5.3 Comparison between the different fibre cables

A comparison between data recorded simultaneously with the iDAS using both the linear cable and helical cable can be made from Figure 5-5. This data from SP9 clearly shows the difference in directivity response between the linear and helical cables. At depth, the seismic arrival is higher amplitude on the linear cable. This is to be expected as at this (near) source offset the arrivals at the bottom of the well are closer to 0° incidence. The linear cable is known to be more sensitive than the helical cable to P-wave arrivals that are in-line with the fibre. However, near the surface the P-wave arrival is not visible on the linear cable. On the helical cable this arrival is clear. This highlights how the helical cable is more sensitive to P-waves arriving broad-side (90° incidence) to the cable than a linear cable. There is a peak in signal strength around 80 Hz on all systems.

At a larger offset (e.g., SP52, Figure 5-6), the P-wave arrival is at high angles of incidence to the fibre for most of the fibre length. This makes the directivity effect clearer between the two types of cable. On the linear cable, it is impossible to see the P-wave arrival. However, on the helical cable, this arrival is detected around 0.09 s after the drop time.

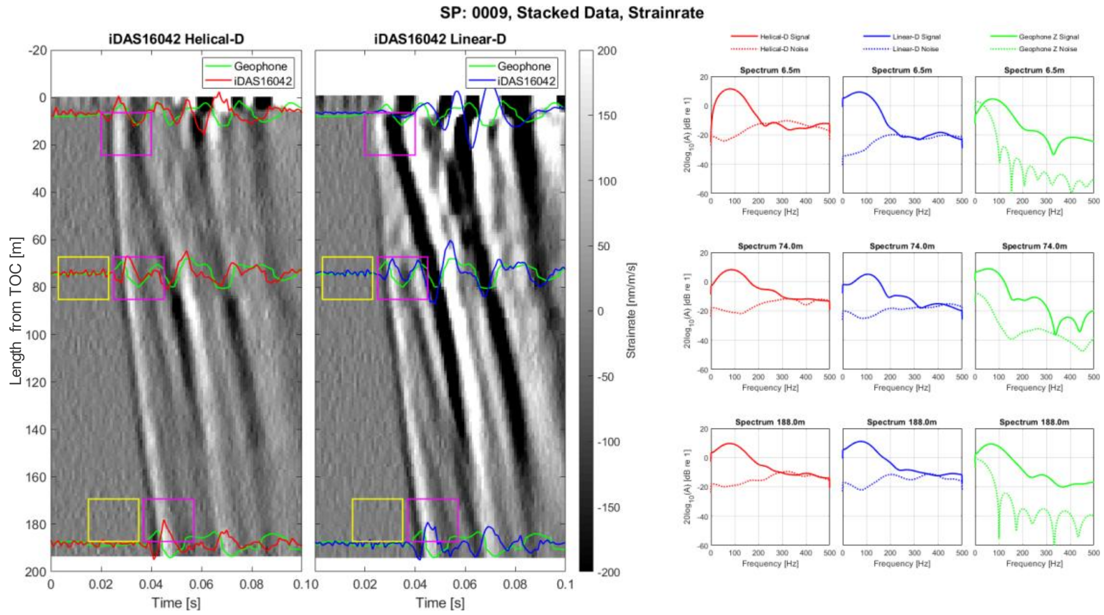

Figure 5-5 *Left: Data recorded at SP9 using the iDAS. Data from the helical (left) and linear (right) cables are shown. The noise (yellow) and signal (right) windows are indicated. The geophone recordings on the Z-component are shown (green), compared to the fibre. Note, the geophone data at 75 m and 188 m deep are plotted with the opposite polarity.*

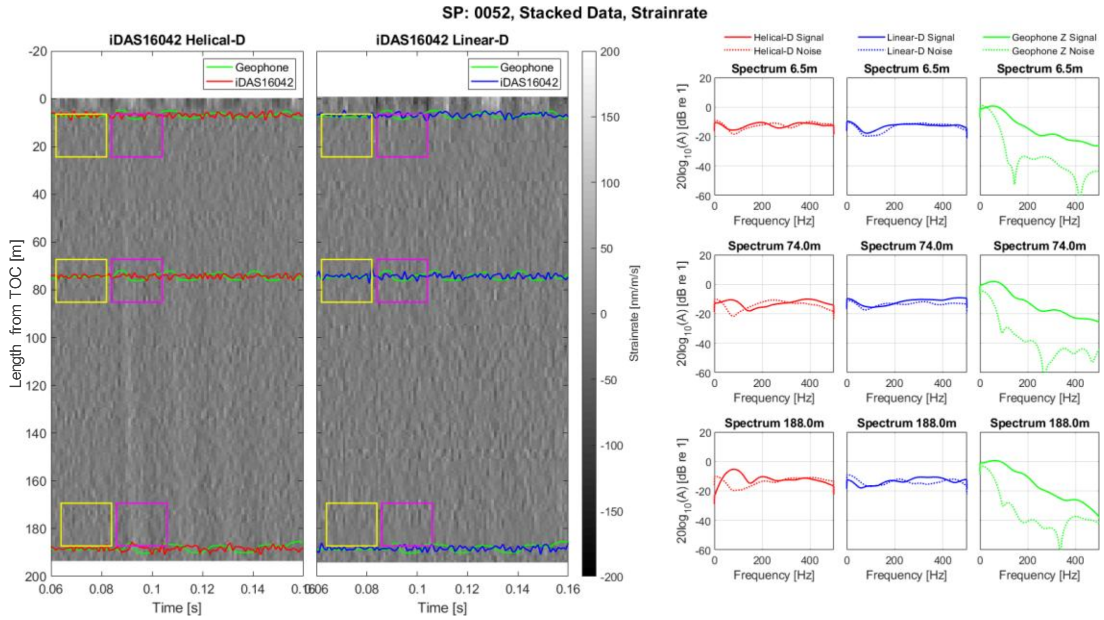

Figure 5-6 Left: *Data recorded at SP52 using the iDAS. Data from the helical (left) and linear (right) cables are shown. The noise (yellow) and signal (right) windows are indicated. The geophone recordings on the Z-component are shown (green), compared to the fibre signal from the channel closest to the geophone. Right: Frequency spectra for the signal and noise recorded on the fibre and geophone Z-component at the geophone depths. Note, the geophone data at 75 m and 188 m deep are plotted with the opposite polarity.*

Figure 5-7 shows the SNR difference between helical and linear cables for all source points, colour-coded by the receiver depth of the measurement. The SNR difference is plotted as a function of source point offset and angle of incidence. The data shows that, at offsets greater than 200m, the helical cable generally has a higher SNR than the linear cable. However, at offsets less than 200 m, the linear cable generally performs better than the HWC with up to 10dB difference in SNR at zero offset. When comparing the difference in SNR values as a function of incidence angle, it is clear that between approximately 60° and 80° the helical cable mostly performs better.

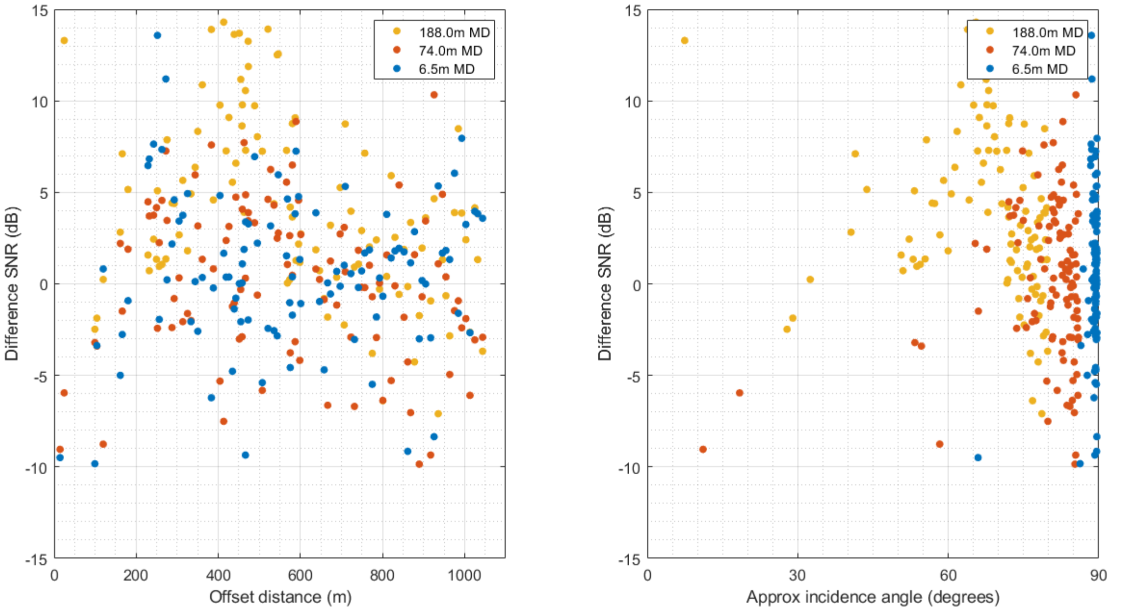

Figure 5-7 *The SNR difference between the helical and the linear cable versus source point offset (left) and versus the approximate P-wave angle of incidence (right) measured using the iDAS. A positive value means the helical cable produces higher SNR than the linear cable.*

5.4 Comparison between recordings with different gauge length

A comparison is also made between the results of data acquired using the Carina-P3 unit configured for a 10 m and an experimental 30 m gauge length, e.g., Figure 5-8 for SP9 at 99 m offset. The leftmost plot in this figure shows the 10 m data and the adjacent plot the 30 m data. A noticeable feature of the 30m data is the "staircase" effect every 15 m. This is inherent in the Carina acquisition architecture where a step is seen at half the gauge length. This is less obvious but also present in the 10 m data. The signal is effectively identical within the 15 m steps so can simply be decimated to 15m channel spacing to remove the staircase effect.

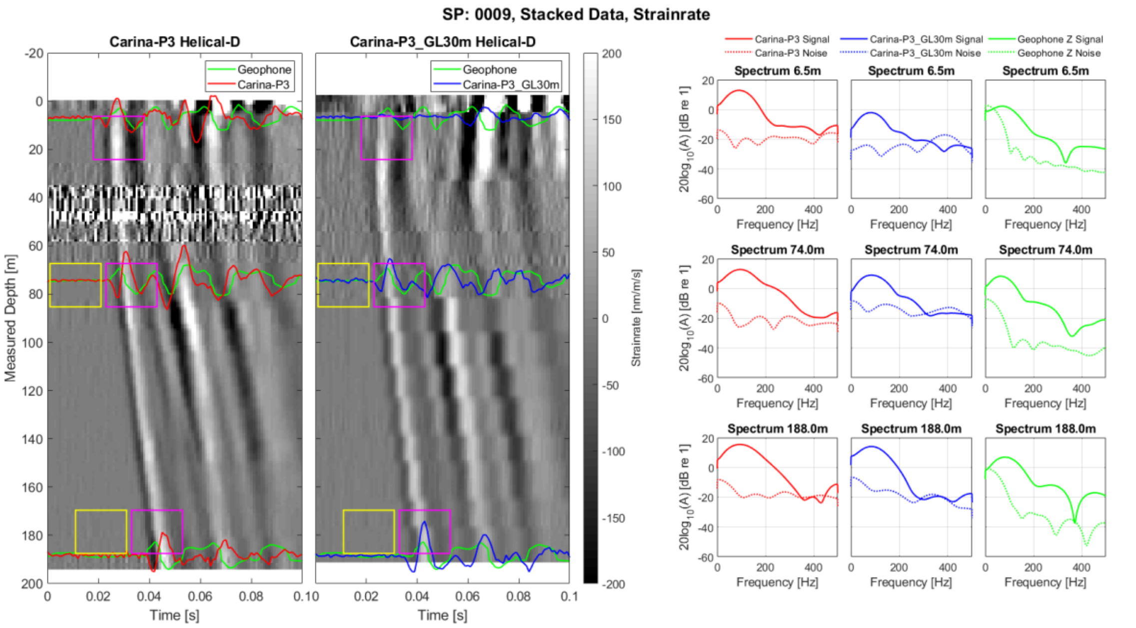

Figure 5-8 *Left: Data recorded at SP9 using the 10m gauge length Carina system (left) and 30m gauge length Carina system (right) are shown. The noise (yellow) and signal (right) windows are indicated. The geophone recordings on the Z-component are shown (green).). Note, the geophone data at 75 m and 188 m deep are plotted with the opposite polarity.*

The SNR is calculated using the windows indicated by the pink and yellow boxes in Figure 5-8, in the same way as previously described. This calculation is done for every source point recorded on the 30 m system. The SNR difference between the 10 m and 30 m system (calculated as SNR30m-SNR10m) is shown in Figure 5-9. On average, the data on the 10 m system has SNR although there is no obvious relationship. Note that a 30 m gauge length system records the total strain-rate over a 30 m length of fibre, whereas the 10 m gauge length system records the total strain-rate over a 10 m length of fibre. Therefore, if the same signal is recorded on 30 m of fibre, the system will natively record 3x higher amplitude on the 30 m system. However, in the conversion of this data to SEGY format, the amplitudes were scaled to true strain-rate values in nm/m/s, which corrects for the different gauge lengths between systems.

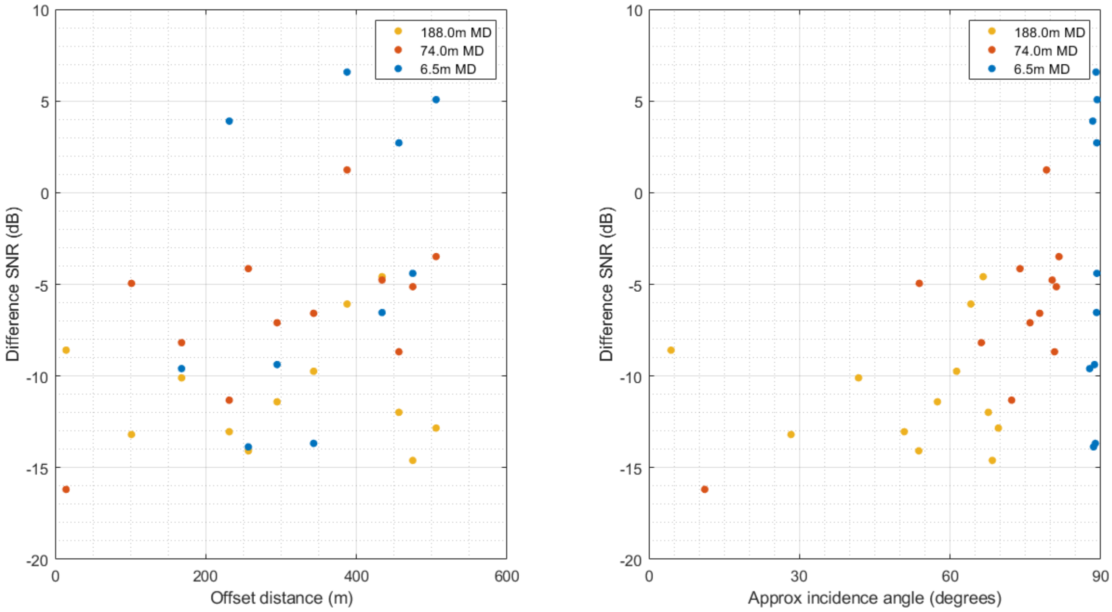

Figure 5-9 *The SNR difference between 30 m and 10 m gauge length Carina systems vs offset (left) and vs approximate angle of incidence (right). A positive value means the 30 m gauge length system is higher than the 10 m system.*

Theoretically, the 30 m system is expected to give data with a higher SNR than the 10 m system. This is because the longer gauge length allows for more light to be put into the fibre, which in turn improves the noise floor of the system. However, the results in Figure 5-9 show that in this instance the 10 m system is performing slightly better than the 30 m system. At 6.5 m depth this is most likely because the signal is being measured over a length of fibre which includes effects from outside the borehole. Similarly, the measurement at 188 m will include parts of both the downgoing and upgoing cable and the measurement at 74 m includes the damaged part of the cable. Testing of the 30 m gauge length system over longer straight cable distances should show the expected increase in SNR.

6 Results – Geophones

6.1 Seismic noise levels

One of the main purposes of the borehole experiment was to measure noise levels at different depths, and to investigate peculiarities in the spectra recorded in very shallow surface boreholes by Lund et al. (2017). Here we will study noise spectra at different depths and at different times in the main borehole and also study the data collected by the vertical component instrument in the shallow borehole, and the broadband Guralp ESPC next to it.

6.1.1 Noise recordings with various instruments at various locations

In Figure 6-1 we show one hour of night time data, between 01:00 and 02:00, for two consecutive nights when we recorded with the Guralp Affinity and the IMS digitiser, respectively. The instrument responses have been deconvolved and the data is shown as power density spectra in decibel referred to a ground motion velocity of 1 m/s.

The noise curves generally agree well, with a broad peak between 8 and 40 Hz, where the lower limit comes from the constraints of the 14 Hz natural frequency of the geophone. The vertical components of the geophones at 6 and 75 m depths have significantly higher noise levels in this band than the vertical component at 188 m depth, and also higher than all horizontal components. There are clear spectral peaks at 25, 50, 100 and 120 Hz, and the 50 Hz over-tones continue up through the spectra up to 1,000 Hz. We see no trace of the 380 Hz resonance observed in the laboratory, so that was probably an artefact of the test environment. The ground motion background noise meets the digitiser noise level at about 150 Hz for the Affinity, and at around 200 Hz for the IMS digitiser. As noted by Lund et al. (2017), there seems to be little noise in Forsmark above some 200 Hz. We note that at around 100 Hz the geophone at 188 m depth starts to pick up more noise than the geophones higher up. This is probably due to the better transmission of high frequency energy at that depth than higher up, and that there is not much surface noise around the borehole (at night) with frequencies above 100 Hz.

The spectral ”humps” observed in the Lund et al. (2017) investigations, with the same type vertical component IMS geophones as used here but loosely installed in 60 cm deep boreholes, are not present in the borehole data in Figure 6-1. Lund et al. (2017) speculated that the humps were resonance phenomena, which could explain why the geophones cemented into the deep borehole do not show this phenomenon. In order to further investigate the issue of the spectral humps, we carried out new measurements with one of the Lund et al. (2017) vertical component IMS geophone in the shallow PFM007946 borehole. The set-up was similar to the Lund et al. (2017) set-up, except that the geophone was now attached to a Guralp DM24 digitiser instead of the IMS digitiser. Results are shown in Figure 6-2, together with data from the vertical component geophone C in the HFM42 borehole, the nearby Guralp broadband sensor and data from site 2 of the Lund et al. (2017) campaign (closest site, approximately 275 m north of HFM42). The Lund et al. (2017) data shows a smaller hump around 150 Hz and a larger hump at 200 – 300 Hz, both clearly visible.

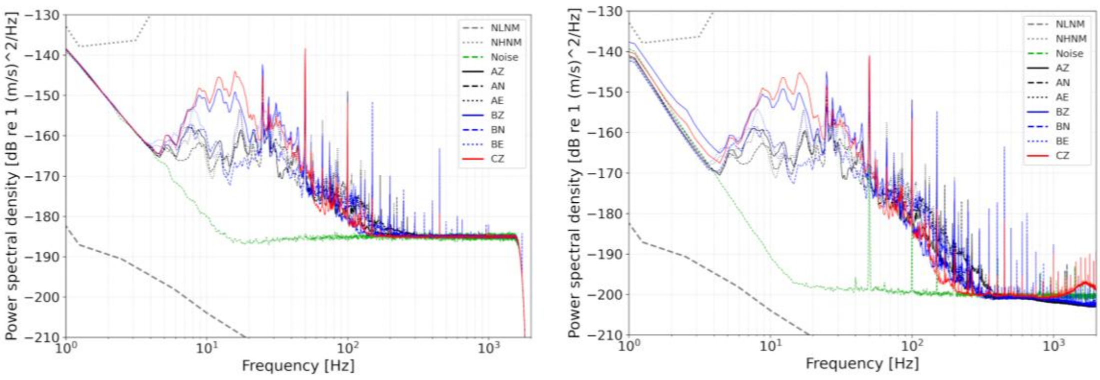

Figure 6-1. *Power spectral densities with one hour of velocity data between 01:00 – 02:00 for all seven geophone components in the borehole. Left) Affinity digitiser at 4 kHz sampling. 2018-08-17. Right) IMS digitiser at 6 kHz sampling. 2018-08-16. "Noise" refers to the individual digitiser system noise, as in Figure 2-9. NLNM is the New Low Noise Model, NHNM is the New High Noise Model (Peterson, 1993)*

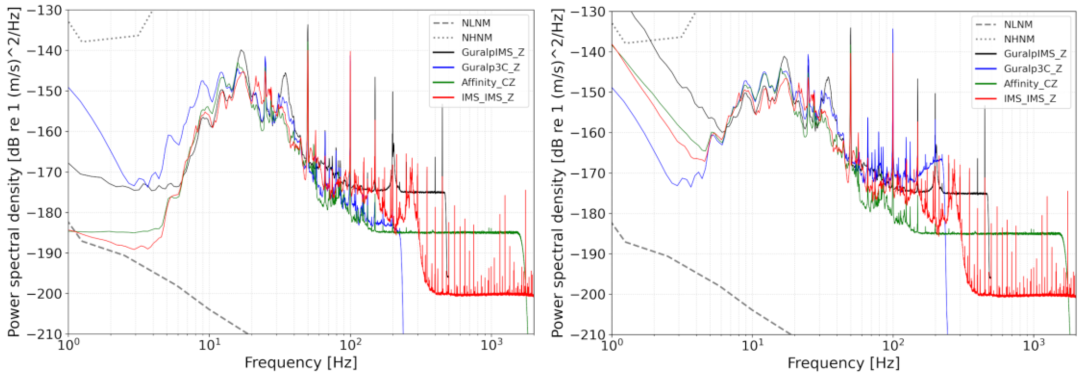

Figure 6-2. *Vertical component power spectral densities from the IMS geophone in the short borehole PFM007946 connected to a Guralp DM24 digitiser (black), a free standing Guralp Compact 60 s sensor connected to a Guralp DM24 digitiser (blue), the IMS geophone at 6.5 m depth in the main borehole connected to the Guralp Affinity digitiser (green), all with one hour of data from 2018-08-17 01-02 UTC. Red line is one hour of data from site 2 of Lund et al. (2017), at 2013-11-14 01-02 UTC. Left) The data have been corrected for instrument sensitivities but not for the shape of the instrument response curve. Right) The data have been corrected for complete instrument responses.*

Figure 6-2 shows that the IMS geophone in PFM007946 does not record high-frequency energy as the geophone at site 2 in Lund et al. (2017). There is a widening of the spectral peak around 200 Hz in the PFM007946 data, but no trace of the 150 and 200 – 300 Hz peaks from site 2. This could indicate that there are resonance issues with the placement of the geophone without proper clamping, but that the resonance frequencies vary with installation. This was also indicated in the comparison of different sites in Lund et al. (2017). It should be noted, as is evident from Figure 6-2, that the combination of the IMS geophone with the Guralp DM24 digitiser is significantly less sensitive, some 25 dB, than the IMS geophone with the IMS digitiser. This is in agreement with the system noise estimates in Figure 2-9.

Comparing to geophone C, cemented into HFM42 at 6 m depth just below the loose overburden, we see that the geophone C (green in Figure 6-2) is significantly quieter than the loose geophones above approximately 60 Hz. Below 60 Hz the five-year older site 2 data is surprisingly similar to the current measurements. The geophone in PFM007946 shows the generally highest noise levels, although a comparison to the site 2 data is difficult as the data was recorded more than 5 years and 275 m apart.

The data from the broadband Guralp sensor (blue in Figure 6-2) shows a similar level of noise as all the geophones between approximately 15 and 50 Hz and between 50 Hz and 200 Hz shows similar levels as geophone C. However, we include two plots in Figure 6-2 to illustrate some of the potential pitfalls when correcting for the instrument response. The data on the left has been corrected for the combined sensitivity of the sensor and digitiser, but the response curves have not been considered. The data on the right in Figure 6-2 have been corrected for both sensitivity and response curves. The left plot indicates that the Guralp broadband instrument is noisier than the geophones at lower frequencies. This is not the case, the effect comes from the decreasing sensitivity of the geophones below the 14 Hz natural frequency. If the response curves are taken into account, to the right, we see that the geophones amplify instrument noise below some 4 – 6 Hz, depending on the digitiser. The broadband Guralp has a flat response between 60 s and 50 Hz, and thus shows the same behaviour at lower frequencies in the two plots. At higher frequencies, however, the Guralp broadband sensor loses sensitivity above 50 Hz. Accounting for this using the response curve over-compensates, as can be clearly seen above 100 Hz in the plot to the right. We know that the rate of decay of the high frequency response in the instrument is somewhat over-estimated in the poles and zeros. A similar effect was seen in Lund et al. (2017).

6.1.2 Temporal variation in seismic background noise

The Affinity digitiser continued operation at HFM42 through the autumn of 2018, and in the spring of 2019 was set up to deliver continuous, real-time 100 Hz data to SNSN in Uppsala. We study the noise evolution during the autumn of 2018 and spring of 2019 with a number of one hour data series extracted between 01:00 and 02:00 in the night. During this time the sampling frequency of the continuous recording was changed twice. The original 4 kHz sampling for the VSP and initial tests was reduced to 1 kHz on 2018-08-21 and then to 500 Hz on 2019-03-22. The real-time stream of continuous data to Uppsala commenced on 2019-03-21.

In Figure 6-3 we show noise spectra for the vertical geophones at 188 m and 75 m depth, respectively. We see that the noise during this hour is relatively constant over time. There is a tendency to higher noise at the lower frequencies later in the year 2018 and spring of 2019. This could be due to higher activity, and more power production, at the nuclear power plants. The noise peaks at 25, 50 and 100 Hz are also highest during the late autumn and spring, corroborating the conclusion of more intense power production.

The most surprising result of the study is the similarity of the noise distribution in the frequency domain. The broad noise peak between 15 and 50 Hz is consistently between 10 and 20 dB higher at the middle sensor B compared to the lower sensor A. The low between 10 and 15 Hz as well as the low between 30 and 40 Hz are permanent in the data from the lowermost sensor. At the middle sensor there is a persistent low between 20 and 30 Hz, except for the 25 Hz peak, which, however, is similar in amplitude to the 20 – 30 Hz band at sensor A. The ground motion recorded at sensor A has decreased to the digitiser noise level at about 200 Hz. At the middle sensor, the ground motion meets the digitiser at about 120 Hz. As concluded above, this indicates that high frequency noise is less attenuated in the rock at 188 m depth than in the rock at 75 m depth.

Figure 6-4 shows the noise spectra for the uppermost sensor, C. The data are similar to those for sensors A and B in that the amplitude distribution with frequency is relatively constant, there are higher noise levels late in the year and the ground motion meets the digitiser noise just over 100 Hz. Interestingly, the noise peak around 15 Hz has grown even higher than at sensor B. We do not know what or where this noise originates from. The amplitudes are generally higher at C than at B, varying between different frequency bands.

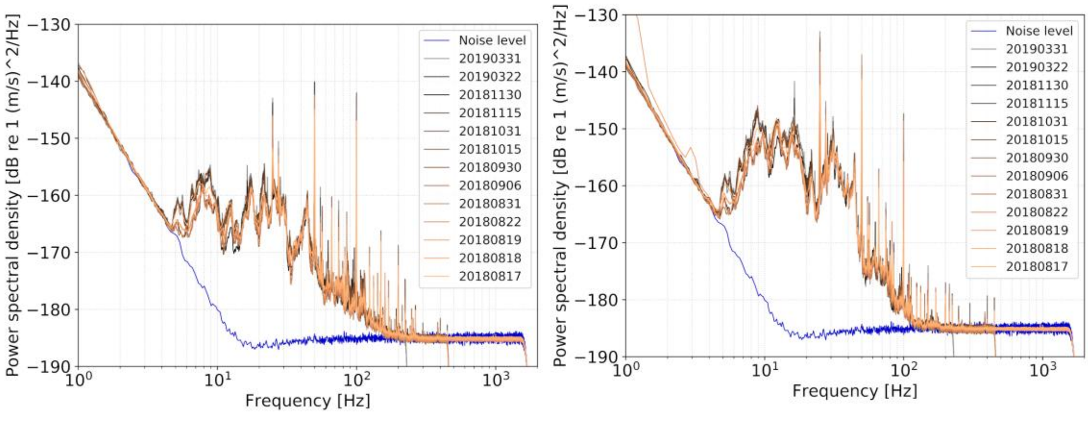

Figure 6-3. *Vertical component spectra using the Affinity digitiser with one hour of data between 01:00 – 02:00 on the dates indicated in the legend. Sampling rates vary from 4 kHz to 500 Hz later in the period. Left) Lowermost sensor (A) at 188 m depth. Right) Middle geophone (B) at 75 m depth. "Noise level" refers to the digitiser system noise, as in Figure 2-6.*

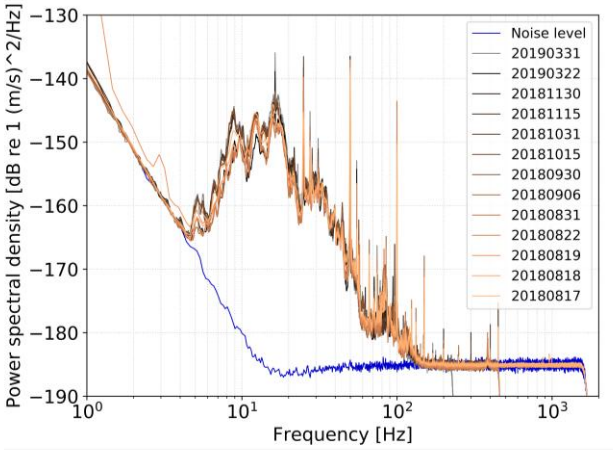

Figure 6-4. *Vertical component spectra using the Affinity digitiser with one hour of data between 01:00 – 02:00 on the dates indicated in the legend. Sampling rates vary from 4 kHz to 500 Hz later in the period. Upper sensor (C) at 6.5 m depth. Noise level" refers to the digitiser self-noise, as in Figure 2-6.*

We look closer at the temporal evolution of the amplitudes in certain frequency bands by plotting the root-mean-square (RMS) of the amplitude time series with time. We define 5-minute segments of RMS as

$$RMS = \sqrt{\sum x_i^2/N}.$$

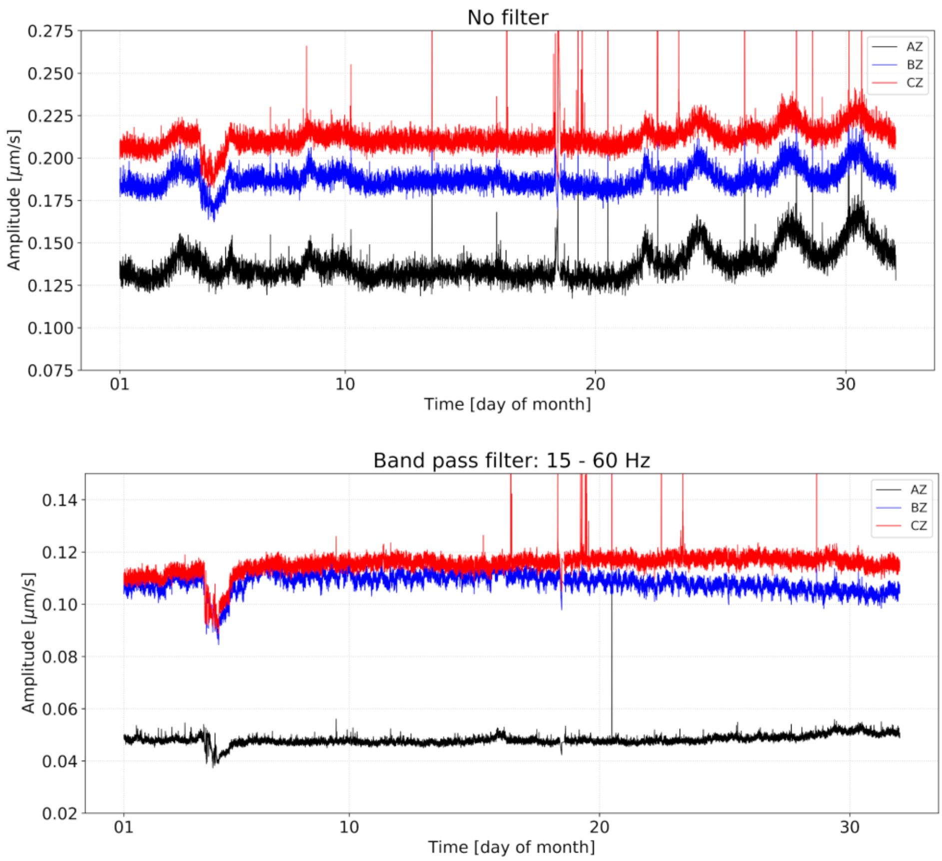

Figure 6-5. *Temporal evolution of ground motion in 5-minute segments of RMS during October 2018. Vertical geophones only, lower (AZ), middle (BZ) and upper (CZ). Upper panel) Unfiltered data, all frequencies. Lower panel) 15 – 60 Hz band pass.*

The RMS calculated here contains all ground motion within the studied frequency bands, in 5-minute segments continuously throughout the day and month. We see in Figure 6-5 how the total ground motion RMS is relatively constant through October 2018. There is a significant difference in the noise levels at different depths, the lower sensor A records only about 60% of the ground motion at the uppermost sensor C, while the middle sensor B records approximately 90% of the motion at sensor C. There is a decrease in noise around 4-5 October, possibly due to repair works or some malfunction in the power generation system. At the end of October there is a general increase in ground motion, together with a temporal variation of a few days length. During the month there are about 10 occasions with short bursts of high ground motions at all depths, probably due to work close to the HFM42 borehole.

The lower panel in Figure 6-5 shows the 15 – 60 Hz frequency band, where much of the ground motion activity is concentrated. We see that in this frequency band there is a factor of two difference between the lower sensor A and the two upper sensors, which have very similar RMS. The levels are approximately constant over the month, with a slight increase at sensors A and C at the end of the month and a similarly sized decrease in RMS at B.

Figure 6-6 shows two additional frequency bands, one around 50 Hz (45 – 55 Hz) and one around 100 Hz (95 – 105 Hz). The RMS amplitudes in these bands are of similar size, but significantly smaller than e.g. the 15 – 60 Hz band. We note that in these two bands the amplitudes at the three sensors are less separated than in Figure 6-5. In the 50 Hz band sensor B sees the highest amplitudes until the middle of the month, when a decrease starts that continues during the latter half of the month. By the end of October, the amplitudes at B are similar to those at A. Oppositely, the amplitudes near the surface, at C, are as small as at A in the beginning of the month, but increase suddenly around the 5th and then vary until they grow largest around the 22nd. The amplitudes at A are relatively constant throughout much of the month, but increase toward the end of the month.

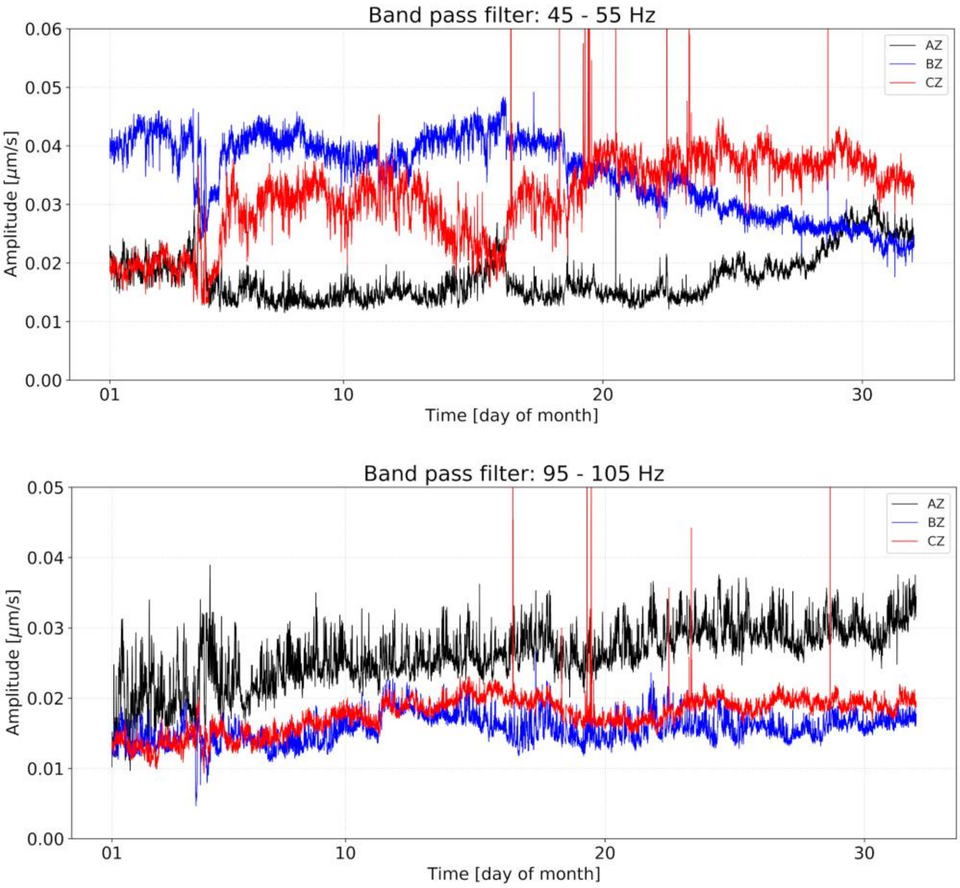

Figure 6-6. *Temporal evolution of ground motion in 5-minute segments of RMS during October 2018. Vertical geophones only, lower (AZ), middle (BZ) and upper (CZ). Upper panel) 45 -55 Hz band pass filter. Lower panel) 95 - 105 Hz band pass filter.*

In the 100 Hz band, the lowermost sensor A has the highest RMS amplitudes, consistently throughout the month, in agreement with lower high frequency attenuation at depth. The amplitudes at A increase gradually throughout the month and have significant high frequency variations. The amplitudes at B and C are very similar throughout the month, but less variable at C, except for the occasional spike in RMS, probably caused by local disturbances.

6.2 Recorded seismic events

During the operation of the borehole geophones a number of seismic events have occurred both in the vicinity of Forsmark and further away. Here we show results for two earthquakes, one small magnitude 0.4 event between Forsmark and Österbybruk and the magnitude 2.9 earthquake in Gävle. We also show results from two local blasts. Table 6-1 has time and location of the events and Figure 6-7 shows the location of the blast sites.

Table 6-1. Seismic events recorded by the borehole geophones in borehole HFM42. Numbers in parenthesis at the location refers to the map in

Type	Date and time [UTC]	Location	Distance [m]	Depth [km]	Size	Affinity settings sampling rate, gain
Earthquake	2018-09-23 14:37:49	Sångarbo 60.2832; 18.0865	14 km	19	M 0.4	1,000 Hz, x8
Earthquake	2018-10-20 11:56:40	Gävle 60.7204; 17.1732	65.7 km	3	M 2.9	1,000 Hz, x8
Blast	2019-04-03 17:07:14	KFM18 (2) 6700286.24; 675300.08 (60.400825, 18.182234)	329	0.0203	8 kg	1,000 Hz, x8
Blast	2019-04-03 17:30:39	KFM20 (3) 6700231.92; 675316.93 (60.400334, 18.182495)	273	0.0305	6 kg	1,000 Hz, x8
Blast	2019-04-03 18:24:55	KFM20 (3) 6700231.92; 675316.93 (60.400334, 18.182495)	273	0.0178	4 kg	1,000 Hz, x8
Blast	2021-02-10 09:17:48	6699717; 675066 (4) (60.395824; 18.177501)	388	surface	?	2,000 Hz, x1

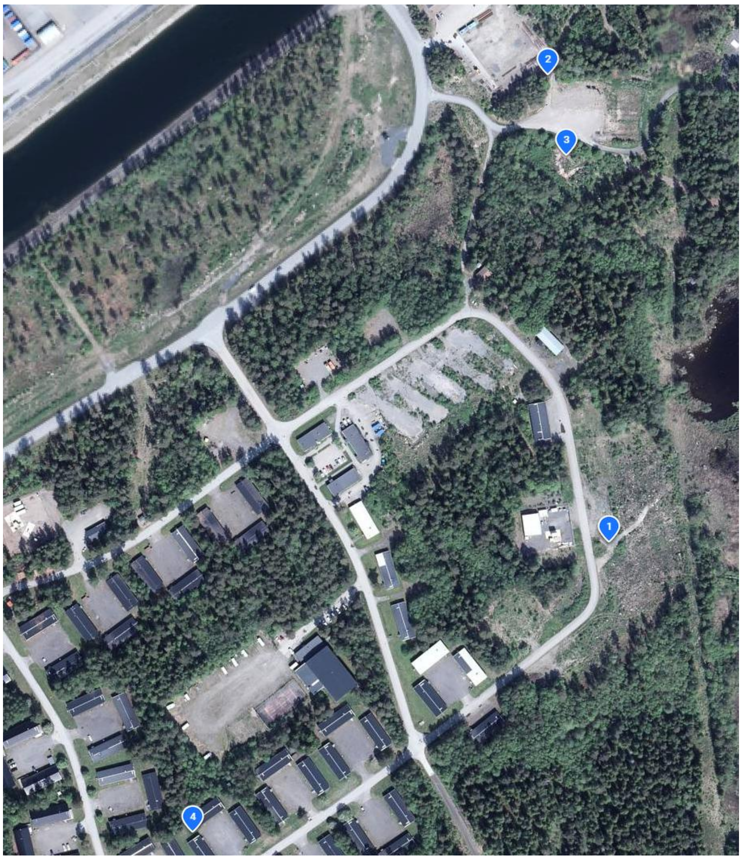

Figure 6-7. *Map of the blast sites for the blasts recorded at HFM42 (point 1). Boreholes KFM18 (point 2) and KFM20 (point 3) and the surface blast (point 4). Distances are approximately 329 m to point 2, 273 m to point 3 and 388 m to point 4.*

6.2.1 Local earthquake

A small local earthquake occurred on the 23 September 2018 approximately 14 km south-west of HFM42. The event was manually analysed on 8 permanent SNSN stations around Forsmark, from station FOR close to the power plants, 12 km away from the epicentre, via Flymyra, Gräsö, Östervåla, Fiby, Norrtälje and Åland to the station south of Falun, 127 km away. This was a strike-slip earthquake, occurring either on a NW-SE striking subvertical fault or a NE-SW striking fault dipping 59 degrees. The event was recorded on the borehole geophones and the permanent station FOR as shown in Figure 6-8.

We see that the earthquake was well recorded on all but the upper geophone, but it is obvious that the ambient noise levels are high on the upper (C) and middle (B) sensors, degrading the signal to noise ratio (SNR). The SNR is better at the deepest geophone (A) and best at the 30 second broadband instrument at FOR. The ground velocities are similar on all sensors, between -0.7 and 0.7 micrometer per second. The data shows, again, that the orientation of the horizontal components in the borehole are good, as the transverse components have very little P-wave energy. We also note in Figure 6-8 that there is less overall noise at FOR. This is due to (i) FOR is located 1.7 km away from the nearest power plant while HFM42 is only 650 m away and (ii) The sampling rate at FOR is 100 Hz, and thus the Nyquist frequency is 50 Hz, which avoids recording of the large 100 Hz and overtones energy. Additionally, the anti-alias filters in the digitiser, as a by-product, removes the 50 Hz noise.

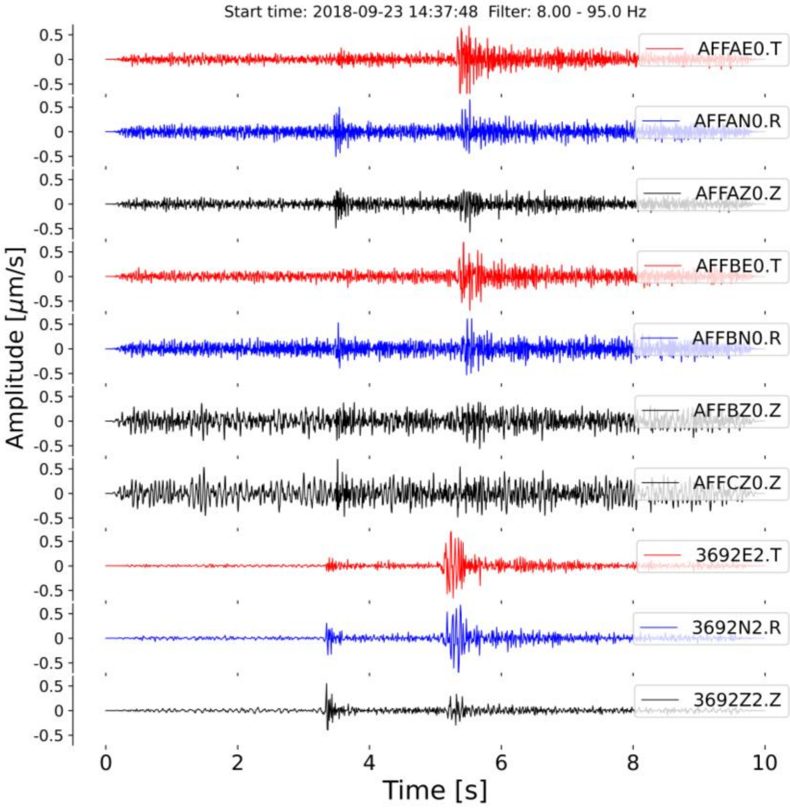

Figure 6-8. *Recording of a local magnitude 0.4 earthquake on 2018-09-23. Geophones in the HFM42 borehole (AFFA, AFFB and AFFC) and the broadband Guralp sensor at permanent station FOR (3692). The horizontal components have been rotated to radial (R, blue) and transverse (T, red), the vertical components are unchanged (Z, black). Band pass filtered signals between 8 and 95 Hz (8-47 Hz for station FOR).*

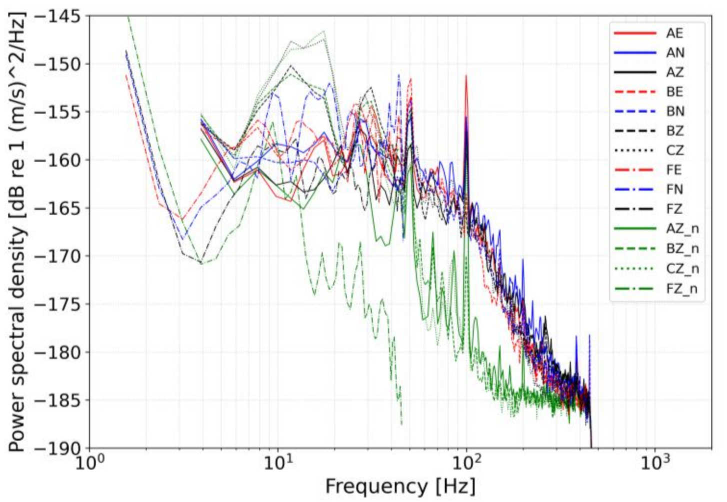

Figure 6-9. *Ground velocity power spectral densities for 10 seconds of data around the local magnitude 0.4 earthquake on 2018-09-23, in dB relative to 1 m/s. All components of the geophones in the HFM42 borehole and the FOR broadband sensor. Instrument responses have been deconvolved. Lower geophone (A, solid line), middle geophone (B, dashed line), upper geophone (C, dotted line), 30 s broadband instrument (F, dash-dotted line). 10 seconds of preceding noise data from the vertical components ("_n" labels, green).*

The spectra in Figure 6-9 show how the vertical components in geophones B and C have high energies between 8 and 20 Hz. Comparing to the noise data we see that this is almost exclusively noise. Similarly, the A geophone and station FOR show noise amplitudes below approximately 12 Hz. Above 12 Hz the noise at FOR decreases rapidly and the earthquake data has about 10 dB higher energies. At geophone A this transition occurs at about 25 Hz while for the shallower B and C geophones it does not occur until above the 50 Hz noise peak. Comparing the signal spectra to the noise spectra we see that the local earthquake signal contains significant amounts of high frequency energy between 50 Hz and 250 Hz, a difference of 5 – 10 dB in most of that range.

It is instructive to calculate station magnitudes in order to investigate the amplitudes in different frequency bands and study the influence of noise on the magnitudes. In Table 6-2 we show Helsinki time domain local magnitudes, ML(HEL) (Uski & Tuppurainen, 1996) in different frequency bands and for both 3 s of data at the S-wave arrival and 3 s data in the noise prior to the P-wave. ML(HEL) is calculated from the largest peak-to-peak amplitude in the data window, using the Sg/Lg phases of a local or regional event. In the noise window it simply uses the largest peak-to-peak signal.

Table 6-2. Local magnitudes, ML(HEL), in various frequency bands for 3 seconds of data around the S-arrival (Earthquake) and 3 seconds of data in the preceding noise (Noise).

Data	Frequency range [Hz]	Geophone A ML	Geophone B ML	Geophone C ML	FOR ML
Earthquake	4 - 20	0.4	0.6	0.8	0.6
Earthquake	10 - 40	0.5	0.6	0.7	0.4
Earthquake	60 - 90	-0.2	-0.2	-0.2	-
Noise	4 - 20	0.3	0.7	0.8	0.4
Noise	10 - 40	0.2	0.6	0.7	0.02
Noise	60 - 90	-0.8	-0.7	-0.8	-

We see in Table 6-2 that it is difficult to pick a frequency window which both contains the maximum signal energy and is not overwhelmed by noise. The 4 – 20 Hz window contains mostly noise at all sensors and in the 10 – 40 Hz window the upper two geophones record mostly noise whereas the lower, A, geophone have amplitudes partly above the noise level giving a better indication of the magnitude. FOR agrees with the SNSN network magnitude. At frequencies above 50 Hz the signal-to-noise level is good at all geophones, but the event amplitudes are too low to give a good representation of the magnitude in this frequency band.

6.2.2 Regional earthquake

On 2018-10-20 a shallow magnitude 2.9 earthquake occurred in the northern suburbs of Gävle, upsetting much of the town. The event was followed by 7 aftershocks in the days after. Signals from an event of this size are recorded over much of Sweden in the permanent seismic network, SNSN. This was a strike-slip event with a significant reverse faulting component.

The event was well recorded on all sensors at Forsmark, we show the waveform data in Figure 6-10, deconvolved with the instrument responses. As for the local event, the amplitudes are similar on the different instruments, here between -10 and 10 micrometer per second, and the transverse components have little P-wave energy. Spectral data, in Figure 6-11, show that the amplitudes of the waves from the event are larger than the site noise at Forsmark over much of the frequency range up to 150 Hz, except at the 100 Hz noise peak and some of the overtones.

This event provides a good example of when instrument response deconvolution helps to extend the nominal frequency range of the sensor. Figure 6-11 shows the power spectral densities for a case when the instrument sensitivities are applied to the data but the shape of the response functions is not deconvolved, and a case when full deconvolution is performed. Without deconvolution the geophone spectra agree well with the broadband sensor down to about 11 – 12 Hz, as expected due to the 14 Hz natural frequency. The broadband sensor shows that much of the energy in the earthquake is contained below 10 Hz, which the geophones do not pick up very well. However, deconvolving the instrument response results in restoration of the amplitudes below the natural frequency, and in this case that works very well, bring the geophone lower frequency data up to amplitudes similar to those recorded on the broadband sensor. Specifically, in the 2 – 12 Hz band there is good agreement between the geophone and broadband data. The lower in frequency we go, the more uncertain this approach becomes, and Figure 6-11 shows that at about 1 Hz the deconvolved signal amplitudes meet the instrument response curve, indicating that no real signal is recorded.

Calculating station magnitudes, ML(HEL), in the 2 – 12 Hz frequency band we find that the deep sensor A estimates a magnitude of 2.6, sensor B 2.6 and sensor C 2.7. The SNSN station FOR with a broadband seismometer estimates 2.9, in agreement with the official SNSN magnitude of the earthquake. The geophone data can thus be used to calculate magnitudes also for events with dominating frequencies below the 14 Hz corner frequency, if the instrument response is properly deconvolved and the energy in the signal large enough. Using frequencies above 12 Hz does not increase the magnitude as those frequencies have lower amplitudes. If the magnitude calculation is performed on the noise data, as above, in the 2 – 12 Hz band we find that the noise has an equivalent ML(HEL) of 1.1, 1.3, 1.3 and 0.9 at sensors A, B, C and FOR, respectively.

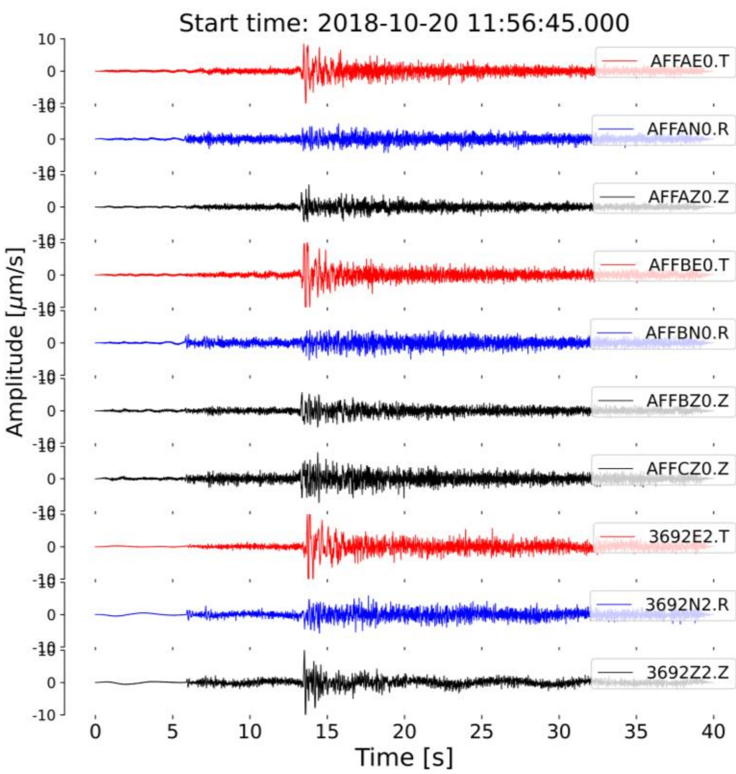

Figure 6-10. Recording of a regional magnitude 2.9 earthquake in Gävle on 2018-10-20. Geophones in the HFM42 borehole (AFFA, AFFB and AFFC) and the broadband Guralp sensor at permanent station FOR (3692). The horizontal components have been rotated to radial (R) and transverse (T), the vertical components are unchanged (Z). The instrument responses have been deconvolved.

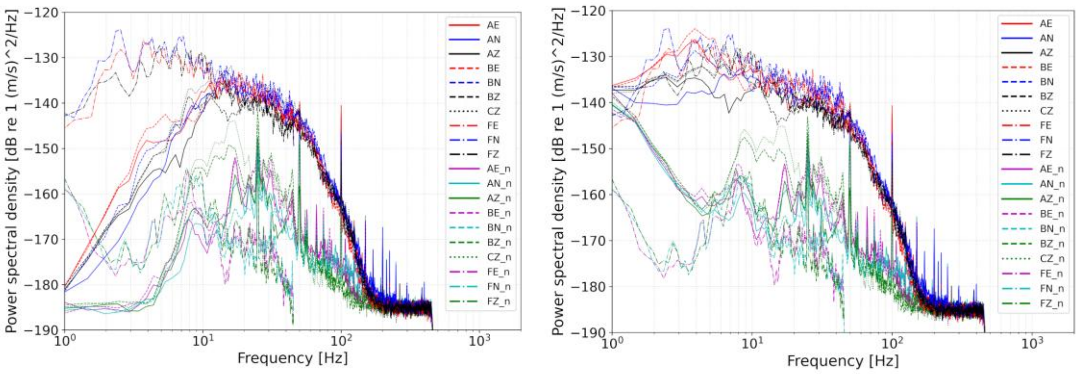

Figure 6-11. *Power spectral densities in dB relative to 1 m/s ground velocity. All components of the geophones in the HFM42 borehole and the FOR broadband sensor. Lower geophone (A, black), middle geophone (B, blue), upper geophone (C, green), 30 s Guralp broadband instrument (F, red). 40 seconds signal data with two character labels (red, blue, black). 40 s preceding noise data with "_n" labels (grey, cyan, magenta). Left) The instrument sensitivities have been applied to the data, but no deconvolution. Right) Instrument responses have been deconvolved.*

6.2.3 Blasts in boreholes in Forsmark, 2019-04-03

On 3 April 2019 10 blasts were performed with varying charge sizes at varying depth in boreholes KFM18 and KFM20, located as indicated in Table 6-1. KFM18 is approximately 329 m from HFM42, at back-azimuth 352 degrees, and KFM20 is 273 meters from HFM42, at back-azimuth 353 degrees. Unfortunately, the geophone wires had been detached from the digitiser during maintenance work and these were not reconnected until in time for the eight blast. The times, depths and charge sizes of the last three, recorded, blasts are noted in Table 6-1. Sampling rate was 1,000 samples per second during the blasting.

All three blasts were well recorded on the geophones in HFM42 and also on an additional Guralp Compact 60 s to 100 Hz seismometer on the outcrop at borehole PFM007946, approximately 30 m east of HFM42. Figure 6-12 shows the recordings of the blast at 17:07:14. We see that the two deeper geophones (A and B) show negative first motions on the vertical component, in agreement with a downward travelling blast signal. Conversely, the C geophone and the Guralp show an upward travelling P-wave. The Guralp and C geophones shows large surface wave motion on the Z- and R-components, indicating a Rayleigh, or Rg, wave. This is also visible on the BZ-component, but much less on the BR, while being absent on the A geophone.

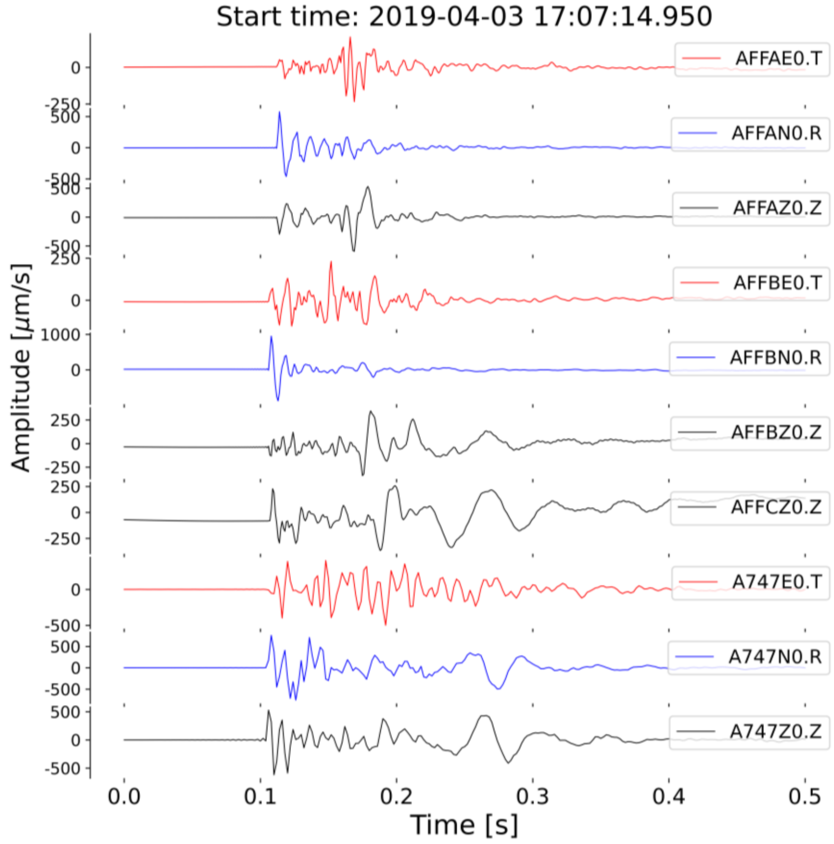

Figure 6-12. *Blast at 2019-04-03 17:07:14 in borehole KFM18 at 20.3 m depth and charge size 8 kg. Recorded at the geophones in the HFM42 borehole (AFFA lowest depth, AFFB middle depth, AFFC upper) and at a Guralp Compact seismometer (A747). Vertical components (.Z, black), radial components (.R, blue) and tangential components (.T, red). The instrument response has been deconvolved.*

Spectra of the data show, Figure 6-13, that the geophones record significant high frequency energy all the way up to the Nyquist frequency. Even at frequencies of 300 to 400 Hz, the data are 50 dB above the background noise and the high energy noise peaks at 50 Hz and 100 Hz are much below the signal strength. The blast data show that high frequency energy is well transmitted over distances of 300 – 400 m in the shallow rock at Forsmark and that the transition from rock domain 1 to rock domain 2 seems to have very little influence on the high frequency content. However, the Rg wave is significantly attenuated at geophone A, at 188 m depth in rock domain 2.

The two later blasts, at 17:30 and 18:24, show similar waveforms and spectra as Figures 6-12 and 6-13 and will not be shown here.

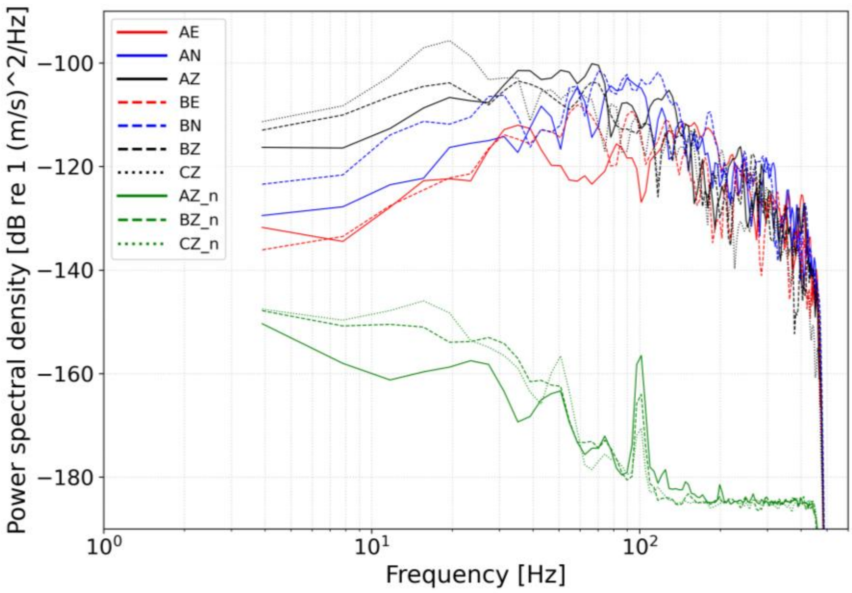

Figure 6-13. *Power spectral densities in dB relative to 1 m/s ground velocity of 1 second of data around the arrivals from the blast at 17:07:14 (red, blue, black) and 10 seconds of noise data from just before the P-wave arrival (green, "_n" labels). The instrument responses have been deconvolved.*

6.2.4 Blast in Söderviken on 2021-02-10

During the civil works in Söderviken we looked more closely at one of the nearby blasts. The blasting was aimed at rock removal.

The blast at 09:17:48 was located 388 m away from the borehole and was well recorded at 2kHz sampling rate on all the geophones in the HFM42 borehole, see Figure 6-14. We see that there is a very clear repeating pattern in the data, which may be due to a ripple fire type of blasting.

Perhaps the most interesting aspect of the blast data is the spectrum. Figure 6-15 shows the power spectral densities at all components and it is striking how much high frequency energy there is in the blast. Previous spectra have shown that the ambient noise decreases to the digitiser noise levels at around 200 Hz. Here we see that the blasts contain significantly more high frequency energy, confirming also that the recording instruments work well in capturing energy up to almost 1,000 Hz. We note in the spectra how there are strong spectral lines at 10, 20, 30 Hz and up, following the 10 Hz variation seen in the time series. We also see how at lower frequencies the vertical components have more energy than the horizontals but that at higher frequencies the horizontals show more ground motion. In addition, the uppermost C sensor show highest amplitudes at lower frequencies, but lowest amplitudes at higher frequencies. This is probably due to higher attenuation in the upper part of the bedrock.

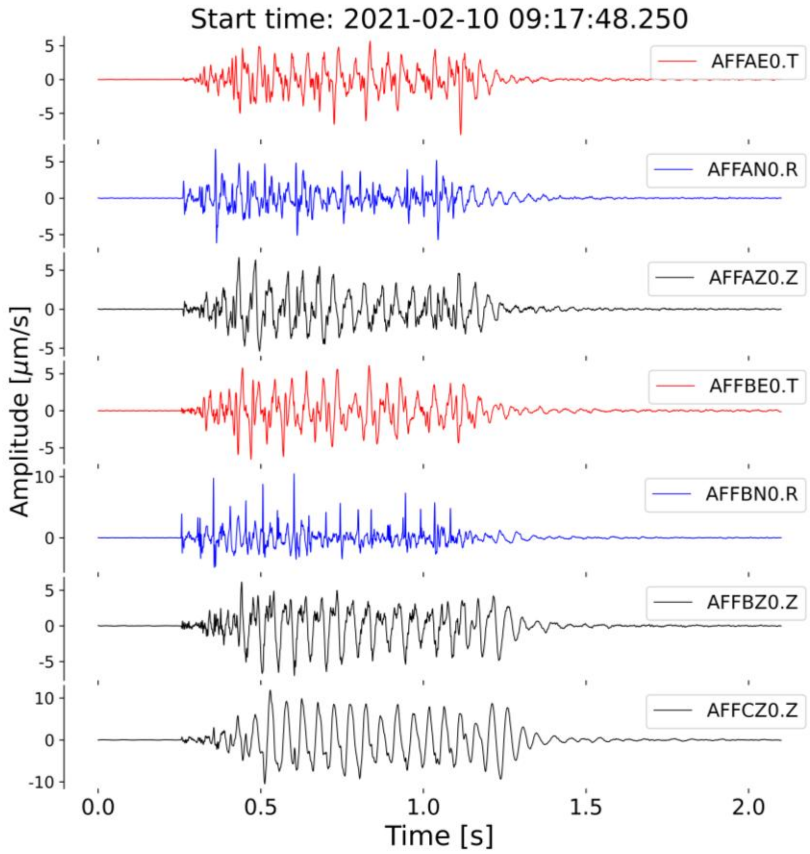

Figure 6-14. *Recording of a local blast in Söderviken, Forsmark at 2021-02-10 09:17 UTC. Geophones in the HFM42 borehole (AFFA, AFFB and AFFC). The instruments are deconvolved and the data rotated.*

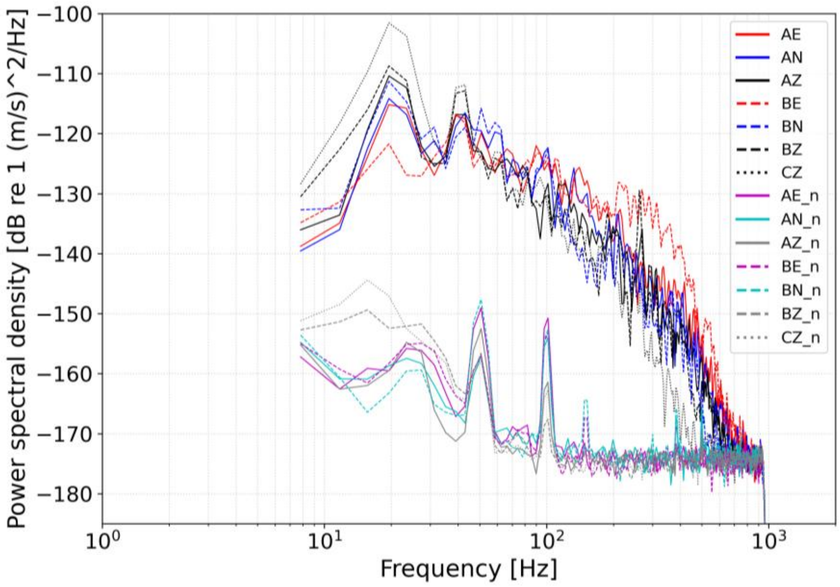

Figure 6-15. *Recording of a local blast in Söderviken, Forsmark at 2021-02-10 09:17 UTC. Power spectral densities in dB relative to 1 m/s ground velocity using 2.1 seconds of data. Blast data in black (Z), blue (N) and red (E). 2.1 seconds of noise data from just prior to the P-wave in grey (Z_n), cyan (N_n) and magenta (E_n). All components of the geophones in the HFM42 borehole. Lower geophone (A, solid lines), middle geophone (B, dashed lines), upper geophone (C, dotted line). Instrument responses have been deconvolved.*

6.3 Active source data

We use the active source data to investigate to which distance the geophones at different depths in HFM42 are able to record the signals and to study the frequency content in the signal. We also use receiver gathers for the three geophones to estimate seismic velocities and discuss attenuation. To increase the signal to noise, the active data is stacked with 10 weight drops per source point. The waveforms from the three-component geophones, A and B, have been rotated to the ray coordinate system, L (in the direction of propagation), Q (in the vertical plane, perpendicular to the propagation direction) and T (transverse, perpendicular to the propagation-vertical plane). The inclination of the incoming waves has been calculated very simplistically from the geometry of source-to-borehole distance and the depth of the geophone, without taking into consideration that the velocity structure is likely to affect the inclination, or take-off angle. The vertical CZ geophone data are not altered.

6.3.1 Examples from individual source points

Source point 1, 13.6 m distance from the top of the borehole. Figure 6-16 shows that the weight drops vertically above the borehole are well recorded at all geophones, and that the P phase shows clearly on the L-component and the S phase on the T-component. There are also significant later S-type phases recorded on the A and B geophones.

The spectra in Figure 6-17 show that geophone C, at 6.5 m depth and thus 15 m distance from SP1, records signal data with frequencies up to 600 Hz. Geophone B at 75 m depth records signal frequencies up to 450 Hz and geophone A, at 188 m depth sees signals up to 300 Hz. Comparing the background noise level in Figure 6-17 to the lab data in Figure 2-6, we note that when stacking 10 data segments the noise does indeed decrease by approximately 10 dB, as expected for random, independent noise.

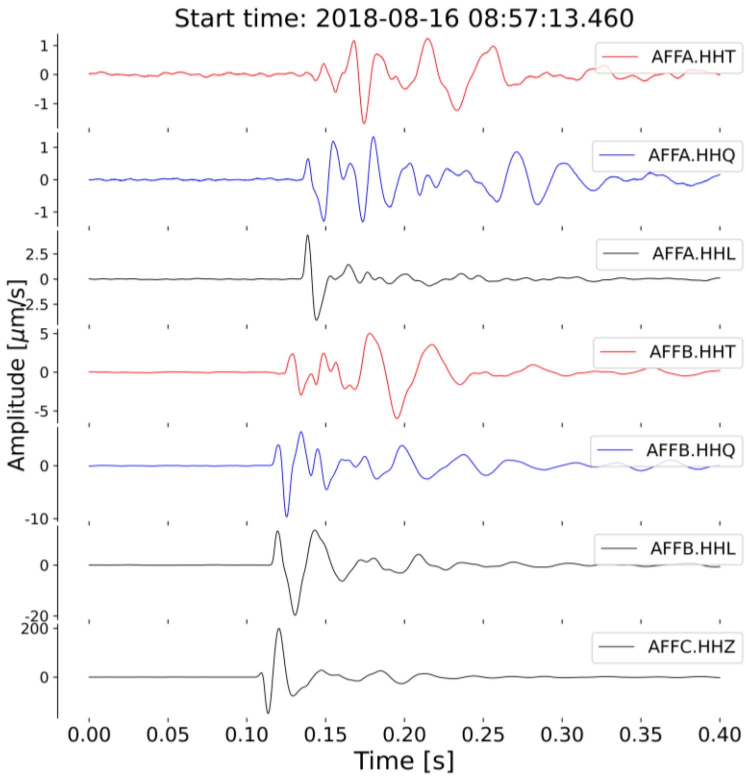

Figure 6-16. *Active source data from source point 1, each component comprises 10 stacked weight drop recordings. The deeper geophones A and B are rotated to the ray coordinate system L (black), Q (blue) and T (red). The shallow geophone C is not rotated. The instrument responses have been deconvolved.*

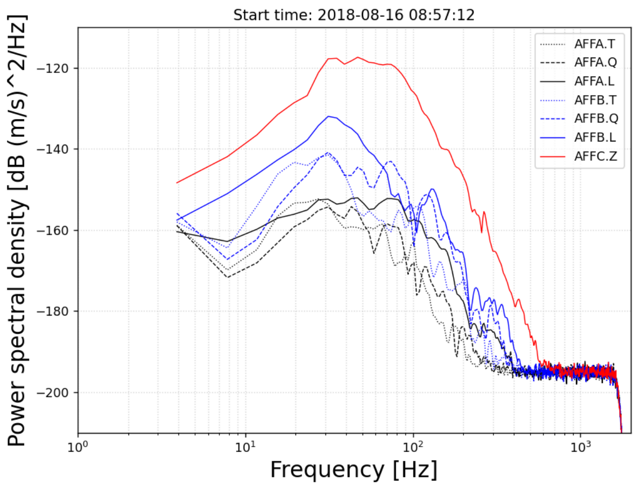

Figure 6-17. *Power spectral densities of the stacked 4 second recordings from source point 1, dB relative to 1 m/s. The deeper geophones A and B are rotated to the ray coordinate system L (black), Q (blue) and T (red). The shallow geophone C is not rotated. The instrument responses have been deconvolved.*

Source point 35, 315 m distance from the top of the borehole. Figure 6-18 shows that the P-wave is well recorded on the L-components and the S-wave on the Q- and T-components at the deeper two geophones. We see that the vertical C geophone shows very little P wave energy, as the P wave arrives almost horizontally to the geophone. The Q-component at geophone B shows more similarities with the L-component than with the T-component, possibly due to surface wave energy, whereas at the deepest geophone the Q-component is more similar to the T. The amplitudes of the largest signals are similar at the A and B geophones, between -1 and 1 micrometer per second, and the vertical C geophone has higher amplitudes, between approximately -2.5 and 2.5 micrometer per second.

The power spectra in Figure 6-19 show that the signal strength has decreased by some 25 dB from the levels at SP1. There is also less high frequency energy recorded from SP35 than from SP1, all three components reach the noise level at approximately 200 Hz and as opposed to SP1, the CZ component has lowest signal strength at higher frequencies.

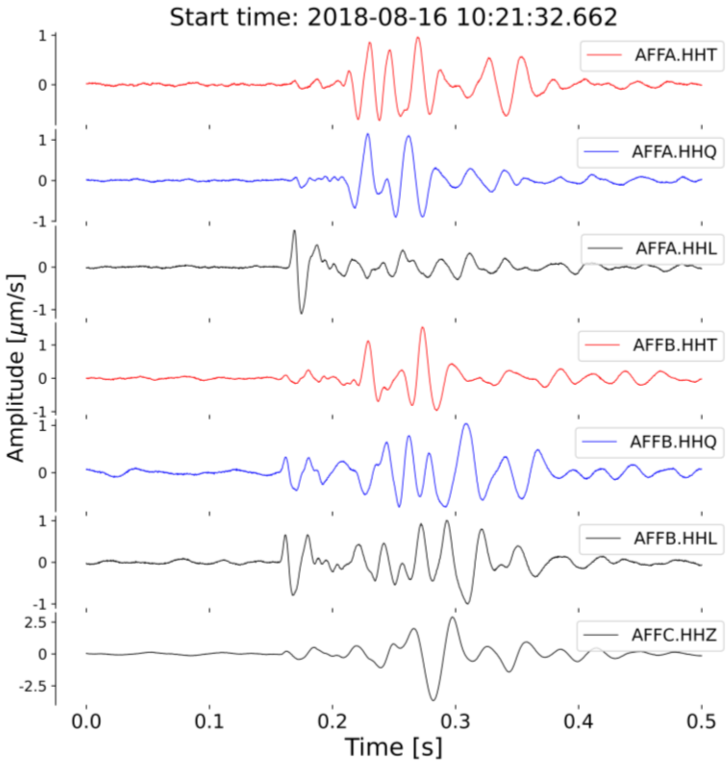

Figure 6-18. *Active source data from source point 35, each component comprises 10 stacked weight drop recordings. The deeper geophones A and B are rotated to the ray coordinate system L (black), Q (blue) and T (red). The shallow geophone C is not rotated. The instrument responses have been deconvolved.*

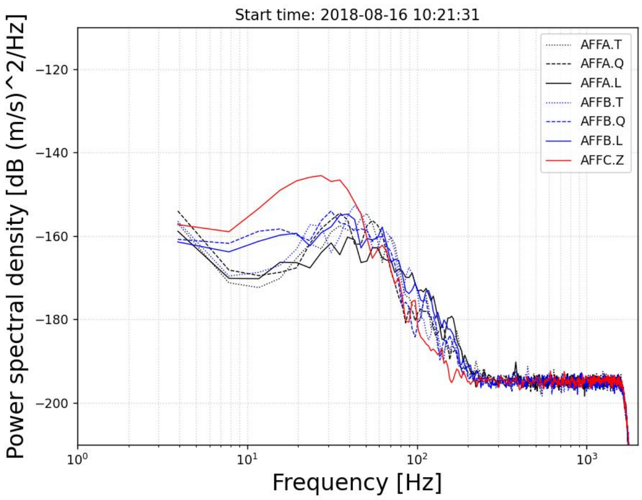

Figure 6-19. *Power spectral densities of the stacked 4 second recordings from source point 35, dB relative to 1 m/s. The deeper geophones A and B are rotated to the ray coordinate system L (black), Q (blue) and T (red). The shallow geophone C is not rotated. The instrument responses have been deconvolved.*

Source point 70, 572 m distance from the top of the borehole. Figure 6-20 shows that at this distance the P wave is still recorded with good signal-to-noise on the L-component and the S wave on the Q- and T-components at the two deeper geophones. At the C geophone the signal-to noise is significantly lower, to the point where the signal is difficult to identify. Amplitudes are higher at the deepest A geophone, approximately -0.5 to 0.5 micrometer per second, than at the other two geophones.

The power spectra in Figure 6-21 show that the background noise at 50 Hz now has a significant effect on the signal and that signal strength has decreased by some 5 dB above 50 Hz compared to the data from SP35. There is slightly less high frequency energy recorded from SP70 than from SP35, except in the L-component of the A geophone, which contains frequencies above the background noise up to 350 Hz. As in the SP35 data, the CZ-component has the least energy above 50 Hz.

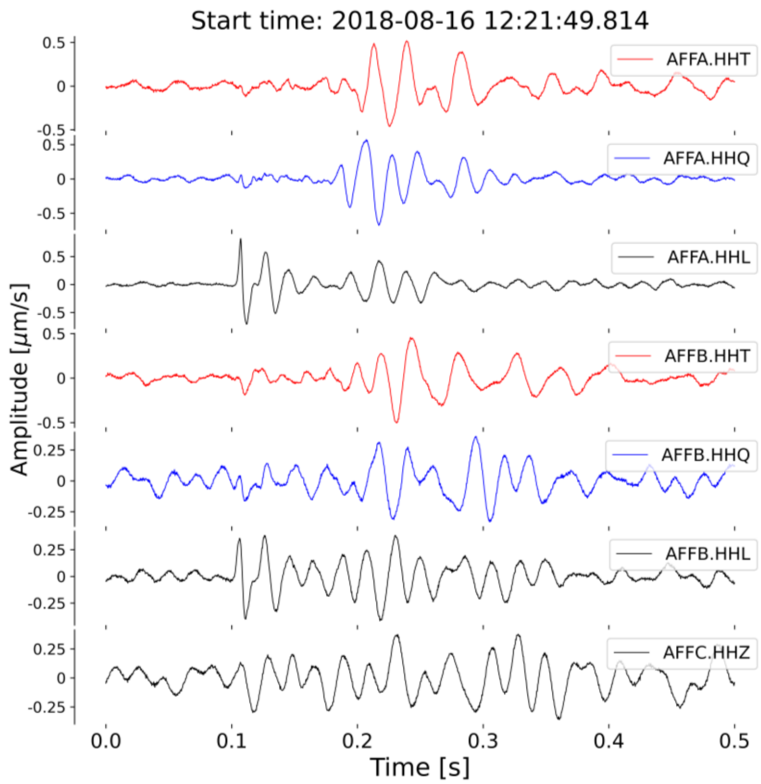

Figure 6-20. *Active source data from source point 70, each component comprises 10 stacked weight drop recordings. The deeper geophones A and B are rotated to the ray coordinate system L (black), Q (blue) and T (red). The shallow geophone C is not rotated. The instrument responses have been deconvolved.*

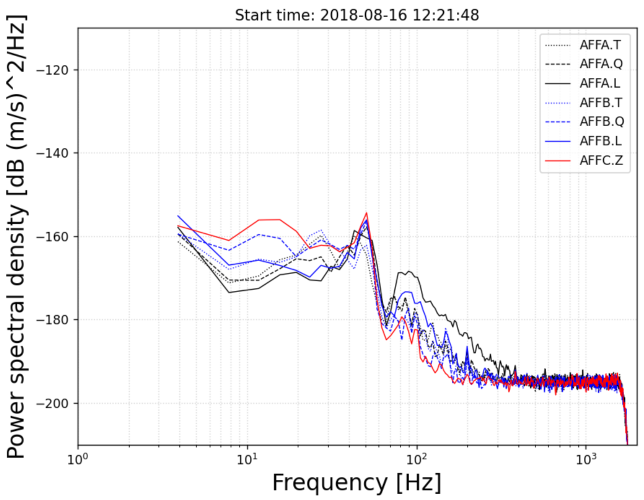

Figure 6-21. *Power spectral densities of the stacked 4 second recordings from source point 70, dB relative to 1 m/s. The deeper geophones A and B are rotated to the ray coordinate system L (black), Q (blue) and T (red). The shallow geophone C is not rotated. The instrument responses have been deconvolved.*

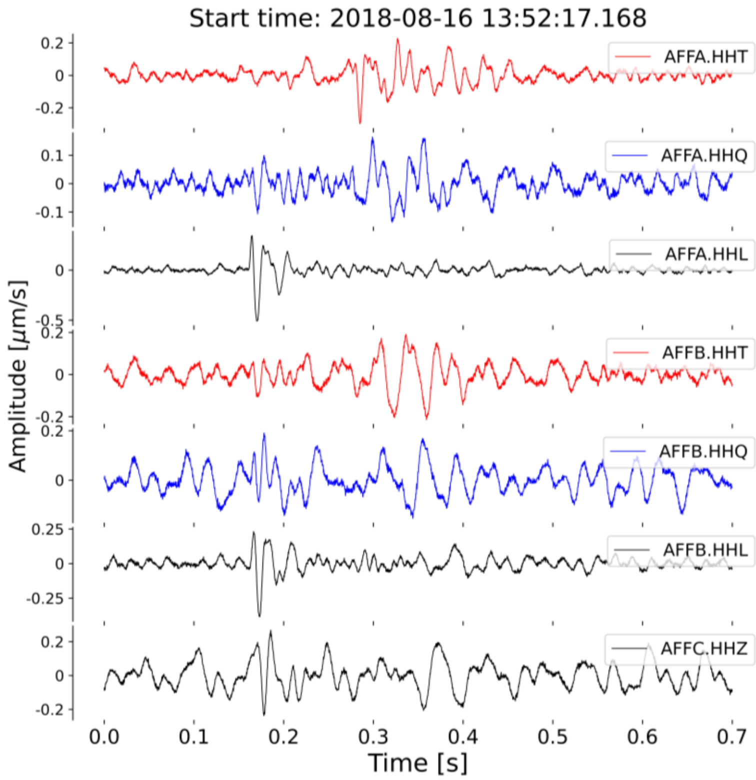

Figure 6-22. *Active source data from source point 110, each component comprises 10 stacked weight drop recordings. The deeper geophones A and B are rotated to the ray coordinate system L (black), Q (blue) and T (red). The shallow geophone C is not rotated. The instrument responses have been deconvolved.*

Source point 110, 897 m distance from the top of the borehole. Figure 6-22 shows increasingly noisy data. The P wave is, however, still well resolved on the L-components of the deeper two geophones, and the S wave is discernible on the Q- and T-components of those geophones. Interestingly, the P wave is now also clearly seen on the vertical C geophone as a sharp, higher frequency phase. This is likely because the source point is now so far away that the wave propagates through higher velocity lower layers and then turns upward toward geophone C. Signal amplitudes are generally lower than those from SP70, with the A geophone S waves particularly smaller.

The power spectra in Figure 6-23 show that at this distance the background noise at both 50 Hz and 100 Hz affects the signal. The signal strength has decreased somewhat compared to the data from SP70. The A geophone has the highest signal strength at high frequencies, as at shorter distances, and the CZ-component has the least energy above 50 Hz.

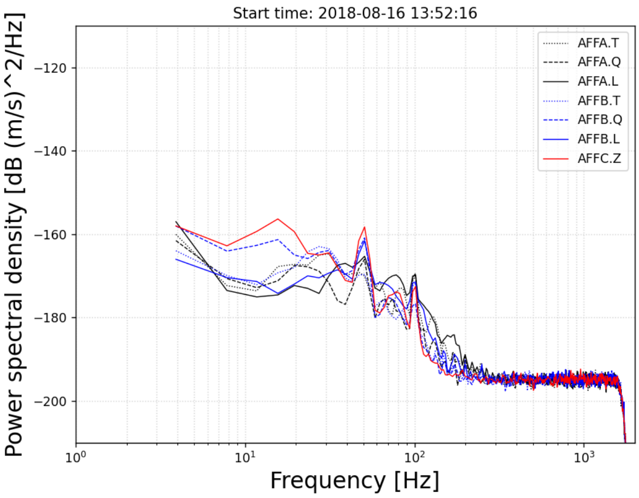

Figure 6-23. *Power spectral densities of the stacked 4 second recordings from source point 110, dB relative to 1 m/s. The deeper geophones A and B are rotated to the ray coordinate system L (black), Q (blue) and T (red). The shallow geophone C is not rotated. The instrument responses have been deconvolved.*

In Figures 6-24 and 6-25 we compare the spectra of the L- and Q-components from the A and B geophones of the four stations above. As discussed above, the energy and frequency content are, of course, largest at the nearest source point, 1, followed by SP35. However, the differences between source points 35, 70 and 110 are not very large, and depend to some extent on the studied component and which frequency we look at. The deepest sensor A tends to record somewhat higher frequencies above the noise floor than the middle geophone B, while B tends to have higher amplitudes than A.

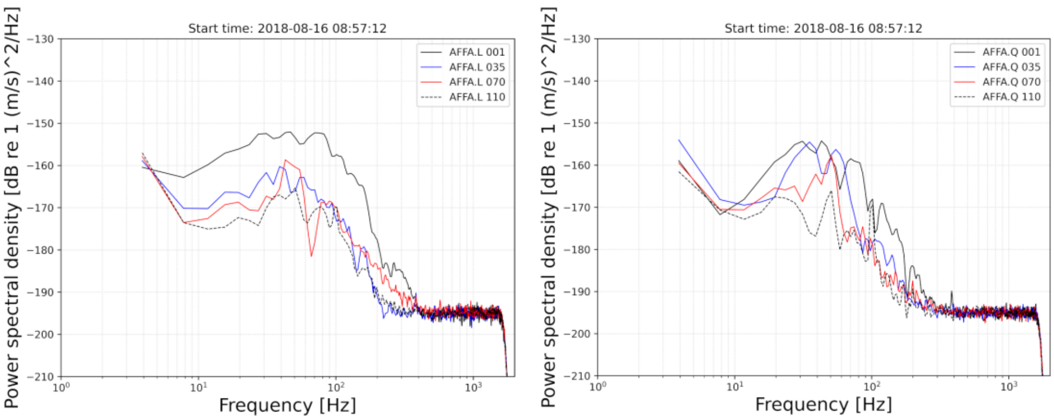

Figure 6-24. *Power spectral densities of the stacked 4 second recordings at geophone A from source points 1 (black, solid), 35 (blue), 70 (red) and 110 (black dashed), dB relative to 1 m/s. The instrument responses have been deconvolved. Left) L-components. Right) Q-components.*

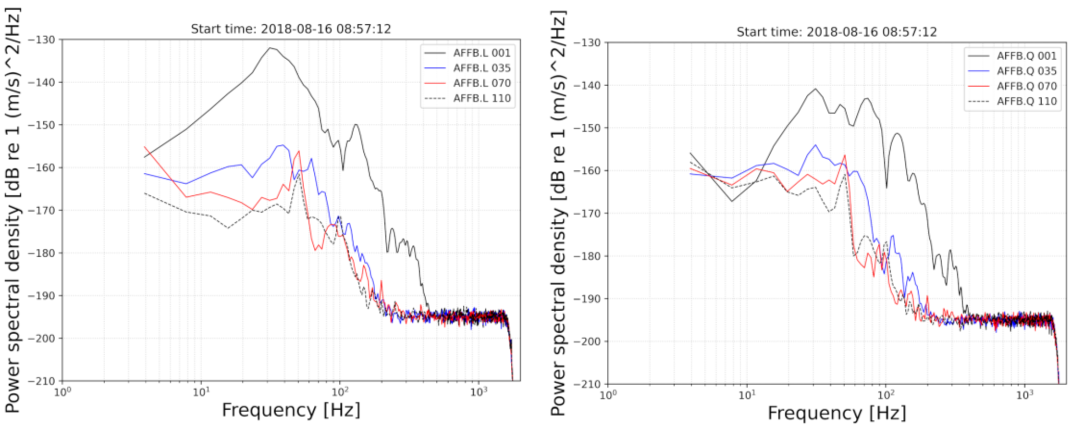

Figure 6-25. *Power spectral densities of the stacked 4 second recordings at geophone B from source points 1 (black, solid), 35 (blue), 70 (red) and 110 (black dashed), dB relative to 1 m/s. The instrument responses have been deconvolved. Left) L-components. Right) Q-components.*

6.3.2 Receiver gathers

In this section we show figures with all the active sources recorded on a certain component at a certain geophone in the borehole. The data has been stacked, every source point has 10 stacked weight drops, increasing signal-to-noise. The traces are rotated to the ray coordinate system, with components L, Q and T, and have been individually normalized. The distance, in the plots have been calculated as the distance from the source point to the geophone at depth, i.e. SP1 is located on the surface 13.6 m from the borehole and as the depth of geophone A is 188 m the data is plotted at a distance of 188.5 m from geophone A. Similarly, the distance of SP1 is 76.7 m for geophone B and 15.1 m for geophone C. The lack of data close to the borehole depends on restrictions whereby no weight drops could be made, and the data gap around 650 m distance is due to the geometry, where source points 70 – 79 are at similar distance to the borehole, and source points 80 and 81 could not be used, see Figure 4-1.

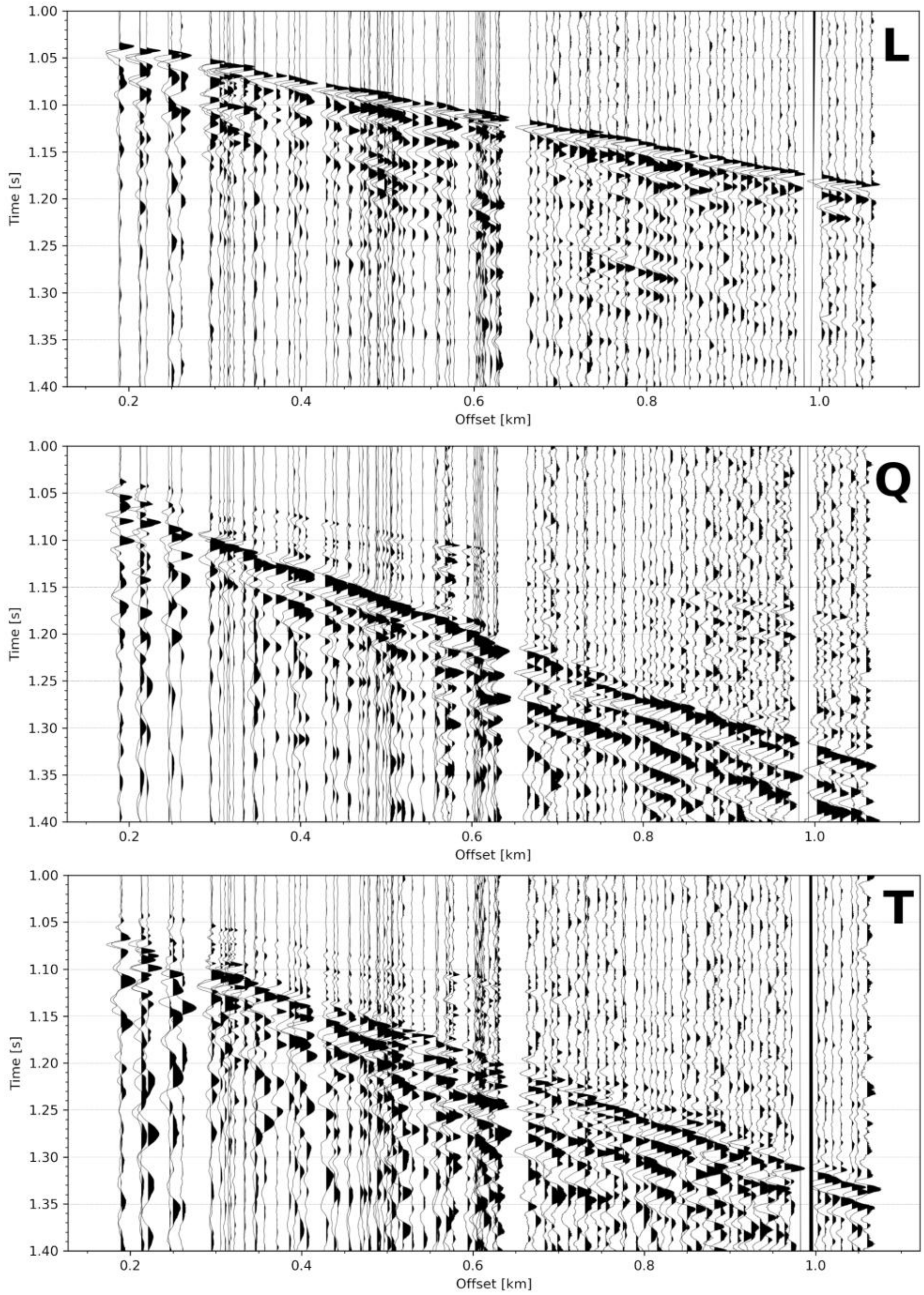

Figure 6-26. *Receiver gathers for geophone A, at 188 m depth. The three components of the geophone have been rotated to the ray coordinate system, LQT. The traces are individually normalized and positive amplitudes are filled with black.*

Figure 6-26 shows that the P-wave is very well recorded on geophone A, where the along-the-ray L-component has good signal-to-noise ratio for all source distances. Similarly, the S-wave is clearly recorded on the Q-component, for all source distances. There are weak indications of P-wave energy on the Q- and T-components, most likely resulting from uncertainties in the true take-off angles in the rotation of the components. The linearity of the arrival data makes it possible to estimate average P- and S-wave velocities, which for geophone A are: Vp = 5.8 km/s, Vs = 3.25 km/s.

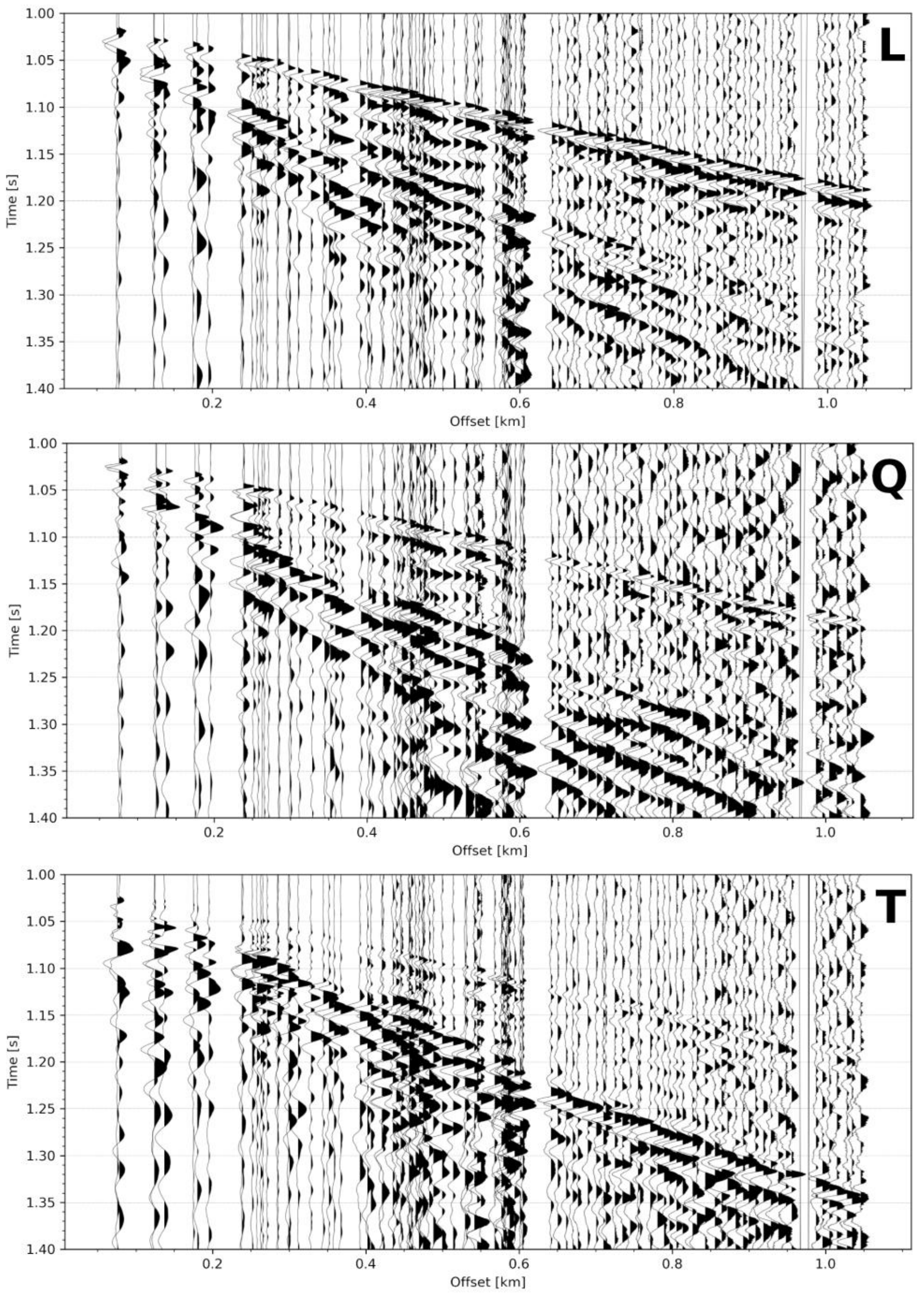

Figure 6-27. *Receiver gathers for geophone B, at 75 m depth. The three components of the geophone have been rotated to the ray coordinate system, LQT. The traces are individually normalized and positive amplitudes are filled with black.*

Geophone B, at 75 m depth, show the P-wave arrivals on the L-component just as clearly as geophone A, with high signal-to-noise ratio even for the furthest sources, see Figure 6-27. The S-wave arrivals on the Q-component are more complex than for geophone A and the phases seem less well separated in the data on geophone B than on geophone A. We see, for example, that there is appreciable P-wave energy on the Q-component, and some on the T-component for geophone B. This is probably due to ray paths that agree less well with the simple straight lines used to rotate the data. It is not unlikely that the rays have penetrated below 75 m to a higher velocity region and then impinged on geophone B from below. Estimating the average velocities from the linearity of the data we find: V_p = 5.5 km/s, V_s = 3.0 km/s, slightly lower values than for geophone A.

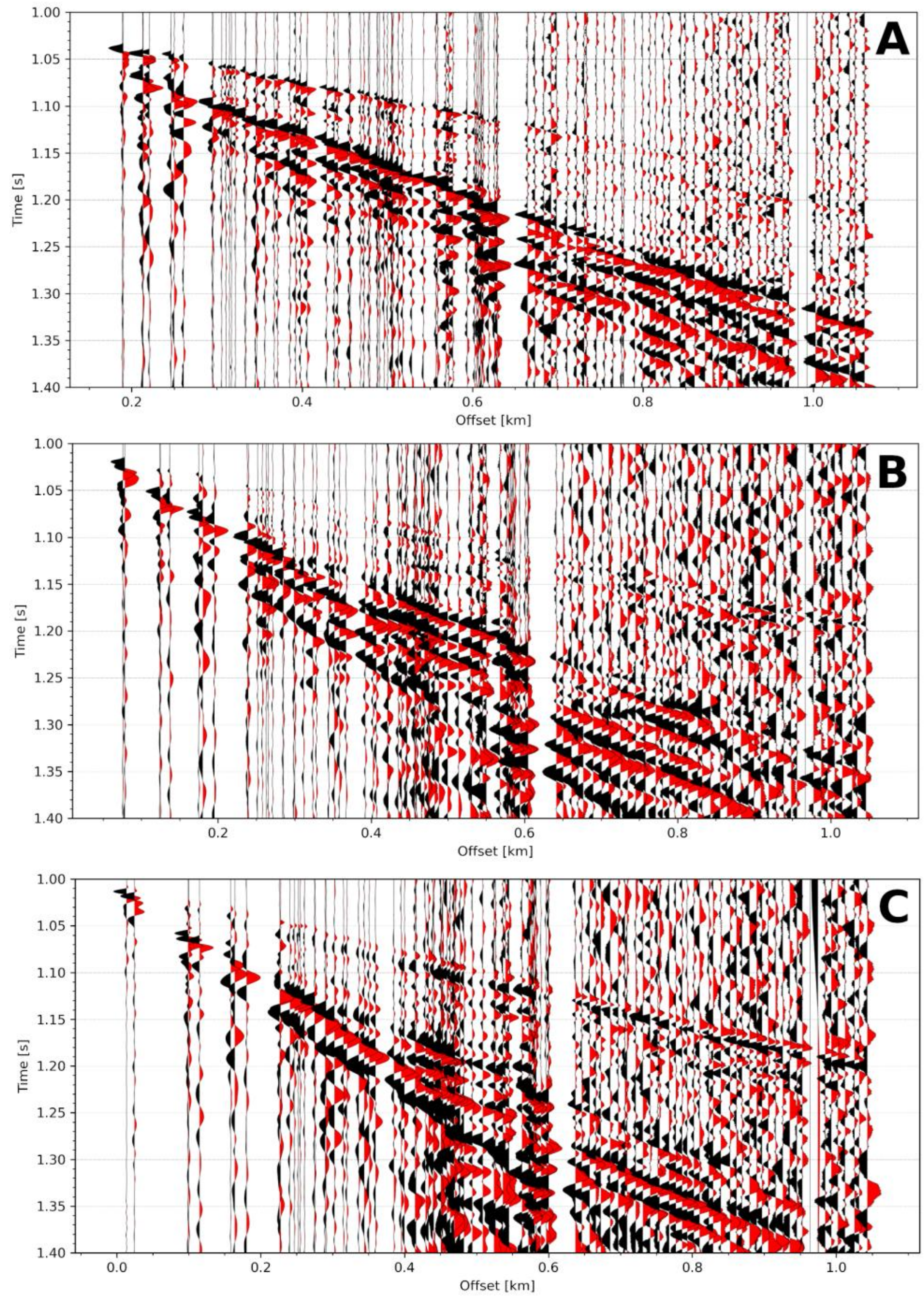

Figure 6-28. *Receiver gathers for the vertical components (Z) at geophones A (188 m depth, top), B (75 m depth, middle) and C (6.5 m depth, bottom). The traces are individually normalized and positive amplitudes are filled with red, negative with black.*

In order to assess the directionality of the incoming waves we plot the vertical component data from geophones A, B and C in Figure 6-28. The wiggles are now coloured red in the positive part and black in the negative. We see for geophone A that the first motions on the Z-component are negative (black), indicating a down-going wave, to as far distances as the P-wave can be identified. This confirms that the wave travels from the surface down to 188 m depth, although from 600 – 700 m distance it propagates more or less horizontally. The vertical component data from geophone B similarly shows that there is very little vertical energy at far distances, but also that there is an indication that the first motions change polarity at about 400 m distance. It is, however, not clear how well this trend continues at longer distance. We conclude that there is a possibility that the rays arriving at geophone B from distance beyond 400 m have propagated below the geophone.

The data from geophone C, which only has a vertical component, in Figure 6-28 clearly show that beyond about 200 m the P-wave arrives from below the geophone, as expected. At shorter distances the incidence angle is less clearly defined. The P-wave arrival does not have very large signal-to-noise ratio but it is relatively well indicated in Figure 6-28. Estimating the average velocities, we find: Vp = 5.5 km/s, Vs = 2.9 km/s where the S-velocity has significant uncertainty.

The P-wave arrival on the L-components of geophones A and B is very clear and in Figure 6-29 we show the signal-to-noise ratio (SNR) for the P-wave on the L-components. Both signal and noise windows are 20 ms long, and in each window we calculate the RMS and then take the ratio of the RMS in the signal and noise windows. We see in Figure 6-29 that SNR is very high at both geophones, decreasing significantly below 3 only for the two poorly recorded sources around 1,000 m. We also note that SNR is generally higher at geophone A, located at 188 meter depth. There is some scatter in SNR from sources near the borehole, which to some extent depends on variations in frequency content in the recorded waveforms. Applying a bandpass filter can significantly alter the SNR values, as can variations in window length.

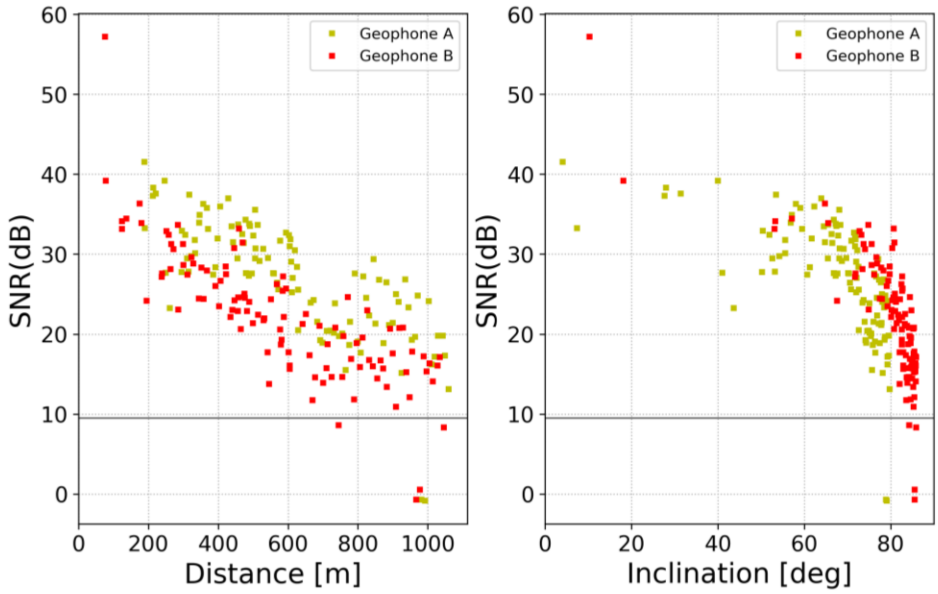

Figure 6-29. *Signal-to-noise ratio (SNR) in decibel versus distance (left) and inclination (angle between vertical and incoming ray, right). L-component at geophone A (yellow), L-component at geophone B (red). The horizontal line indicates SNR = 3.*

6.4 Summary

Three IMS high-sensitivity geophones were installed in borehole HFM42; one three-component geophone at 188 m depth, one three-component at 74 m depth and on vertical component geophone at 6.5 m depth. The geophones all operate as expected. Studying ambient noise levels, recorded seismic events and the active source data, we find:

- The ambient noise recorded in HFM42 shows a similar spectral shape as that observed by Lund et al. (2017); there is a wide noise peak between 3 Hz and approximately 200 Hz and there are strong noise peaks at 25 Hz, 50 Hz, 100 Hz, 150 Hz and further overtones.
- The ambient noise slightly decreases from the 6.5 m geophone to the 74 m geophone, but significantly decreases from 74 to 188 m, by as much as 10 – 20 dB. Interestingly, the lower frequency noise is strongest at the uppermost geophones but the 100 Hz noise is stronger at the lowermost geophone. This is likely due to lower noise attenuation because of more competent rock at depth.

- We find good agreement between the absolute ground motion recorded by different instruments near the surface; the uppermost HFM42 vertical IMS geophone with the Affinity digitiser, a nearby vertical IMS geophone in a shallow (60 cm deep) borehole connected to a Guralp DM24 digitiser, a broad-band Guralp seismometer connected to a Guralp DM24 digitiser and old recordings (Lund et al., 2017) with a shallow vertical IMS sensor and an IMS digitiser.
- Ambient noise recordings at night during the time period August 2018 to March 2019 show a surprising general stability in terms of spectral amplitudes. There is a slight increase in lower frequency amplitudes with time, potentially due to increased power production during winter, but it is small. At particular frequencies, such as at 50 Hz and 100 Hz, there are significant temporal variations.
- The geophones in HFM42 successfully recorded both a magnitude 0.4 local earthquake at 14 km distance and a magnitude 2.9 regional earthquake 65 km away. Single station magnitude estimates in agreement with the SNSN magnitudes were possible to estimate in specific frequency ranges.
- Local blasts near the HFM42 borehole were recorded at sampling rates 1 kHz and 2 kHz. The records show that the geophone systems can detect energy above the system noise levels at frequencies up to 800 Hz.
- Active source data, from stacked weight drops, were used to investigate the variation in spectral amplitudes with distance. For a near-by source we found that the geophone system recorded ground motion above the system noise up to 600 Hz. At 315 m distance the active source signal is still recorded above the ambient noise levels. At 572 m distance the P- and S-waves are well recorded on the two deeper geophones but the signal is affected by the 50 Hz noise. At 897 m distance the P-wave is still well resolved and the S-wave discernible, but the data is now affected both by the 50 and 100 Hz noise peaks and the general ambient noise.
- The active source data was also used for receiver gathers, rotating the three-component geophones into the ray coordinate system in order to maximize P- and S-wave energy. The gathers show arrivals all the way out to 1.05 km distance making it possible to estimate effective seismic velocities for the three geophones in HFM42. We find for geophone A velocities of Vp = 5.8 km/s, Vs = 3.25 km/s, for B: Vp = 5.5 km/s, Vs = 3.0 km/s and for C: Vp = 5.5 km/s, Vs = 2.9 km/s, where the S-wave velocity for C has significant uncertainty.
- We calculate signal-to-noise ratios (SNR) for the active source P-wave data, rotated to the along ray L-component, for the 74 m and 188 m deep geophones. The SNR is above 3 for both geophones at all shot points, except for two poor shots at about 1 km distance. The SNR at the geophone at 188 m depth is generally higher than at the 74 m deep geophone.

In combination with the results of Lund et al. (2017), we see that noise levels generally decrease away from the nuclear power plants, and at deeper levels in the bedrock. Since we only have three geophones in the borehole we cannot say exactly how noise decreases with depth, but since the geophone at 74 m depth is located in a less competent rock mass (FFM02) than the geophone at 188 m depth (in FFM01), and the difference between the 6.5 m and the 74 m geophones is not very large, it seems that the lower rock mass FFM01 is quieter than rock mass FFM02. This indicates that the Forsmark seismic network should aim to locate as many sensors as possible in rock mass FFM01. We do not yet know if this conclusion holds in areas where rock mass FFM01 is shallower, this will be tested with the installation of the network. However, as a good 3D sensor coverage of the volume of interest is very important, not all sensors can be located at depth.

7 Comparison of Carina and surface seismic data using an active source

The active source weight drop and the layout of source points and CDP-line was outlined in Section 4.1. First, we present some results from active source recordings on the Carina cable and then results from recording on the surface geophones. Ideally, reflections observed on the surface seismic would also be observed on the borehole data. However, this turns out not to be the case. We also compare the new CDP data to a previously acquired profile in the area.

7.1 Carina data

The unstacked Carina data appeared quite noisy, with some difficulty in identifying the first arrivals from the far offset source points. After sorting by source point and then stacking (vertical fold of 10) the signal to noise ratio improved. Two source gathers close to the borehole are shown in Figure 7-1. The Carina data will later be compared to the geophone data (geophones installed at c. 6 m, 75 m and 187 m). Therefore, it is of interest to look at receiver gathers from these depths for the Carina data (Figure 7-2).

In order to test if there is any noticeable decrease in amplitude of the downgoing wave that can be attributed to attenuation in the rock the data from SP1 (closest to the borehole so the ray path is nearly vertical) were corrected for geometrical spreading, filtered (30-50-150-250 Hz) and linear moved out (velocity 5750 m/s with a time shift of 100 ms) (Figure 7-3: left). After linear moveout the first arrivals appear nearly at the same time at about 100 ms. It is only in the uppermost 10 meters or so that there is a slight delay. This indicates that at the location of the borehole the seismic velocity is nearly constant at 5750 m/s below the uppermost 10 m. The velocity may be lower in the noisy zone at about 50 m depth (Figure 7-3: left), but the actual value cannot be determined from the data due to the noise. The noise in the 40-60 m interval is due to the cable being defective as mentioned previously. After linear move-out the peak amplitude of the first arrival was picked and plotted (red curve in Figure 7-3). There is no clear decreasing trend in the amplitude with depth that would indicate that a Q value can be calculated. Instead the amplitude variations appear to be governed by borehole coupling and local variations in scattering near the borehole.

After linear move-out with the appropriate velocity waves that are propagating vertically down the borehole will arrive at the same time (100 ms for the case of the first arrival). These waves can be removed or nearly removed by applying a median filter that rejects waves with the same arrival time. This is a standard procedure in VSP processing, allowing waves propagating at another angle to better stand out. After median filtering and removal of the linear move-out (Figure 7-3: right), there are still no arrivals propagating up the borehole (or at any other angle) that can be identified as reflected P-waves. There is one coherent event at about 190 ms that could possibly be a reflected S-wave. Its apparent upward propagating velocity is about 3800 m/s. If indeed an S-wave, it is then arriving at angle to vertical of about 30 degrees.

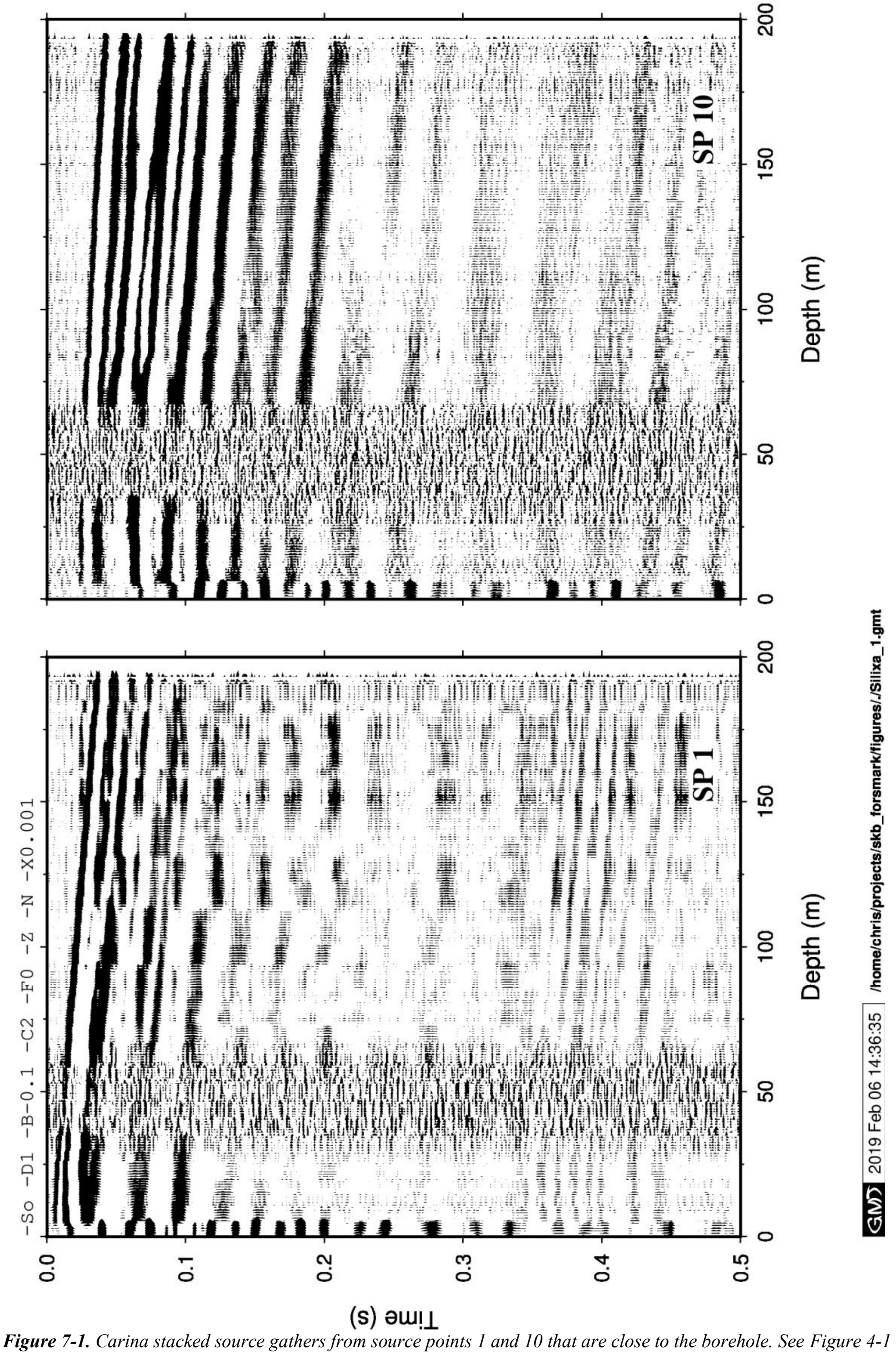

Figure 7-1. *Carina stacked source gathers from source points 1 and 10 that are close to the borehole. See Figure 4-1 for locations. Data have been trace normalized prior to plotting.*

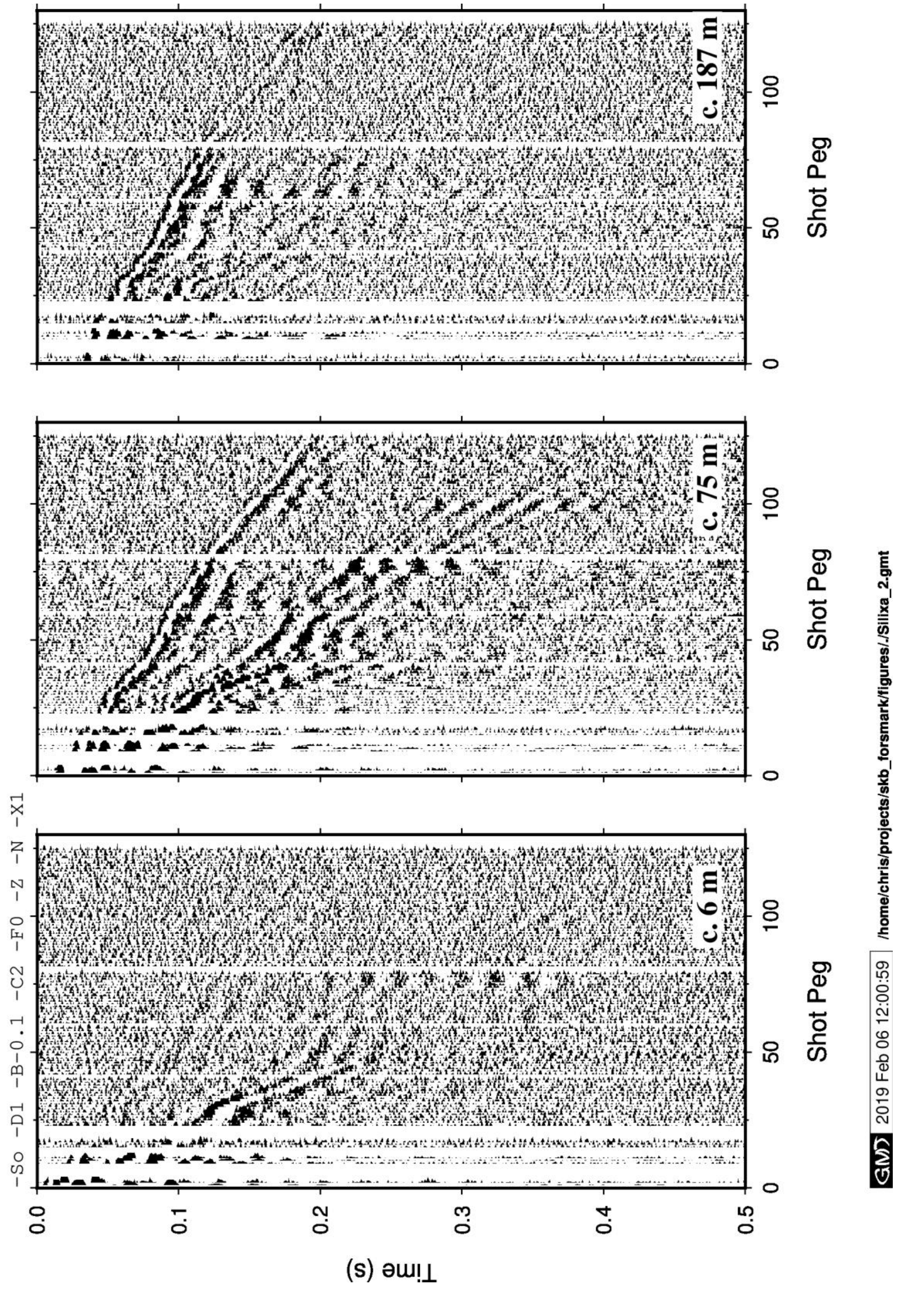

Figure 7-2. *Carina stacked data for depths corresponding to c. 6 m, 75 m and 187 m. Data have been trace normalized prior to plotting.*

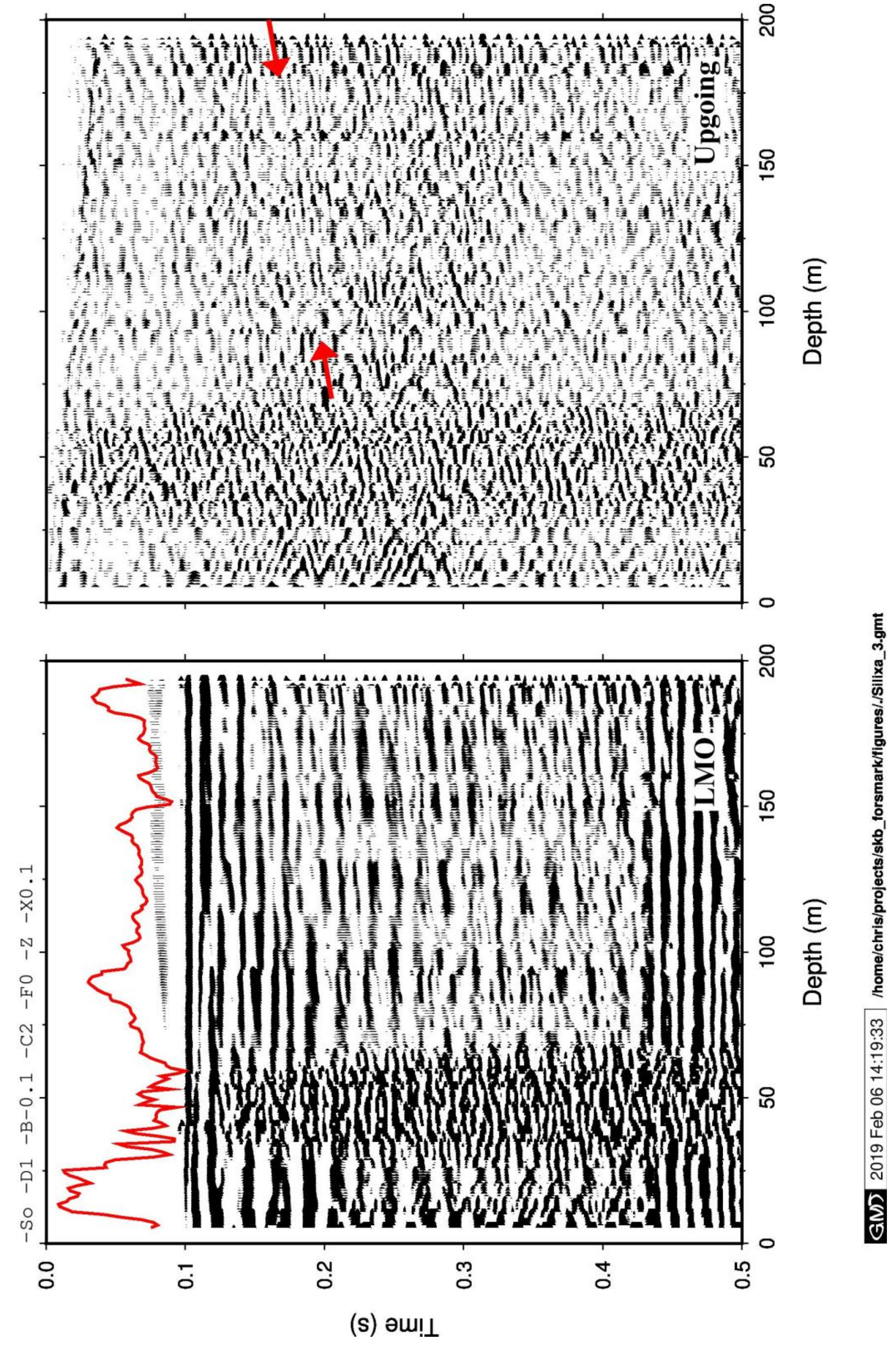

Figure 7-3. *Carina data from source point 1. Data have been time shifted by distance to the source point divided by a velocity of 5750 m/s and then shifted down 100 ms. Red curve on top is the picked maximum amplitude in the first arrival after corrections for geometrical spreading of the wave-front. Data have not been trace normalized prior to plotting. (right) Up-going wavefield after removal of the down-going wavefield by median filtering. There are no clear P-wave reflections in the up-going wavefield. There may be a potential S-wave reflection (marked by red arrows).*

7.2 CDP processing of the surface seismic profile

The surface seismic data that were acquired along the active source line were processed as CDP data following a similar processing sequence as used in the past (e.g. Juhlin et al., 2002). Main processing steps included refraction statics, bandstop filtering of 50 and 100 Hz noise, deconvolution, bandpass filtering (60-90-240-Hz at 0 s to 40-60-150-250 Hz at 0.4 s), trace balance, median filter (3300 m/s and 5800 m/s), NMO, stack and FX-decon. The purpose of this processing was to ensure that the active source was powerful enough to generate clear signals that could be detected by the borehole sensors and to investigate if any new structures could be detected. Previous profile 4 (Juhlin et al., 2002) was partly acquired along the same road as the active source profile in this study, but with a dynamite source. Note that the northern part of the active source profile is not coincident with previous profile 4 so that the two surveys did not cover exactly the same sub-surface (see Figure 4-1).

Figure 7-4 shows stacks of the active source profile and that part of profile 4 that runs nearly parallel to it and covers approximately the same N-S section. At times of about 1 s the results are very similar with the active source profile showing clearer reflections on its southern part. Given that 1 s time corresponds to depths of about 3 km (travel paths of 6 km) it is clear that the source was powerful enough to generate strong signals, at least along the southern part. The fact that the image deteriorates towards the north at these times may be due to poorer coupling of the source or to geometrical effects. Considering the 2nd point, profile 4 extended farther to the north and sources from north of the profile are included in the processing. For a fairer comparison the profile should be reprocessed using just sources and receivers corresponding to those locations which were used for the active source profile in this study. The moderately steeply dipping reflectivity between 0.4 and 0.7 s (A1 reflection in Juhlin et al., 2002) is better imaged on the dynamite data (previous profile 4). This may be either due to geometrical effects, as mentioned above, or to that the dynamite source generated higher frequencies.

In the uppermost 0.1 s there are number of apparent sub-horizontal reflections present on the active source profile that are absent on profile 4. None of these are obvious in the source gathers, making them uncertain. However, every effort has been made to remove noise and the influence of first breaks stacking in as reflections. Furthermore, the reflection at about 0.08 s stacks in at about 5600 m/s, a velocity close to what is expected based on the fibre-optic measurements in the borehole (Figure 7-3). At present, it is likely that these sub-horizontal reflections represent a real structure in the subsurface. In the 3D survey acquired in 2016 (Lundberg et al., 2018) and in two high resolution profiles acquired in 2011 (Brojerdi et al., 2011) reflections originating from similar depths have been observed. These reflections appear to be localized to certain areas and do not have lateral extents of more than a few 100s of meters. It is not currently clear whether these reflections originate from fracture zones or lithological boundaries. Fracture zones near the surface may be highly heterogeneous with rapidly varying thickness, resulting in that observable reflections are generated where the zones are thicker. Lithological contrasts may also vary rapidly and it is possible that small lenses of mafic rock are present at depth. Such lenses could also generate localized reflections. Since previous profile 4 had a different sub-surface coverage it may not have crossed the structure with such a geometry that it could be imaged. High resolution seismic surveying (2 m station spacing with a dynamite source with some offset shot points for 3D coverage) or drilling to 300 m could confirm (Figure 7-5) the structure and supply information on its nature. EM methods may also provide additional clues.

The sub-horizontal reflections at 0.08 s (Figure 7-5) are not observed on the Carina cable data. However, it is not clear if these potential structures extend all the way to the borehole in which the cable was installed.

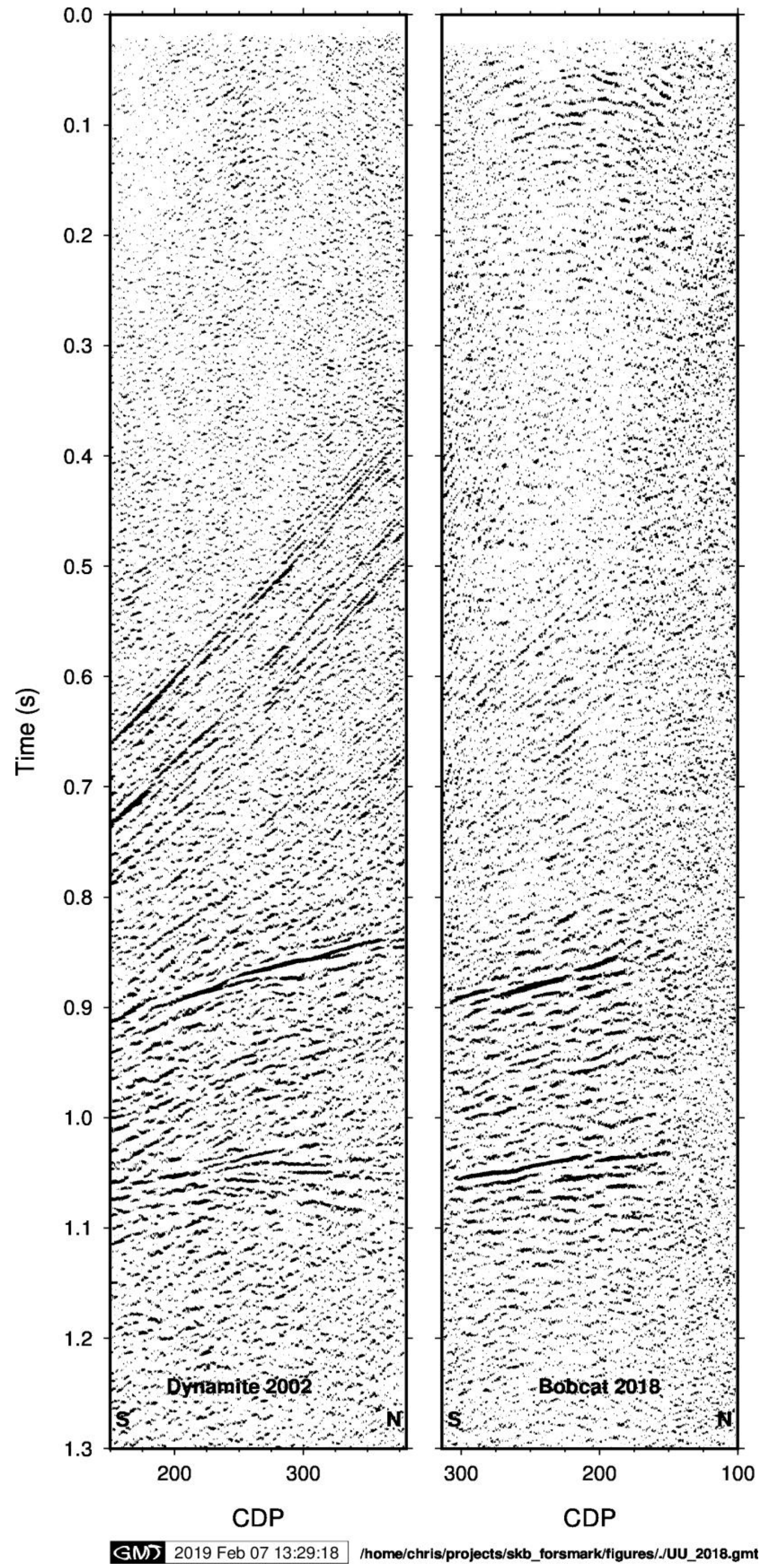

Figure 7-4. *Comparison of stacks from previous profile 4 (Juhlin et al., 2002) and the active source profile in this study. For location of CDP points (horizontal scale) see Figure 4-1. CDP spacing is 5 m.*

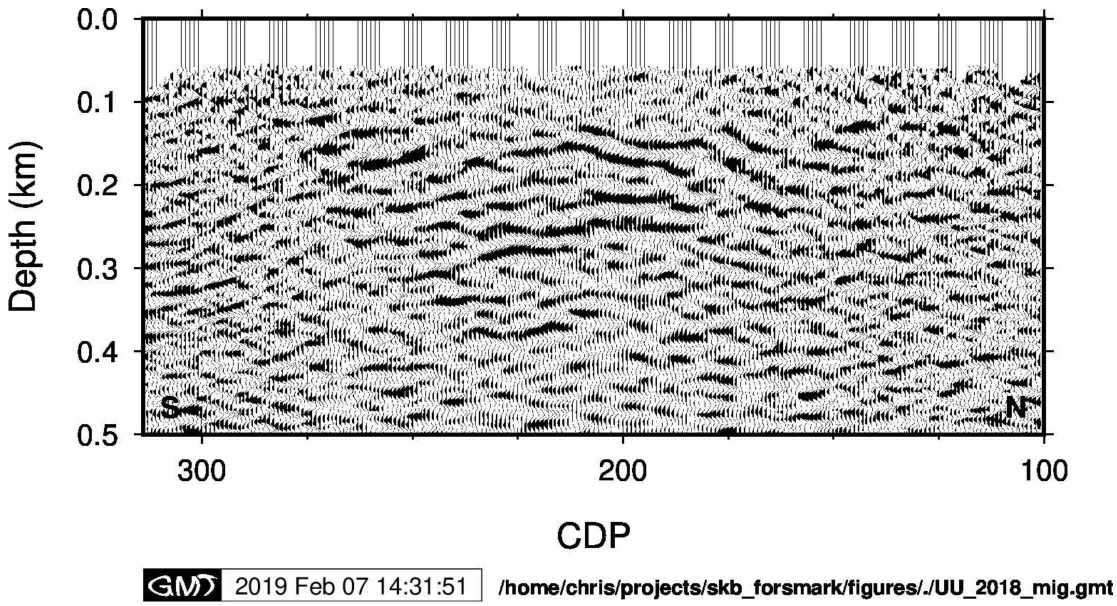

Figure 7-5. *Migrated and depth converted section of the active source profile showing the uppermost 500 m. A velocity of 5600 m/s was used for the depth conversion.*

8 Comparison between fibre and geophones

One aim of the field test is to compare the performance of the iDAS, Carina and geophones. A direct comparison is difficult as there are differences in both the measurements and the coupling with the formation of the geophones and the fibres. The differences in measurement characteristics of the technologies are summarised in Table 8-1.

As earthquakes, or other events generating seismic events, generally do not occur repeatedly in the same location during a short period of time with similar source mechanisms we start this section by looking at individual and stacked recordings of weight drops on the fibres and geophones. We then study similarities in stacked weight drop recordings, investigating phase, amplitude, signal-to-noise ratio (SNR) and frequency content.

When rotating the three-component geophone data to the ray coordinate system below, incidence angles have been calculated by a simple, straight ray geometry. This is not quite correct, as the analysis in Section 7.1 showed that the uppermost 10 meters of the subsurface at the borehole has lower velocity than the more intact bedrock below and thus incidence angles are slightly underestimated. As the low-velocity layer below the weight drops in most places only is a few meters thin, we estimate that the effect is small.

Note, due to data recording the Carina data has the wrong polarity and is corrected in the following analysis.

Table 8-1: Summary of general geophone and DAS measurement characteristics in borehole deployments.

Characteristic	Geophone	DAS
Measurement type	Point measurement of particle motion	Distributed measurement of strain/strain-rate
Spatial sampling	m-scale	Down to 0.25m
Instrumentation coverage in borehole	Generally up to 100s m	The full length of the borehole (max 10s km)
Number of components	Often 3C	1C
Sampling rates	Up to 4 kHz	Up to 10kHz (100kHz can be available)
Temperature	Standard up to 80°C (max approx. 210°C)	Standard up to 85°C (max >300°C)
Lifetime	Standard <10 years	10s years
Electronics & parts	No electronics. Mechanical parts.	Electronics at surface. No mechanical parts downhole
Other		Multiple simultaneous measurements possible (e.g. temperature & strain-rate)

Comparing individual and stacked recordingsFigure 8-1 shows the Carina records of each of the 10 weight drops at SP58, 469 meters from the borehole, recorded at 188 m depth. The data have been time integrated but not amplitude converted. There are appreciable differences in the recordings, although all 10 weight drops were performed during a time period of only 60 seconds. Differences could be due to slight variations in the impact of the weight, or perhaps more likely, variations in the noise conditions close to the borehole. On recordings 4 and 7 it would be non-trivial to detect the incoming phase, or determine the first arrival. However, when the 10 recordings are stacked (lower black seismogram in Figure 8-1) the noise is significantly suppressed and the phase arrivals clearer.

Comparing all recordings at 188 m depth of the first weight drop at SP58, we see in Figure 8-2A that the Carina and helical iDAS record show a similar first arrival and that the Carina data has better SNR. On the linear iDAS the first arrival is not visible. The geophone data shows a rather small vertical first arrival and significantly clearer north component arrival, indicating that the incoming wave is close to horizontal. Figure 8-2A shows that the noise on the geophone is generally lower than that on the fibres. Stacking the 10 weight drops, Figure 8-2B, improves the SNR of the Carina and iDAS helical data considerably, but the iDAS linear data is still too noisy to identify the P-wave, due to its horizontal incidence. Making use of the dense spatial sampling of DAS, it would also be possible to improve fibre data SNR using channel stacking over, for example, a gauge length.

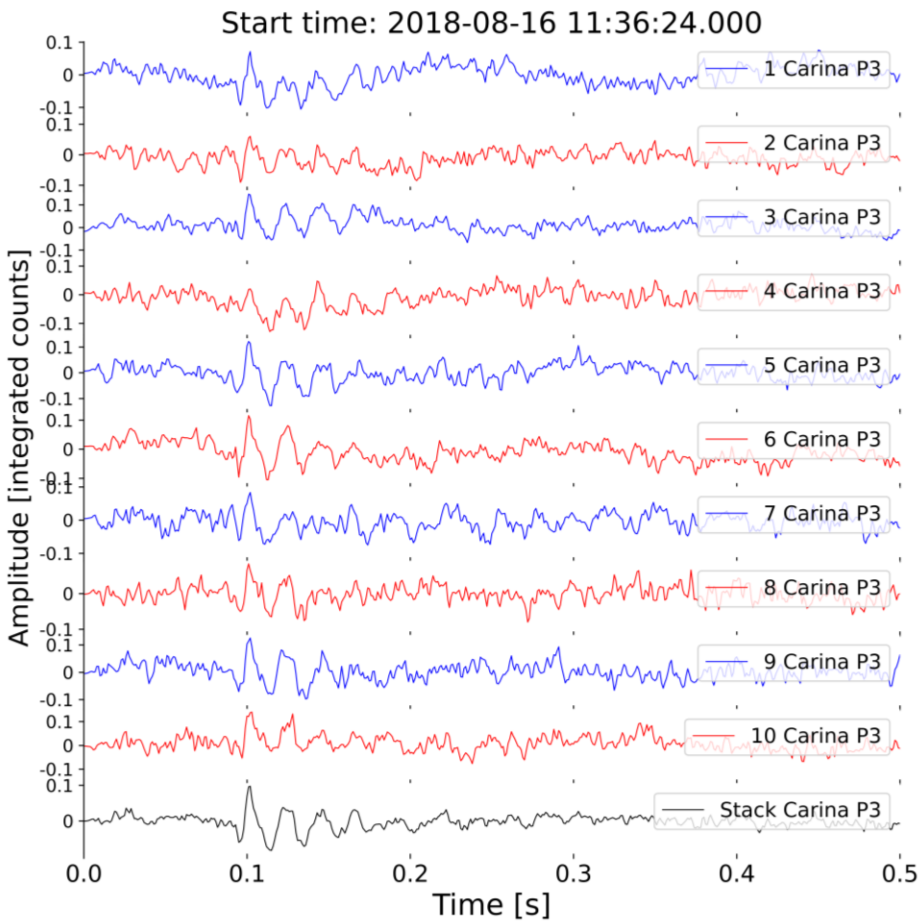

Figure 8-1. *Recordings of the 10 weight drops at source point 58 on the down-going Carina fibre at 188 m depth, and at the bottom a stack of the 10 recordings. The data has been time integrated and high-pass filtered above 10 Hz.*

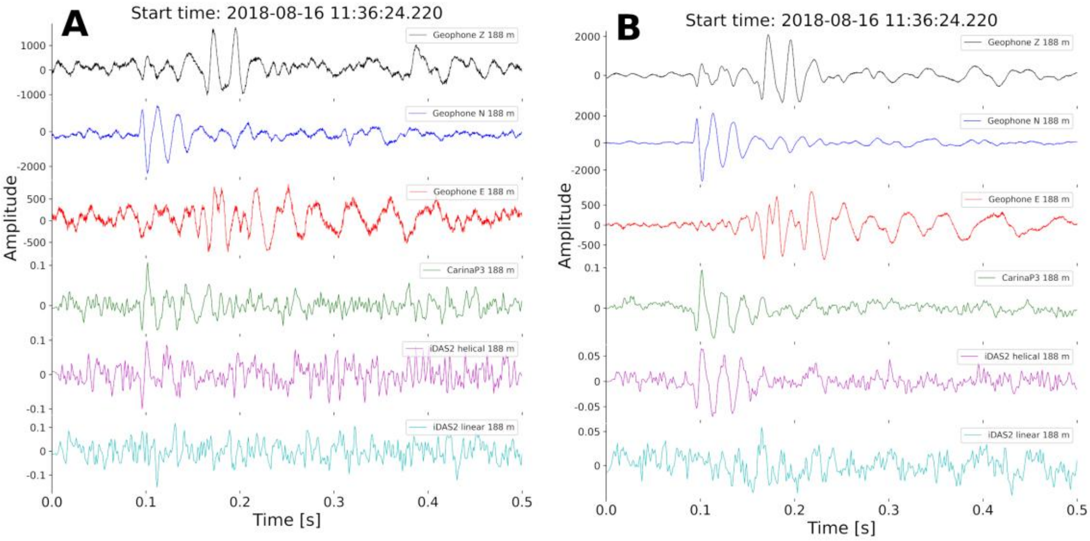

Figure 8-2. *Recordings from 188 m depth of weight drops at source point 58, 469 m from the borehole. Upper three recordings are from geophone A, with the Z-component in black, N-component (blue) and E-component (red). The lower three are fibre recordings, time integrated and high-pass filtered at 10 Hz. Carina (green), iDAS helical (magenta) and iDAS linear (cyan). A) First weight drop in the series. B) 10 stacked weight drops.*

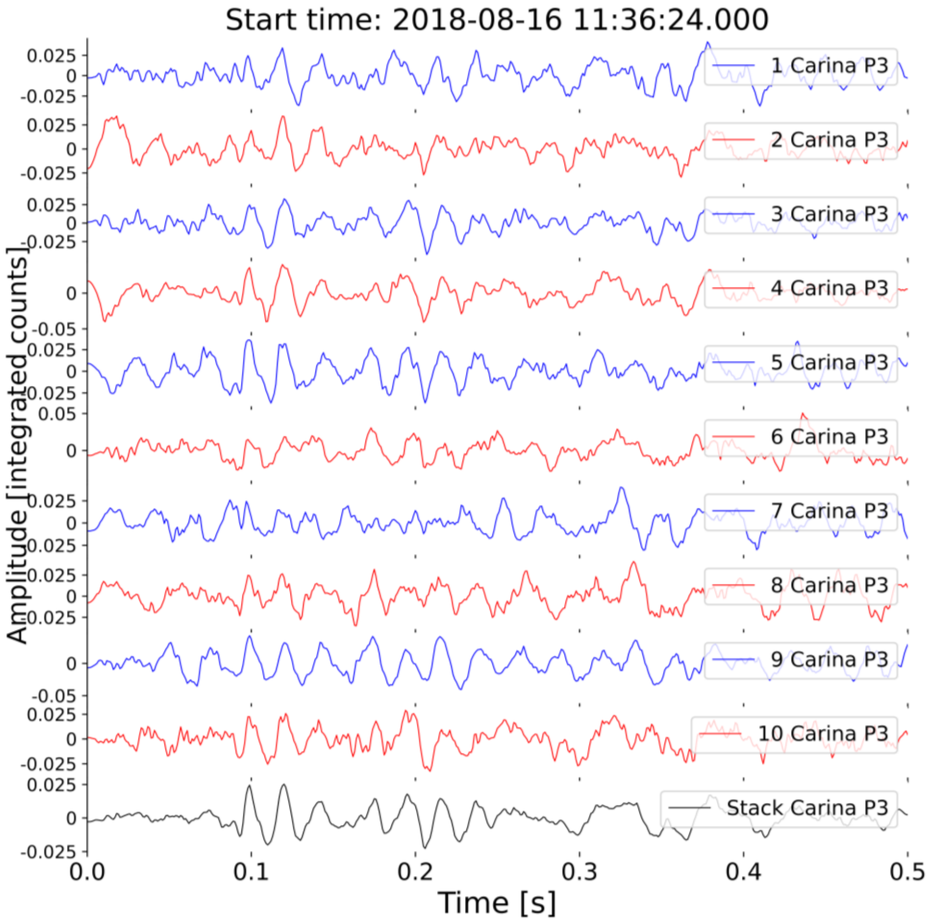

Figure 8-3. *Recordings of the 10 weight drops at source point 58 on the down-going Carina fibre at 75 m depth, and at the bottom a stack of the 10 recordings. The data has been time integrated and high-pass filtered above 10 Hz.*

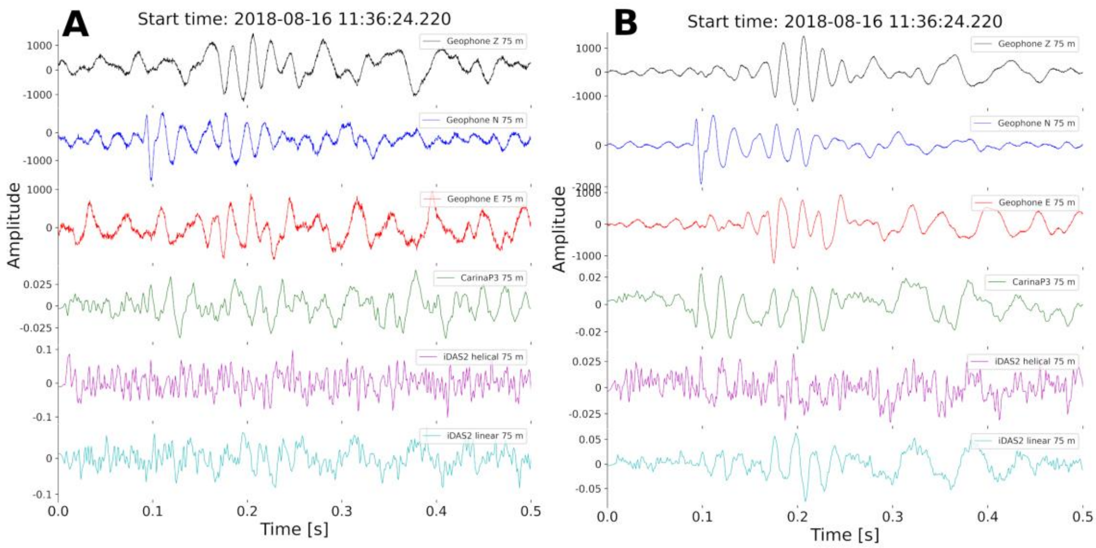

Figure 8-4. *Recordings from 75 m depth of weight drops at source point 58, 469 m from the borehole. Upper three recordings are from geophone B, with the Z-component in black, N-component (blue) and E-component (red). The lower three are fibre recordings, time integrated and high-pass filtered at 10 Hz. Carina (green), iDAS helical (magenta) and iDAS linear (cyan). A) First weight drop in the series. B) 10 stacked weight drops.*

At 75 m depth in the borehole, the signals from the weight drops at SP58 come in even more horizontally, see

Figure 8-3, and the single event recordings on the fibres have lower SNR than they do lower down in the borehole. Stacking the 10 weight drop recordings, however, improves the SNR significantly. Figure 8-4 shows the comparison between different fibres and the geophones, and we see in Figure 8-4A that the P-arrival is not identifiable on the single traces of the iDAS fibres, and the onset is difficult to pick on the Carina fibre. It is, however, very clear on the geophone N-component. Stacks of the data shows, in Figure 8-4B, that the arrival is now visible on the linear iDAS and the Carina fibres, also on the helical iDAS but less clear. The noise on the geophone is also suppressed but for the large amplitude first arrival on the N-component that is less relevant for the SNR.

The waveforms from the geophone, Carina and iDAS helical fibres are plotted on top of each other in Figures 8-5, 8-6 and 8-7 in order to compare phase arrivals. The amplitudes are normalised to a maximum of 1. Figure 8-5 shows that the Carina and iDAS helical data are very similar over the interval, with the Carina having less noise. Compared to geophone A's Z-component, Figure 8-5A, the fibres have similar phase behaviour in the first 0.06 seconds after the P-onset, after which the similarity degrades. The geophone has highest amplitudes later in the waveform, corresponding to the arrival of the S-wave. Comparing instead to the L-component, the motion along the direction of the ray, Figure 8-5B, the geophone and fibres have very similar behaviour in the first 0.06 seconds, albeit with different polarities. Differences in polarities occur because the fibre has a different directional sensitivity pattern to geophones (Zhan, 2019; Baird, 2020). The amplitudes also agree better, with highest amplitudes for the P-arrival. Figure 8-5C compares the fibre data to the Q-component of the geophone, which focuses on the S-wave. The agreement between fibres and the Q-component is not very good, except perhaps for the phase at about 0.23 seconds.

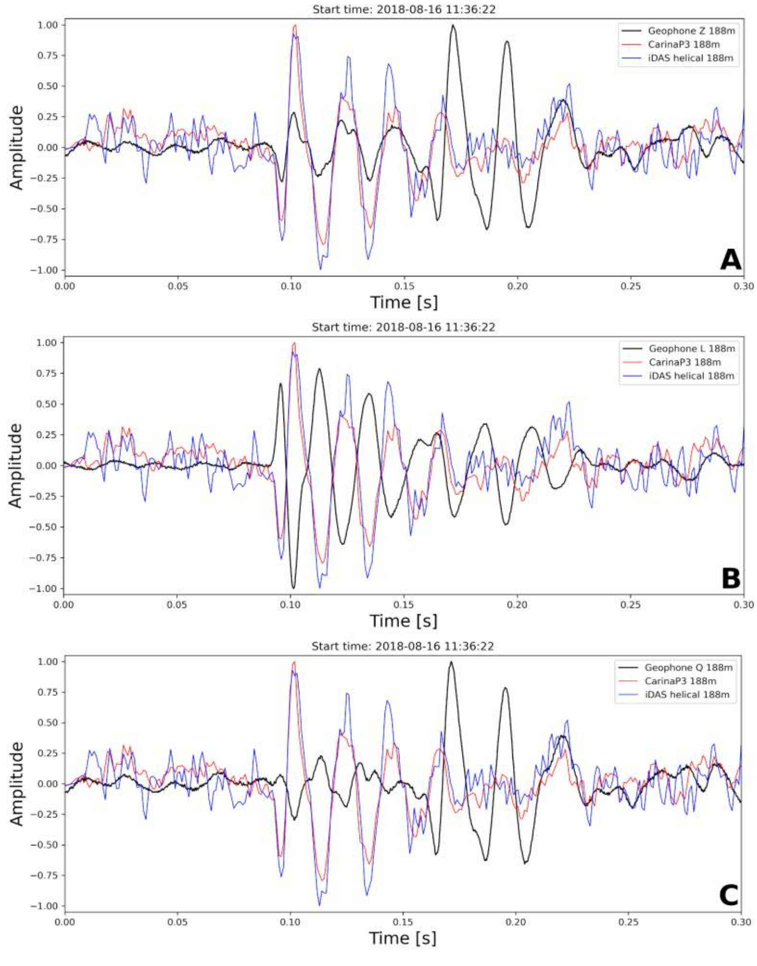

Figure 8-5. *Stacked recordings from 188 m depth of weight drops at source point 58, 469 m from the borehole with incidence angle 68° for geophone A. Geophone A (black), Carina (red) and iDAS helical (blue). The fibre data is integrated and high-pass filtered at 10 Hz. The recordings are individually normalised to maximum amplitude 1. The*

fibre data is identical in A, B and C. A) Geophone Z-component, B) Geophone L-component, C) Geophone Q component.

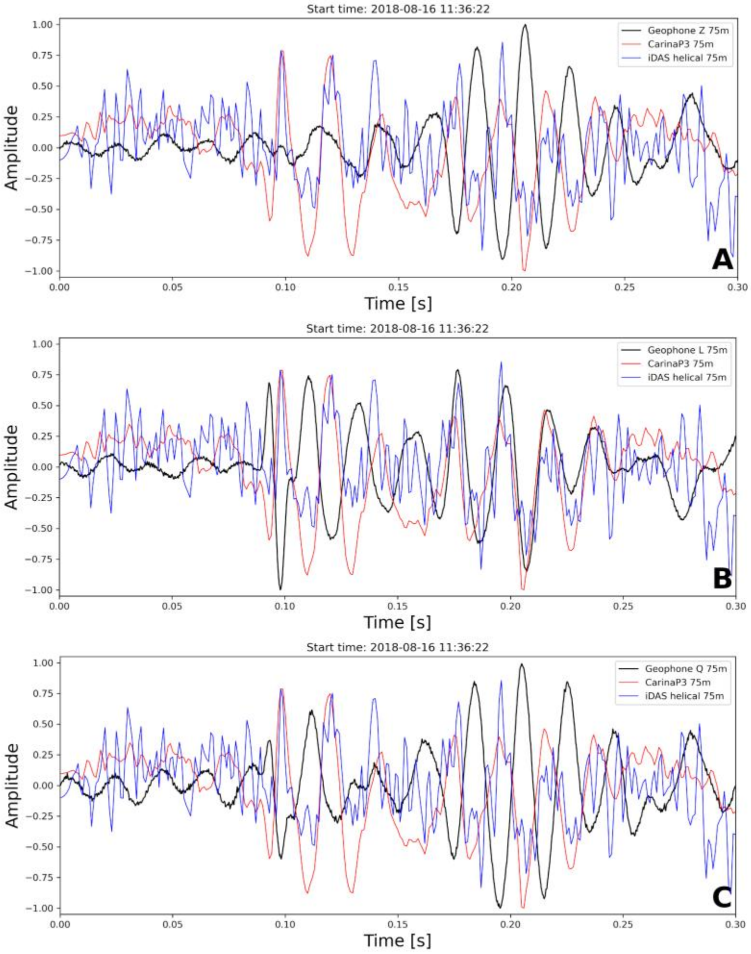

Figure 8-6. *Stacked recordings from 75 m depth of weight drops at source point 58, 469 m from the borehole with incidence angle 81° for geophone B. Geophone B (black), Carina (red) and iDAS helical (blue). The fibre data is integrated and high-pass filtered at 10 Hz. The recordings are individually normalised to amplitude 1. The fibre data is identical in A, B and C. A) Geophone Z-component, B) Geophone L-component, C) Geophone Q component.*

In Figure 8-6 we show the waveform data from 75 m depth, for SP58. Although the fibre data is noisier at 75 m depth than at 188 m depth, the behaviour is similar in that the Carina and iDAS helical data agree fairly well, and that the fibre data is similar to the early part of the L-component of the geophone data, but polarity reversed. However, Figure 8-6 also shows that there is more similarity between the fibre data and the later, S-wave dominated geophone data at 75 m depth. The fibre data has the same polarity as the later L-component data but opposite polarity to the Q-component data. The estimated incidence angle of the waves at 75 m depth thus does seem favourable for both P- and S-recordings on the fibres, as intended by the helical design.

Data from SP2, in Figure 8-7 show that the large amplitude waves, incoming more directly from above, are recorded very similarly on the geophone Z-component and the fibre data, especially for the first arrival. There is a clear difference between the geophone and fibre data soon after the first arrival, which could be due to the incoming S-wave.

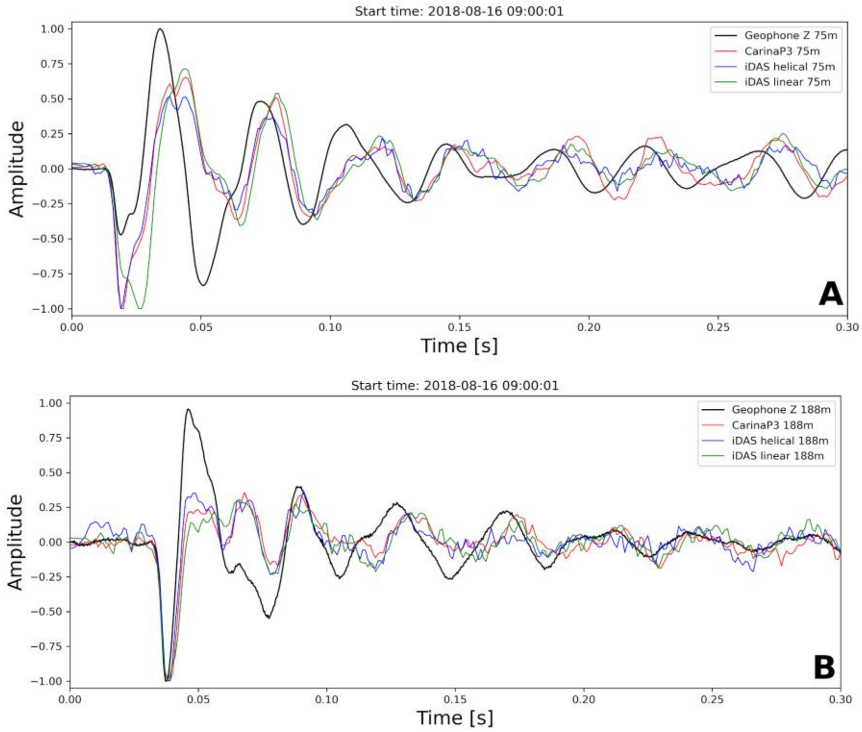

Figure 8-7. *Stacked recordings of weight drops at source point 2, 24 m from the borehole. Geophone (black), Carina (red), iDAS helical (blue) and iDAS linear (green). The fibre data is integrated and high-pass filtered at 10 Hz. The recordings are individually normalised to maximum amplitude 1. A) Data from 75 m depth, geophone B. B) Data from 188 m depth, geophone A.*

8.1 Comparing amplitudes and signal-to-noise

In Section 0 normalised amplitudes of DAS and geophone data are compared. For a comparison in true ground motion, in velocity units, DAS data must be transformed because the systems measure strain-rate whereas the geophones measure particle velocity. Strain along the fibre, in the z-direction, ε_{zz}, is related to particle velocity along a linear fibre, $\dot{u}_z$, via

$$\varepsilon_{zz} = \frac{-1}{c}\dot{u}_z, \qquad [1]$$

where c is the apparent velocity of the seismic wave along the fibre. So, time integration of the DAS strain-rate data allows the data to be converted to velocity. This is an easy conversion to make with a linear fibre but the response of a helical fibre is more complicated (see Baird 2019 for sensitivity of HWC to P- and S-waves).

Example waveforms recorded on the geophones and the fibre-optic cables are given in Figure 8-8a in units of nm/s. The geophone recordings are converted by removing the instrument response and the fibre data are converted using Equation 1. The observed difference in amplitude between the recordings is due to several effects. The conversion does not take into account:

1. The dependence of the P- and S-wave response of on incidence angle,
2. The frequency response of the fibre,
3. The effects of cable or fibre coupling, cable construction and cement type.

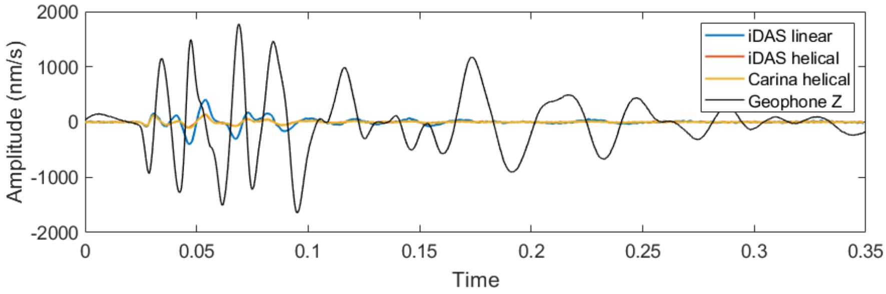

a)

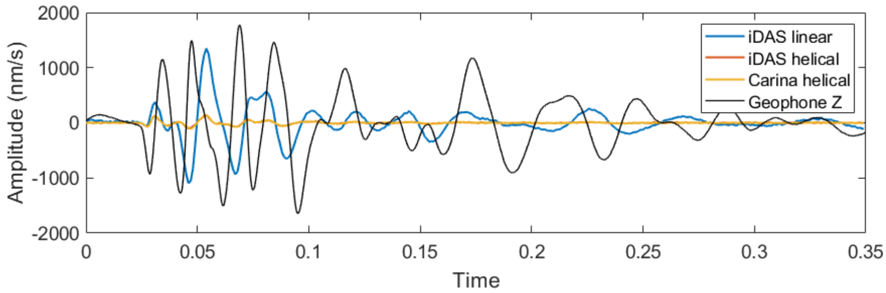

b)

Figure 8-8 *a) Example stacked waveforms for (SP9) recorded on the deepest geophone A; and the linear and helical fibre-optic cables at the same depth (the average amplitude over 10 channels is given). Data is in nm/s. b) The same waveforms but linear iDAS data is corrected for frequency response.*

Geophones have a cos(i) dependent response on incidence angle, i, to P-waves whereas DAS has a cos2(i) response. Similarly, geophones have a sin(i) response to S-waves and DAS has a sin(2i) response (Figure 8-9). The theoretical frequency response of the linear fibre is known (Figure 8-10) and therefore the recorded amplitudes on the linear cable can be corrected for frequency and incidence angle effects assuming an approximate incidence angle and seismic velocity at the geophone depths.

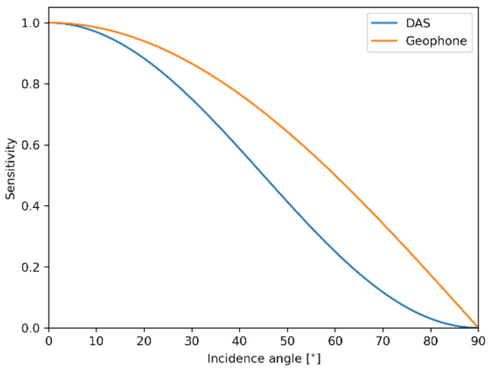

a)

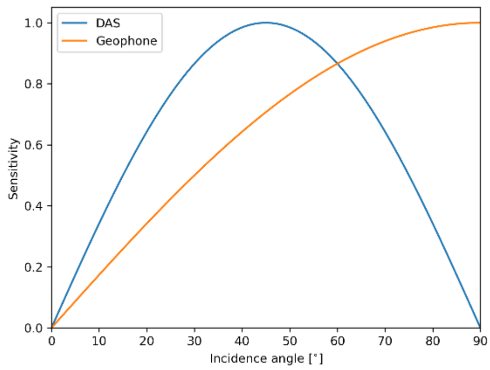

b)

Figure 8-9 *a) P-wave sensitivity patterns and b) S-wave sensitivity patterns for linear fibre DAS (blue) and geophones (orange). Incidence angle is measured from in-line with the fibre or geophone component.*

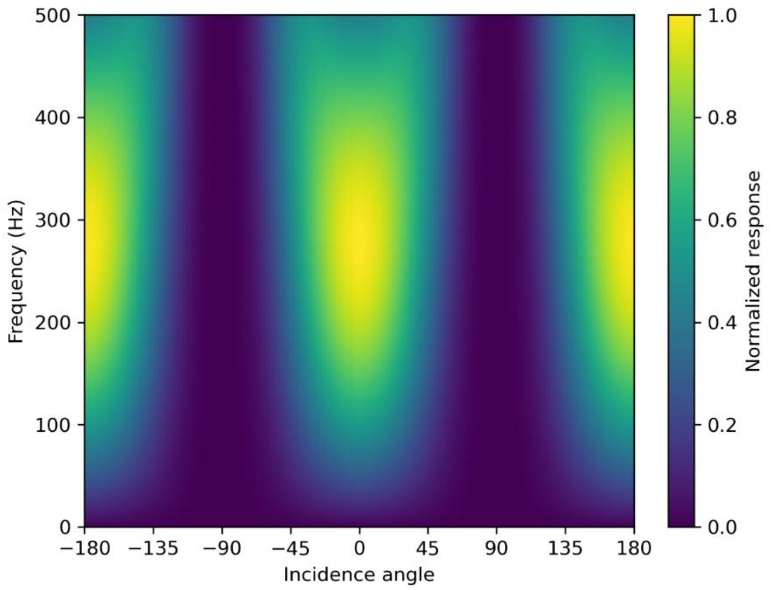

Figure 8-10 *Theoretical frequency response of the iDAS linear system for P-waves at different incidence angles for a 10 m gauge length and V_P = 5450 m/s.*

An example of the frequency response corrected linear cable iDAS data is shown in Figure 8-8b. With the correction the amplitude of linear fibre iDAS data is comparable with the geophone data. However, there remains some difference in the estimated velocity waveforms due to the other, uncorrected, effects, such as the cable response and differences in coupling.

A helical cable introduces an additional mechanical response to the overall data that is not currently completely understood theoretically. In Figure 8-8b the helical cable data were converted to velocity in the same way as the linear cable for comparison with the geophones. However, this does not provide a true measurement of velocity as a helical cable does not directly measure strain-rate in the axial direction along the fibre. Further theoretical work and laboratory tests are required to fully understand the mechanical response of the helical cable.

The velocity seismograms recorded on the geophones and the cables cannot be compared directly and therefore the noise floor of the instruments cannot be compared directly. However, the SNR is also an important factor to consider for performance because SNR affects the probability of a signal being detected. One example visual comparison of SNR on the different systems can be made from Figure 8-7. This shows a signal recorded on all three fibres with similar SNR at this shot point.

For a comparison of the P-wave SNR of stacked velocity signals recorded on the vertical geophones and cables, the geophone data are converted to velocity recordings by removing the instrument response and the DAS data is converted according to Equation 1 (Figure 8-11 and Figure 8-12). All data is bandpass filtered 5 Hz – 200 Hz. The iDAS data recorded on the linear fibre is also corrected for frequency response. Signals are recorded with a maximum SNR up to ~35dB on all systems. Overall, the data acquired by the Carina system is higher SNR than the iDAS data as would be expected. All systems have the highest SNR at short offsets (<200m) as would be expected because the P-wave is arriving in-line with the sensor. For shot point distances greater than approximately 450 m from the borehole (SP>50) the signal on the iDAS data is close to or below the instrument noise and therefore SNR ~ 0 dB at these distances. The Carina system has a lower noise floor and therefore signal is visible at greater shot distances, up to 1 km. The data recorded on the HWC shows better SNR than the linear fibre at high incidence angles, as expected, particularly at depth. The purpose of using a HWC is to improve the sensitivity to P-waves arriving broadside to the cable.

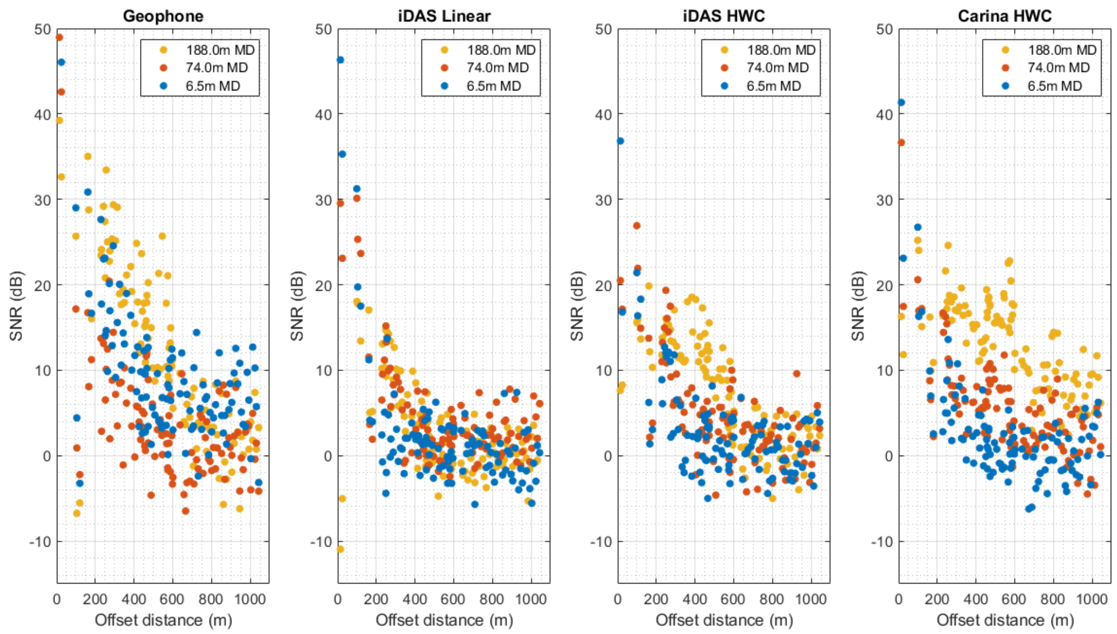

Figure 8-11 *The P-wave SNR as a function of shot offset distance for stacked data. Data are shown for velocity recordings measured on the vertical geophone components and the downgoing fibre on the DAS interrogators. All data are bandpass filtered 5 Hz – 200 Hz.*

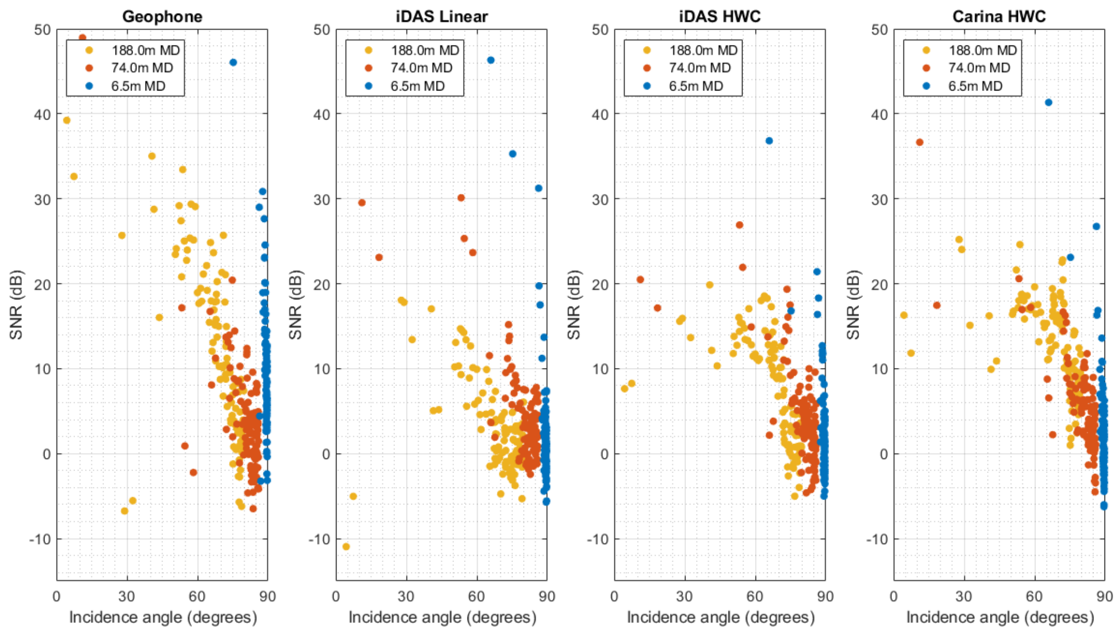

Figure 8-12 *The P-wave SNR as a function of approximate incidence angle for stacked data. Data are shown for velocity recordings measured on the vertical geophone components and the downgoing fibre on the DAS interrogators. All data are bandpass filtered 5 Hz – 200 Hz.*

For both systems the P-wave SNR decreases with offset as would be expected, although they decrease at a different rate. This is due to the difference between the instrumentation types in P-wave sensitivity, $cos\ \theta$ versus $cos^2\theta$ for geophone and linear fibre, respectively.

At very near offsets (<200 m) the P-arrivals are close to in-line with the fibre and therefore the cable has maximum sensitivity to these arrivals and high SNR recordings are obtained for the deeper receiver depths (74 m and 188 m). As expected, the geophones also record good signals.

The geophones and Carina system record P-wave with a similar range of SNR at near offsets (200 m – 600 m) although the shallower geophone has higher P-wave SNR than the Carina system. The low SNR on the fibre at shallow depths is most likely due to very near-surface noise (1.5 m – 11.5 m depth) influencing the DAS measurements at 6.5 m depth. iDAS SNR values are a few dB lower that the Carina system.

At mid to far offsets (600 m – 1000 m) some shots are around the noise level of the iDAS system. It is expected that the HWC fibre performs better at larger offsets for the recording of P-waves with near broadside arrivals, and this is seen in the Carina data where the signal is above the noise at these distances.

We compare recordings at individual shot points (SP1, SP9, SP31 and SP52, Figure 8-13) from all three systems, iDAS, Carina and the geophones, to cover signals in the near- to mid-offset range. Further offsets are not shown as the SNR is often too low to make any meaningful conclusions.

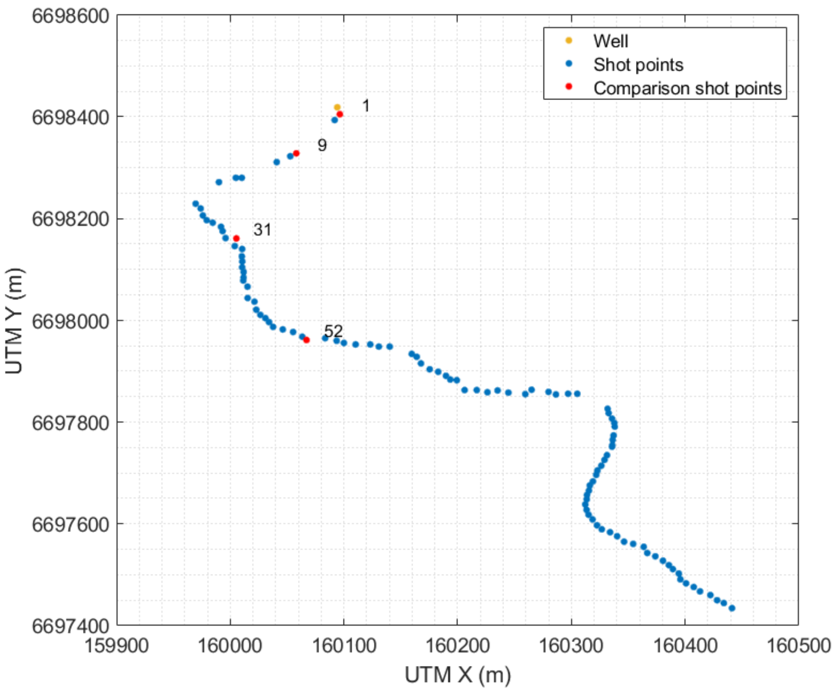

Figure 8-13. *Location of source points identified for comparison (red). The location of the wellhead is shown in yellow.*

In Figure 8-14 to Figure 8-17 the stacked shot data is displayed in various ways. The left most plot shows the iDAS down-going helical fibre source record for all depths. Overlain on this plot are the iDAS and geophone traces at the geophone depths. This overlaid data is normalised prior to plotting. Also plotted are the boxes (magenta and yellow) used to calculate the signal and noise, respectively. The noise box is placed before the signal box, prior to the first arrival, where possible. Where this was not possible, the box is placed at the end of the 4 second record. The plot, second-right, shows the data for the Carina down-going helical fibre. On the right is a grid of plots that show the frequency spectrum calculated within each the signal and noise boxes. The solid lines are the response in the signal box. The dashed lines are the response in the noise box. These plots give an indication of the signal-to-noise separation at different frequencies.

SP1 is the closest source point, and the recorded data is displayed in (Figure 8-14). The signal is travelling almost vertically between source and receivers and the first arrival is very clearly seen on the fibre data. The frequency content of the DAS signal drops as you get deeper due to attenuation effects. At the surface, the maximum frequency detected is approximately 350 Hz.

Since most signal is travelling vertically, the first arrival amplitude is constant with depth except for attenuation effects and differences in coupling in certain places. This changes as the source moves further away and the angle of incidence introduces directivity related amplitude effects.

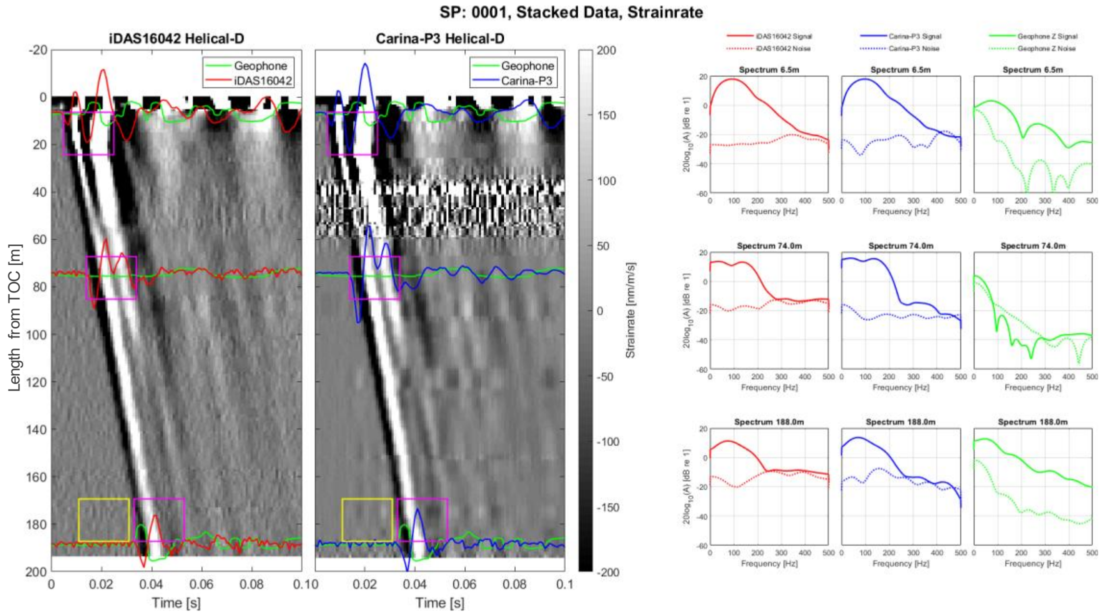

Figure 8-14. *Comparison of data recorded at SP1. Left: Data recorded on a helical cable with an iDASv2. Middle: Data recorded on a helical cable with a Carina system. The time windows used to calculate SNR are shown in yellow and magenta. Note, this figure does not contain the correct geophone data. The correct geophone data for this shot point is displayed in Figure 4-14. Right: Comparison of the frequency spectra of noise and signal recorded by all three systems using the red, blue and green traces on the left-hand plot.*

The signal level on SP9 (Figure 8-15) is quite significantly weaker than SP1. When looking at every source point there are some clear variations in source strength which could be due to source coupling in different locations. With the increase in offset, the arrival has a minor curved shape due to the seismic wave propagation path. Variation in amplitudes due to different coupling is clearer in this plot and there is a clear region around 90 m that has better coupling than other locations in the well. This could be an indication of cement quality.

At SP31 (Figure 8-16) the signal level is quite weak, even after stacking. However, the first arrival is still visible. At this source offset the angle of incidence to the upper portion of the well is now almost 90°. This results in a weakened detection of the first arrival on the DAS system. The helical cable is more sensitive to broad-side arrivals than a linear cable but is has a slight decrease in sensitivity at 90° arrivals compared to 0°. The broad-side arrival in the upper section of the well can be seen however, and this would not be the case for the linear cable. The SNR is lower for this source point than for previous ones but the Carina system has good SNR up to 300 Hz at the lowest level and the geophone has good signal up to 500 Hz.

At SP52 (Figure 8-17) the arrival is almost entirely broadside but the signal is visible on the HWC data. A faint first arrival can be seen in the data around 0.09 s and the Carina system has good SNR up to 250 Hz at the lower level. The geophone has good signal up to 500 Hz.

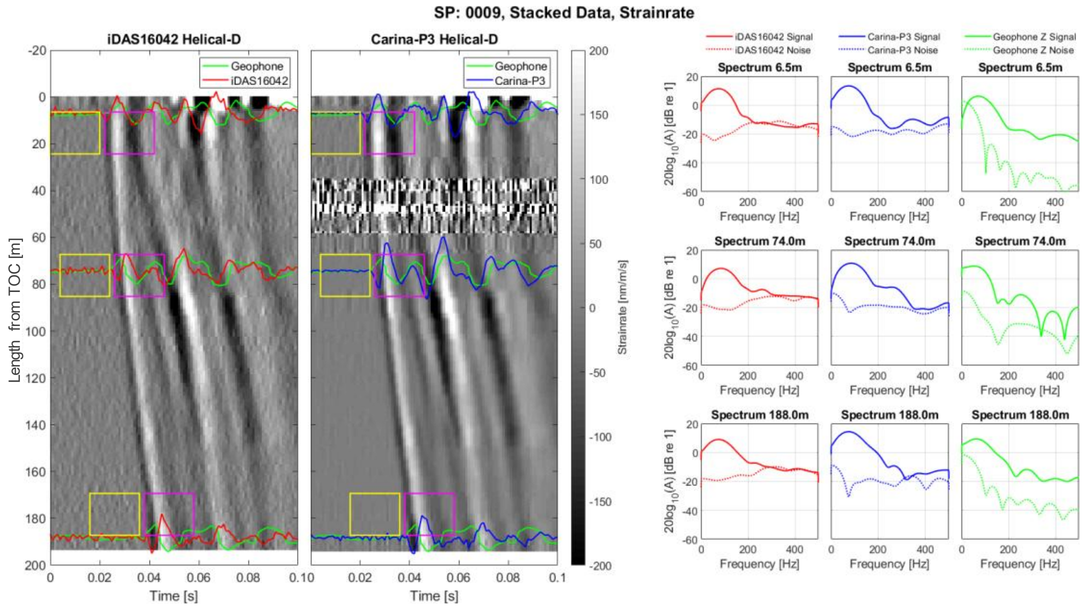

Figure 8-15. *Comparison of data recorded at SP9. Left: Data recorded on a helical cable with an iDASv2. Middle: Data recorded on a helical cable with a Carina system. In both figures the geophone Z-component data is shown in green and the time windows used to calculate SNR are shown in yellow and magenta. Right: Comparison of the frequency spectra of noise and signal recorded by all three systems, using the red, blue and green traces on the left-hand plot.*

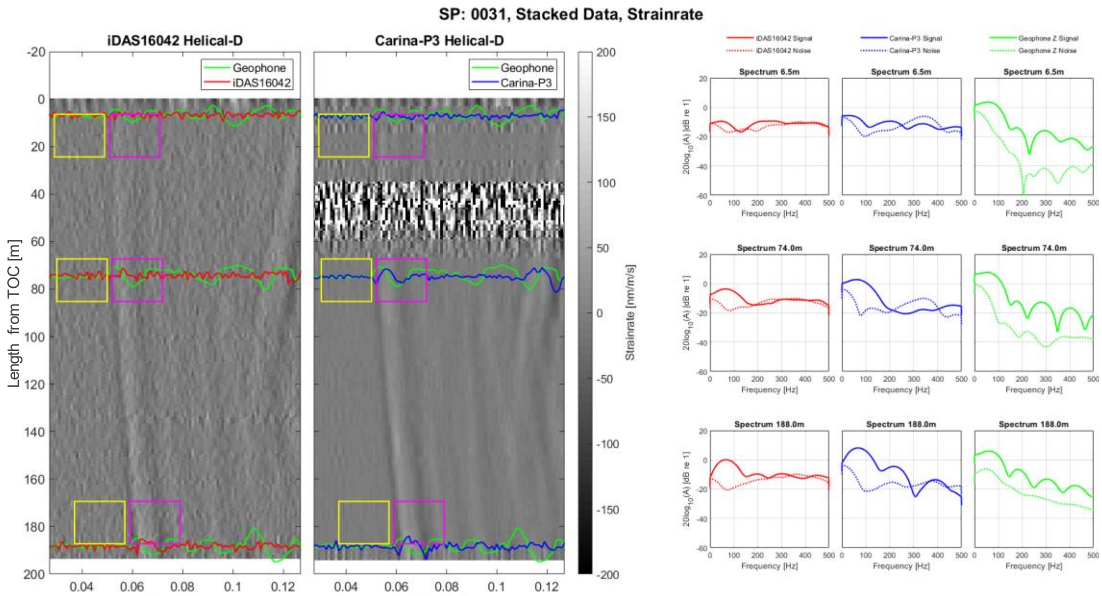

Figure 8-16. *Comparison of data recorded at SP31. Left: Data recorded on a helical cable with an iDASv2. Middle: Data recorded on a helical cable with a Carina system. In both figures geophone Z-component data is shown in green and the time windows used to calculate SNR are shown in yellow and magenta. Right: Comparison of the frequency spectra of noise and signal recorded by all three systems, using the red, blue and green traces on the left-hand plot.*

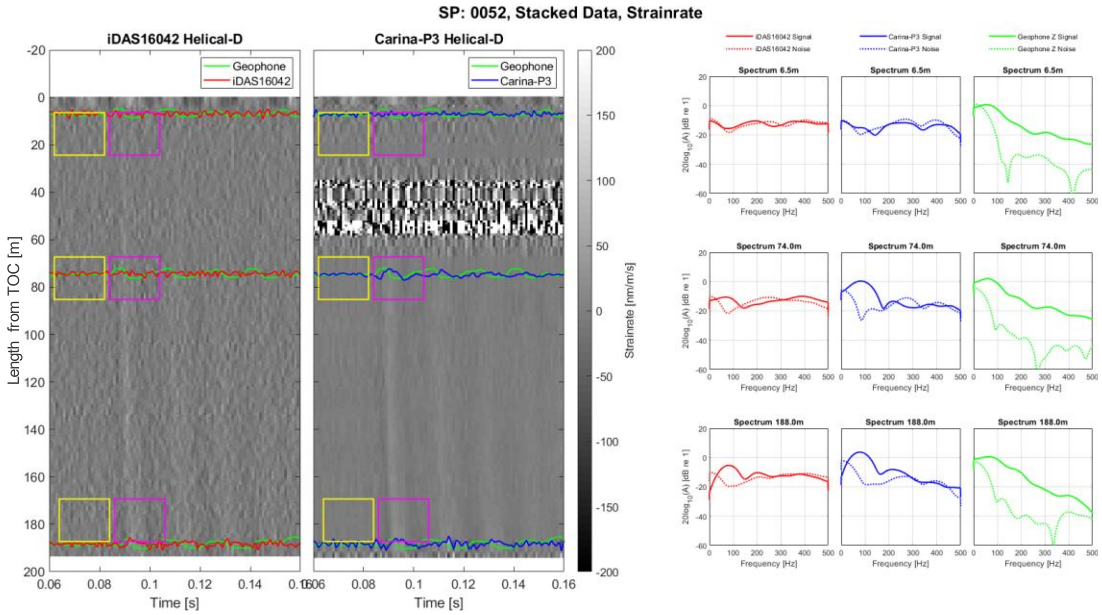

Figure 8-17. Comparison of data recorded at SP52. Left: Data recorded on a helical cable with an iDASv2. Middle: Data recorded on a helical cable with a Carina system. In both figures the geophone Z-component data is shown in green and the time windows used to calculate SNR are shown in yellow and magenta. Right: Comparison of the frequency spectra of noise and signal recorded by all three systems, using the red, blue and green traces on the left-hand plot.

On all figures described above, the manufacturing defect is visible in the Carina data on these plots between 40 m and 60 m. This defect results in a region of data that is very noisy and unusable.

Differences in recorded SNR between the systems are caused by a variety of factors:

- There could be a difference in coupling between the fibre and geophones. However, both were cemented in the borehole.
- The angular sensitivity of geophones and fibres differ. The difference between a geophone component and the linear fibre sensitivity to P-waves as a function of incidence angle is illustrated in Figure 8-9. The $cos^2\theta$ sensitivity of the fibre results in a lower sensitivity than the geophone at all angles for P-waves. Linear fibres have a $sin2\theta$ response to S-waves. Theoretically, HWC with 30° wrapping angle, as used here, have a more even angular response to P-waves at approximately 30% of the maximum amplitude of a linear fibre. However, they remain insensitive to S-waves with 0° or 90° incidence and the overall S-wave response is reduced compared to a linear cable (Baird, 2020).
- The instrumentation types have different frequency responses.
- The effects of the cable and cement type on the fibre response are not considered.

8.2 Noise floor and frequency content comparison

Due to uncorrected effects, an absolute comparison of the noise floor of the geophones relative to the DAS data is not made, although a comparison of the relative noise floors between the DAS interrogators is shown in Figure 5-2 and Figure 5-3.

The frequency content of recorded signals is also an important consideration for seismic monitoring. The instrumentation must record the signals in the frequency band expected. Signals from regional earthquakes (up to ~1000 km from the station) have a frequency content ~3 - 50 Hz. Local microseismic events with magnitudes < 0 recorded at very short distances (<1 km) can be recorded with signals containing frequencies up to several 100 Hz. For the field test at Forsmark, the recording frequency of the geophones was 4,000 Hz and 1,000 Hz for the fibre-optic systems. As discussed above, the P-wave signal up to 300 Hz is visible in the Carina data. The geophone has good SNR up above 500 Hz (e.g., Figures 6-13 and 6-15). Both systems record signal frequencies >200 Hz above the noise level, important for microseismic monitoring.

Figure 8-18 shows the power spectral densities for integrated Carina and iDAS helical data, at the geophone depths and for both down-going and up-going fibres. Comparing to the geophone data in Figure 6-3 and Figure 6-4 (where the earliest data is from the exact same time interval as the fibre data here) there is a large difference in the spectral content. The fibre data lacks the low frequency (5-50 Hz) noise which dominates the geophone data at all depths. There is an indication of this, present as two separate noise peaks, in the iDAS helical near-surface data but not at other depths or the Carina data. Similar to the geophone data, the fibre data shows the 25, 50 and 100 Hz noise peaks as the geophone data but in addition there is also a wide hump at 4 Hz and a number of additional peaks not coincident with the geophone data. There is no general decrease in energy with frequency 20 Hz – 100 Hz, as in the geophone data.

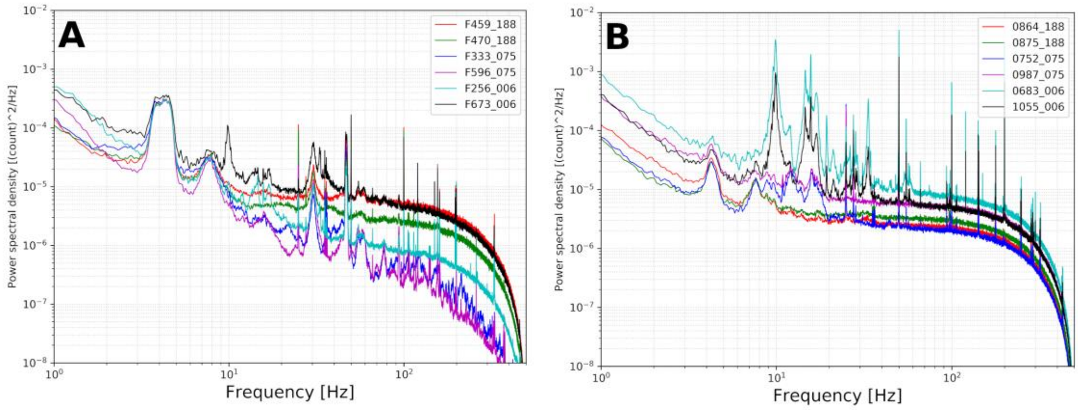

Figure 8-18. *Power spectral densities of one hour of time integrated fibre noise data from 2018-08-17 01:00 – 02:00. A) Carina data extracted at 6.5 m depth (down-going F256, cyan, up-going F673, black), 75 m depth (down-going F333, blue, up-going F596, magenta) and 188 m depth (down-going F459, red, up-going F470, green). B) iDAS helical data extracted at 6.5 m depth (down-going F683, cyan, up-going F1055, black), 75 m depth (down-going F752, blue, up-going F987, magenta) and 188 m depth (down-going F864, red, up-going F875, green).*

The overall characteristics of the power spectra are expected from known DAS characteristics. The noise floor of the DAS interrogators increases with decreasing frequency below 100 Hz (Shatalin et al., 2021), as is seen in Figure 8-18, and there is a fall off at high frequencies (>300 Hz) which is expected due to the frequency response of the DAS (Figure 8-10).

9 Conclusions

This study was designed to investigate a number of important issues with respect to the future installation of a high-resolution local seismic network in the forthcoming nuclear waste repository area at Forsmark. The objectives were:

1. Investigate the suitability of a variety of digitisers.
2. Investigate how the background seismic noise levels vary with depth and time, and if the noise “hump” at approximately 200 Hz found by Lund et al. (2017) was due to natural causes.
3. Test a variety of fibre-optic technologies in a 200 m deep borehole.
4. Compare fibre-optic measurements to geophone measurements.
5. Provide input data to the selection of instruments for the future local seismic network.
6. Investigate attenuation and near-surface structures in the area.

In in early April 2018 a 195 m deep borehole (HFM42) was drilled under SKB supervision in the Forsmark area. Two three-component high sensitivity geophones from the Institute of Mine Seismology (IMS; similar instruments to those used in Lund et al. (2017)) were installed at 188 m depth, in rock domain FFM01, and at 74 m depth, in rock domain FFM02. A one-component vertical IMS geophone was installed at 6.5 m depth. Three fibre-optic cables were installed in the borehole, two helical cables and one linear cable attached to a Carina and an iDASv2 interrogator. The borehole was grouted from bottom to top for optimal coupling of the instruments and cables to the rock. For reference, both a free-standing vertical component geophone in a 60 cm deep borehole (the installation type in Lund et al., 2017) and a surface seismometer were installed in the vicinity of the deep borehole. The three component geophones were oriented with a weight drop source at three different azimuths.

Laboratory tests including noise measurements and suitability for the field work deployment were carried out at Uppsala University on digitisers from Guralp, Nanometrics and the IMS. The Nanometrics Centaur and the Guralp Minimus digitisers were removed from the test suits, the Centaur because of limited sampling frequency for 7 channels and the Minimus due to a timing problem and the lack of an analogue low-pass filter for anti-alias purposes. The system noise of the Guralp Affinity digitiser with a simulated IMS geophone was approximately -185 dB above the geophone corner frequency. The IMS NetADC digitiser performed slightly better, at -195 dB, but the Affinity was found to be better suited for long term field experiment due to easier practical handling. The IMS digitiser was, however, used for 24 hours of measurements in the field.

Measurements of the ambient seismic noise at Forsmark showed that:

- The spectrum of background noise measured in the borehole is very similar to the measurements of Lund et al. (2017), with significant broadband noise from 3 – 100 Hz and high-amplitude narrow peaks at 25, 50, 100, 150 Hz and over-tones. Above 150 – 300 Hz the ground motion noise reaches the digitizer noise levels, depending on digitizer.
- There is no sign of the Lund et al. (2017) spectral “hump” at 200 Hz in the data from the geophones cemented into the HFM42 borehole, but the free-standing reference geophone shows such a hump. This confirms that the hump is likely due to resonances in the installation and does not come from the instrument system.
- The broadband ambient noise is slightly reduced from the geophone at 6.5 m to the geophone at 74 m depth in the borehole, and then significantly decreased from 74 m to 188 m. The deepest sensor is quieter over most of the lower frequency spectrum by 10 – 20 dB, but does record more high frequency ground motion than the upper sensors, indicating that although it is less noisy at depth, the more competent FFM01 rock unit transmits high-frequency signals better.
- The ambient noise levels were surprisingly stable over time, from August 2018 to March 2019. There is a small amplitude increase later in the time period, perhaps due to winter conditions and increased production in the nuclear power plants. However, at specific frequency bands, such as 50 Hz and 100 Hz, there were significant temporal variations in the recorded energy.

Recordings of nearby blasts showed that the instrumentation in HFM42 recorded high frequency ground motion above the system noise levels up to 800 Hz, confirming the potential to record high frequency seismic events. Recordings of local and regional earthquakes showed that the sensitivity is good enough to record a magnitude 0.4 event at 14 km distance and a magnitude 2.9 event at 65 km distance, and that the recorded amplitudes can estimate station magnitudes in agreement with those calculated by the Swedish National Seismic Network.

Distributed acoustic sensing measurements compared data collected on linear and helically wound cables (HWC). In most cases, these measurements confirmed the theory that the HWC provides data with higher P-wave arrivals are near-broadside arrivals, at source offsets 200 m – 600 m.

The active seismic survey also demonstrated the improved SNR of data collected using a Carina system, with engineered Constellation fibre, over data collected using an iDAS v2 on standard single mode fibre.

It was not possible to fully explore the effect of gauge length (GL) in this survey because the borehole length (195 m) was too short to evaluate the 30 m GL data in comparison to the 10 m GL data.

DAS data analysis techniques are developing rapidly and future deployments would provide a more sophisticated understanding and processing of the data.

DAS measures strain-rate on a fibre and geophones measure particle motion in the ground. Therefore, a direct comparison between geophone and fibre-optic is difficult as there are inherent differences in the measurements and also differences in the coupling with the rock. Comparing the systems we found:

- All systems are able to record data with good signal-to-noise (SNR) out to 500 m for stacked weight drop data. The geophones have significantly better SNR for single event data than any of the fibre systems. If the three-component geophones are rotated to the ray direction SNR increases further, out to 1.1 km.
- The Carina system is better than the iDAS helical system, and the linear system shows the poorest SNR response, which is to a large degree due to the fact that the seismic signals are incoming almost perpendicular to the fibre.
- We find that the geophones have good SNR to above 500 Hz and the Carina system to 250 – 300 Hz, depending on the distance to the source.
- The fibre systems show high spatial resolution arrivals throughout the borehole, with the Carina system having the highest SNR.
- The fibre systems and the geophones tend to be in phase in the early part of the signal waveform but then grow increasingly out of phase.
- As true ground motion is difficult to measure with the fibres due to varying frequency and incidence angle response we do not find good agreement between fibre and geophone amplitudes, neither in time series data nor in the spectra.

The active source data was used to investigate potential reflectors in the underlying rock. The Carina fibre data was somewhat noisy but indicated a reflected S-wave incoming at 30 degrees angle to the borehole. The surface seismic recordings were CDP processed and a number of sub-horizontal reflections could be identified at 150 – 300 m depth in the section. These reflections appear to be localized to certain areas and do not have lateral extents of more than a few 100s of meters. It is not currently clear whether these reflections originate from fracture zones or lithological boundaries.

The active source data was also used to estimate seismic velocities along the profile. The Carina data showed that the P-velocity between 10 and 195 m depth is almost constant at 5.75 km/s, with the uppermost layer being slower. The surface seismic recordings found a similar velocity of 5.6 km/s below the uppermost layer. In receiver gathers from the three geophones we found that the lower geophone, at 188 m depth, estimates a velocity of 5.8 km/s for the P-wave and 3.25 km/s for the S-wave. The middle geophone observes slightly lower velocities, 5.5 km/s for P and 3.0 km/s for S whereas the upper geophone observes similar velocities of 5.5 km/s and 2.9 km/s albeit with larger uncertainties.

This study was initially aimed also at estimating the attenuation in the two rock domains FFM01 and FFM02. However, as another project was undertaken in Forsmark with measurements in a 500 m deep borehole more suitable for attenuation studies, we did not pursue that further with this data. It also turned out that due the variation in coupling of the weight drops to the ground, an attenuation study may have been difficult to perform.

Comparing geophones and fibre-optics for a seismic network, three-component geophones provides data on true ground motions for magnitudes, focal mechanisms and moment tensors which the fibre data cannot easily do. Geophones of the type tested here are also more sensitive than the fibre systems. Fibre-optics, on the other hand, provides high density measurements, can be used for simultaneous multi-parameter measurements (strain, temperature and seismic) and can remain in the ground for decades without requiring maintenance. The DAS interrogators are currently relatively expensive but can be used with tens of kilometres of fibre cable.

For a future seismic network in Forsmark we primarily recommend a network of high-sensitivity borehole geophones at various depths in order to detect events and obtain magnitudes, focal mechanisms and potentially moment tensors. To increase detection and location capabilities, now or in the future, we suggest that fibre-optic cables be installed in the boreholes in preparation for later connection to interrogators, either as part of the monitoring system or during campaign measurements. The design of the fibre-optic cable network needs careful analysis as individual cables in boreholes would require multiple interrogators, while continuous buried cables from borehole to borehole would reduce the number of interrogators and provide additional surface ground motion data.

Acknowledgements

We thank Nanometrics for providing the Centaur digitiser and Guralp for providing the Minimus digitiser for testing. SKB provided the borehole and the installation of equipment in the borehole.

References

SKB's (Svensk Kärnbränslehantering AB) publications can be found at www.skb.com/publications. SKBdoc documents will be submitted upon request to document@skb.se.

Baird, A, 2020. Modelling the Response of Helically Wound DAS Cables to Microseismic Arrivals, First EAGE Workshop on Fibre Optic Sensing.

Brojerdi FS, Zhang F, Juhlin C, Malehmir A, Lehtimäki T, Mattsson H, Curtis P, 2014. High resolution seismic imaging at the planned tunnel entrance to the Forsmark repository for spent nuclear fuel, central Sweden. Near Surface Geophysics, 12, 709-719.

Institute of Mine Seismology, 2020. www.imseismology.org, last visited 2021-08-31

Juhlin C, Bergman B, Palm H, 2002. Reflection seismic studies in the Forsmark area - stage 1. SKB R-02-43, Swedish Nuclear Fuel and Waste Management Co.

Lund B, Bödvarsson R, Shomali H, Dynesius L, 2012. Study of seismic background signals in the Forsmark area, SKB P-12-08, Swedish Nuclear Fuel and Waste Management Co.

Lund B, Bödvarsson R, Dynesius L, Schiescke M, 2017. Study of high-frequency seismic signals in the Forsmark area, SKB P-17-12, Swedish Nuclear Fuel and Waste Management Co.

Lund B, Schmidt P, Shomali ZH, Roth M, 2021. The modern Swedish National Seismic Network: 20 years of intraplate microseismic observation, Seismol. Res. Lett., 92, 1747-1758, doi:10.1785/0220200435.

Lundberg, E, Juhlin, C, Zhang, F and Behrendt, R, 2018. Seismic reflection, refraction and tomography results from 3D seismic data, Forsmark. SKB P-17-25, Swedish Nuclear Fuel and Waste Management Co.

Merchant BJ, Slad G, 2018. 2018 Nanometrics Centaur Digitizer Evaluation, Sandia Report SAND2018-11442, Sandia National Laboratories, Albuquerque, New Mexico, USA.

Muanenda Y, Oton CJ, and Di Pasquale F, 2019. Application of Raman and Brillouin Scattering Phenomena in Distributed Optical Fiber Sensing, Front. Phys., 7, 29 October 2019 | https://doi.org/10.3389/fphy.2019.00155.

Nilsson G, 2018. Drilling of percussion boreholes HFM42–HFM46 in Forsmark to be used as monitoring wells. SKB P-18-09, Svensk Kärnbränslehantering AB.

Obspy 2020. www.obspy.org

Shatalin, S., T. Parker and M. Farhadiroushan, 2021. High Definition Seismic and Microseismic Data Acquisition Using Distributed and Engineered Fiber Optic Acoustic Sensors in Distributed Acoustic Sensing in Geophysics: Methods and Applications, Eds. Y. Li, M. Karrenbach, J. B. Ajo-Franklin, AGU Monograph Series, doi: 10.1002/9781119521808.

Sleeman R, van Wettum A, Trampert J, 2006. Three-Channel Correlation Analysis: A New Technique to Measure Instrumental Noise of Digitizers and Seismic Sensors, Bull. Seismol. Soc. Am., 96, 258-271, doi: 10.1785/0120050032

Uski M, Tuppurainen A, 1996. A new local magnitude scale for the Finnish seismic network, Tectonophysics, 261, 23 – 37.

Zhan Z, 2019. Distributed Acoustic Sensing Turns Fiber-Optic Cables into Sensitive Seismic Antennas, Seismol. Res. Lett. 91, 1–15,doi: 10.1785/0220190112.

Appendix 1: Helically wound loose tube cable specifications

Spec Sheet
DH-7S4M1X-1NY250-01-BL
Helically wound loose tube cable

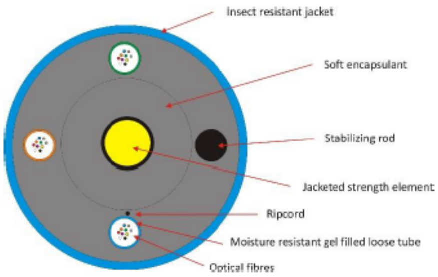

*** Drawing not to scale**

Product description

7 x G657.a1, 4 x OM4 and one Constellation™ optical fibre, contained in three jelly filled loose tube (4 fibres per tube),laid up around a sheathed central non-metallic strength member, Sheathed to encapsulate the tube then Nylon (insect resistant & low coefficient of friction) jacketed

Typical characteristics

Fibre Type	**Constellation Fibre**	**Singlemode**		**MM**	
Fibre Count	1	7		4	
Core Diameter		9 µm		50 µm	
Cladding Diameter		125 µm		125 µm	
Coating		Acrylate		Acrylate	
Wavelength		**1310 nm**	**1550 nm**	**850 nm**	**1300 nm**
Maximum Attenuation		0.38 dB/Km	0.29 dB/Km	2.95 dB/Km	0.90 dB/Km

Mechanical Properties

	CABLE
Nominal Overall Diameter	25mm
Tube Diameter	2mm
Approximate Weight	500 kg/km
Max Crush Resistance	2 kN/100mm
Max Pulling Tension	10 kN
Bend Radius – Under Load	20 x OD mm
Bend Radius – No Load	10 x OD mm
Operating Temperature	-40 to 70°C

Colour sequence for tubes: Blue, Orange, Green
Colour sequence for fibres –
Blue tube: Blue Orange Green & Constellation fibre (Nat)
Orange tube: Blue Orange Green & Brown
Green Tube: Blue Orange Green & Brown

Silixa Ltd
Silixa House, Centennial Park
Centennial Avenue, Elstree
WD6 3SN, UK

t: +44 (0) 208 327 4210
f: +44 (0) 208 953 4362
w: www.silixa.com
e: enquiries@silixa.com

Appendix 2: Composite hybrid fibre optic cable specifications

Spec Sheet
HS-2S2M2C-1TPX064-01-BL
Composite Hybrid Fibre Optic Cable

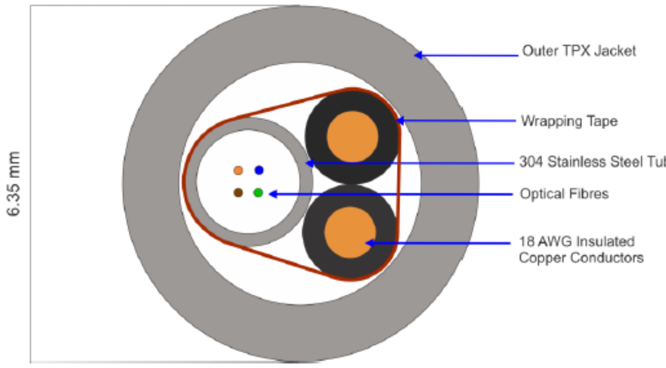

* **Drawing not to scale**

Typical characteristics

Fibre Type	**Multimode**		**Singlemode**	
Coating	High Temp Acrylate (150 °C)		High Temp Acrylate (150 °C)	
Fibre Count	2		2	
Core Diameter	50 µm		9 µm	
Cladding Diameter	125 µm		125 µm	
Wavelength	**850 nm**	**1300 nm**	**1310 nm**	**1550 nm**
Maximum Attenuation	2.7 db/km	0.90 dB/Km	0.40 dB/Km	0.30 dB/Km

Mechanical Properties

	ENTIRE ARMOURED CABLE
Nominal overall Diameter	6.35 mm (0.250 in)
Approximate Weight	65.45 kg/km (43.81 lbs/kft)
Tensile Strength	1,287 N (289.3 lbs)
Yield Strength	1115 N (250.7 lbs)
Strain at Yield	0.464%
Coefficient of thermal expansion	1.73E-05 m/m°C (9.60E-06 in/in°F)
Dynamic Bend Radius	240 mm (9.4 in)
Static Bend Radius	60 mm (2.4 in)
Temperature rating	Rating Pending, Est: -40°C to +150°C
	STEEL TUBE
Material	304 Stainless Steel
Thickness	0.2 mm
	CONDUCTOR WIRES
Material	ETFE Insulated Stranded Copper
Cross Sectional Area	18 AWG
DC Resistance	21 Ohms/km (6.4 Ohms/kft)

Silixa Ltd
Silixa House, Centennial Park
Centennial Avenue, Elstree
WD6 3SN, UK

t: +44 (0) 208 327 4210
f: +44 (0) 208 953 4362
w: www.silixa.com
e: enquiries@silixa.com

Appendix 3: iDASv2 and Carina data sheets

sense the difference

iDAS™

iDAS DATASHEET

Oil & Gas Downhole

Oil & Gas SURF

Mining

Environmental & Infrastructure

The world's finest distributed acoustic sensor, the iDAS, has a novel optoelectronics architecture that allows for digital recording of acoustic fields at every location along a singlemode or multimode optical fibre. Amplitude, frequency and phase fidelity allows for numerous advanced applications.

Benefits of iDAS

» Finest Sampling Resolution = 25cm
» Sampling Frequency = 1kHz-100kHz
» Range = up to 40km
» Easily deployed in remote and hostile environments
» Finest Spatial Resolution = 1m
» Frequency Range = 0.01Hz to 50kHz
» Dynamic Range = > 120dB
» Compatible with standard singlemode and multimode optical fibre

Product Specifications

Sensing Capabilities

Range	Channels	Frequency		Resolution	
		Range	Sample	Sampling	Spatial
0 - 40km	1	0.01Hz - 50kHz	1kHz*	down to 25cm*	down to 1m*

* Range and application dependent. Eg. Seismic iDAS has spatial resolution of 10m, sample interval of 25cm and sample rate of 10kHz on a 10km optical fibre.

Power Supply Requirements

AC Power
100 - 240V, 50 - 60Hz

Communication Options

Ethernet	USB
2x 10Gb/s	2x USB 3.0
2x 1Gb/s	4x USB 2.0

Physical Dimensions [19in rack compatible]

Height	Width	Depth	Weight
6.97in / 177.1mm	18.30in / 464.8mm	18.40in / 467.4mm	16.9kg / 37.3lb

Certification & Compliance

Safety	CE	FCC
• EN60825-1:2014 • Class 1 Laser Product • 21 CFR part 1040.10	RED 2014/53/EU • EN61326-1:2013 • EN301 489-19 v1.2.1 • EN303 413 v1.1.1 • EN61010-1:2010	47 CFR Part 15 Sub Part B

Data Monitoring

iDAS Viewer	iDAS DAQ

Contact Us

Silixa Ltd
230, Centennial Park, Elstree,
Hertfordshire
WD6 3SN, UK

t: +44 (0) 20 8327 4210
f: +44 (0) 20 8953 4362

Silixa LLC
16203 Park Row, Suite 185, Houston
TX 77084, USA

t: +1 832 772 3333
f: +1 832 772 3530

www.silixa.com

 iDAS-LDAT10

Achilles JQS empowered by Achilles Qualified

Certificate Number: 9032 ISO 9001: 2008

Appendix 4: IMS geophone specifications

The two first pages of the Appendix have the original specification of the five element geophone build from IMS in 2013.

institute of mine seismology

Sensor Specification

Uppsala Special Build

Document Number
SKB-SPEC-201309-EdK rev 0

Accelerometer Element		
Description	**Value**	**Tolerance**
Type	25 kHz	-
Configuration	Uniaxial, Vertical	-
Sensitivity	100 mV/g	±5%
Broadband Noise	150 μg	-
Geophone Element		
Description	**Value**	**Tolerance**
Type	Omni directional	-
Natural Frequency	14 Hz	±7%
Configuration	Uniaxial, Vertical	-
Open Circuit Damping	0.185	+10/-5%
Coil Resistance	3500 Ω	±5%
Open Circuit Sensitivity	80 V/m/s	+5/-10%
RtBcFn	49931 Ω Hz	-
Moving Mass	10.2 g	-

Assembled Configuration	
Geophone	5 elements, series, vertical
Accelerometer	1 element, vertical
Geophone Assembly	
Open Circuit Damping	0.185
Coil Resistance	17500 Ω
Open Circuit Sensitivity	400 V/m/s
RtBcFn	249655 Ω Hz
Nominal damping resistor	41 kΩ
Damping ratio with above	0.49
Sensor Cable	
Signal	**Colour**
Geophone (+)	Red
Geophone (-)	Blue
Not Used	Yellow
Not Used	Green
Accelerometer (+)	White
Accelerometer (-)	Black
Not Used	Brown
Not Used	Purple

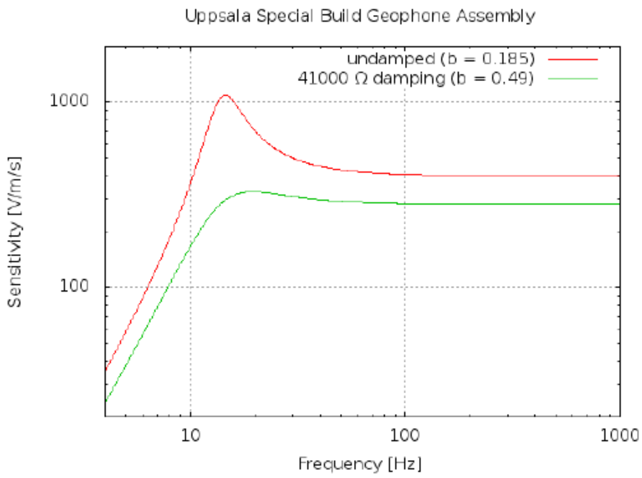

Sensor production test records for the first two sensors, where sensor 180001.208 with 100 m attached cable turned out to have a cable damage on delivery.

IMS SYSTEMS ENGINEERING

Sensor – Production Test Record

institute of mine seismology

Geophone Type:	3G14				
Serial No:	180001.208	**Senscon ID No:**	208		
Element Type:	SM6 14Hz OB (Brass_Cap)	**Element Batch #:**	November 2017		
Cable Type:	HGS_4pr_28AWG	**Cable Length:**	100 Meters		
Meter Markings:	42 – 142				
Casting Chemical:	VYTAFLEX-60	**Sensor Housing:**	*5x3_SM6_S3G16_A_S8534_SC_N*		
Trigger Test:	OK	**Tested By:**	MK	**Date:**	06 March 2018
Polarity Test:	OK	**Tested By:**	MK	**Date:**	06 March 2018
Relay Test:	OK	**Tested By:**	MK	**Date:**	06 March 2018

Geophone Connection Details:	
N / S (X)	Red(+) / Blue(-)
E / W (Y)	Yellow(+) / Green(-)
Up / Down (Z)	White(+) / Black(-)

Smart Sensor:	
Smart Sensor PCB:	SENS-PCB-016-6
PCB Serial:	ZT0003716

Junction Box:	
Junction Box PCB:	JB-PCB-002-6
PCB Serial:	ZT0003346

Smart Sensor Connection Details:	
BROWN (+)	ID +
VIOLET (GND)	ID Return

Note:

Care should be exercised to ensure that the external insulation of the cable is not damaged in any way as this may allow the ingress of water into the core of the cable.

IMS SYSTEMS ENGINEERING
Sensor – Production Test Record

institute of mine seismology

Geophone Type:	5 X 3G14				
Serial No:	180002.208	Senscon ID No:	208		
Element Type:	SM6 14Hz OB (Brass_Cap)	Element Batch #:	November 2017		
Cable Type:	HGS_4pr_28AWG	Cable Length:	200 Meters		
Meter Markings:	3 – 253				
Casting Chemical:	VYTAFLEX-60	Sensor Housing:	*5x3_SM6_S3G16_A_S8534_SC_N*		
Trigger Test:	OK	Tested By:	MK	Date:	06 March 2018
Polarity Test:	OK	Tested By:	MK	Date:	06 March 2018
Relay Test:	OK	Tested By:	MK	Date:	06 March 2018

Geophone Connection Details:	
N / S (X)	Red(+) / Blue(-)
E / W (Y)	Yellow(+) / Green(-)
Up / Down (Z)	White(+) / Black(-)

Smart Sensor:		Junction Box:	
Smart Sensor PCB:	SENS-PCB-016-6	Junction Box PCB:	JB-PCB-002-6
PCB Serial:	ZT0003731	PCB Serial:	ZT0003434

Smart Sensor Connection Details:	
BROWN (+)	ID +
VIOLET (GND)	ID Return

Note:

Care should be exercised to ensure that the external insulation of the cable is not damaged in any way as this may allow the ingress of water into the core of the cable.

Sensor production test record for the replacement geophone, 180003.208

IMS SYSTEMS ENGINEERING
Sensor – Production Test Record

institute
of mine
seismology

Geophone Type:	5X3G14				
Serial No:	180003.208	**Senscon ID No:**	208		
Element Type:	5 x SM6 14Hz OB (Brass_Cap)	**Element Batch #:**	November 2017		
Cable Type:	Teledyne_4PR_24AWG	**Cable Length:**	100 Meters		
Meter Markings:	917 – 1017				
Casting Chemical:	VYTAFLEX-60	**Sensor Housing:**	*5x3_SM6_S3G16_A_S8534_SC_N*		
Trigger Test:	OK	**Tested By:**	MK	**Date:**	28 May 2018
Polarity Test:	OK	**Tested By:**	MK	**Date:**	28 May 2018
Relay Test:	OK	**Tested By:**	MK	**Date:**	28 May 2018

Geophone Connection Details:	
N / S (X)	Red(+) / Blue(-)
E / W (Y)	Yellow(+) / Green(-)
Up / Down (Z)	White(+) / Black(-)

Smart Sensor:		**Junction Box:**	
Smart Sensor PCB:	SENS-PCB-016-6	Junction Box PCB:	JB-PCB-002-6
PCB Serial:	ZT0004044	PCB Serial:	ZT0003910
Smart Sensor Connection Details:		Custom damping	R=41k
BROWN (+)	ID +		
VIOLET (GND)	ID Return		

Note:

Care should be exercised to ensure that the external insulation of the cable is not damaged in any way as this may allow the ingress of water into the core of the cable.

The geophone transfer function for removal of the instrument response, as supplied by IMS 2018.